The role of the *adhesion and degranulation promoting adapter protein* (ADAP) in platelet production

****

Die Rolle des *adhesion and degranulation promoting adapter* Proteins (ADAP) in der Thrombopoese

Doctoral thesis for a doctoral degree

at the Graduate School of Life Sciences,

Julius Maximilians-Universität Würzburg,

Section: Biomedicine

submitted by

Markus Spindler

from Geroldsgrün, Germany

Würzburg, 2019

Submitted on: _____

Office stamp

Members of the *Promotionskomitee*:

Chairperson: _____

Primary Supervisor: Dr. Markus Bender

Supervisor (Second): Prof. Dr. Antje Gohla

Supervisor (Third): Prof. Dr. Christoph Kleinschnitz

Supervisor (Fourth): _____

Date of Public Defence: _____

Date of Receipt of Certificates: _____

„Es wird ja fleißig gearbeitet und viel mikroskopiert, aber es müsste mal wieder einer einen gescheiten Gedanken haben.“

Rudolf Ludwig Karl Virchow (1821 - 1902)

SUMMARY

Bone marrow (BM) megakaryocytes (MKs) produce platelets by extending proplatelets into sinusoidal blood vessels. Although this process is fundamental to maintain normal platelet counts in circulation only little is known about the regulation of directed proplatelet formation.

As revealed in this thesis, ADAP (adhesion and degranulation promoting adapter protein) deficiency (constitutive as well as MK and platelet-specific) resulted in a microthrombocytopenia in mice, recapitulating the clinical hallmark of patients with mutations in the *ADAP* gene. The thrombocytopenia was caused by a combination of an enhanced removal of platelets from the circulation by macrophages and a platelet production defect. This defect led to an ectopic release of (pro)platelet-like particles into the bone marrow compartment, with a massive accumulation of such fragments around sinusoids. *In vitro* studies of cultured BM cell-derived MKs revealed a polarization defect of the demarcation membrane system, which is dependent on F-actin dynamics. ADAP-deficient MKs spread on collagen and fibronectin displayed a reduced F-actin content and podosome density in the lowest confocal plane. In addition, ADAP-deficient MKs exhibited a reduced capacity to adhere on Horm collagen and in line with that the activation of β1-integrins in the lowest confocal plane of spread MKs was diminished. These results point to ADAP as a novel regulator of terminal platelet formation.

Beside ADAP-deficient mice, three other knockout mouse models (deficiency for profilin1 (PFN1), Wiskott-Aldrich-syndrome protein (WASP) and Actin-related protein 2/3 complex subunit 2 (ARPC2)) exist, which display ectopic release of (pro)platelet-like particles. As shown in the final part of the thesis, the pattern of the ectopic release of (pro)platelet-like particles in these genetically modified mice (PFN1 and WASP) was comparable to ADAP-deficient mice. Furthermore, all tested mutant MKs displayed an adhesion defect as well as a reduced podosome density on Horm collagen. These results indicate that similar mechanisms might apply for ectopic release.

ZUSAMMENFASSUNG

Die Megakaryozyten (MKn) des Knochenmarks produzieren Thrombozyten durch die Ausbildung und Verlängerung von Proplättchen in die sinusoidalen Blutgefäße. Obwohl dieser Prozess für die Aufrechterhaltung der normalen Thrombozytenzahl in der Blutzirkulation von grundlegender Bedeutung ist, ist über die Regulation der gerichteten Proplättchenbildung und damit der Thrombozytenproduktion nur wenig bekannt.

Wie in dieser Arbeit gezeigt, führte sowohl die konstitutive als auch die MK- und Thrombozyten-spezifische Defizienz von ADAP (*adhesion and degranulation promoting adapter protein*) in Mäusen zu einer Mikrothrombozytopenie, ähnlich wie dies bei Patienten mit Mutationen im *ADAP* Gen zu beobachten ist. Die Thrombozytopenie wurde durch eine Kombination aus einer verstärkten Entfernung (*clearance*) von Thrombozyten aus der Zirkulation durch Makrophagen und einem Defekt in der Thrombozytenproduktion verursacht. Dieser Defekt führte zu einer ektopischen Freisetzung von Proplättchen-ähnlichen Partikeln ins Knochenmark und zur Anreicherung derartiger Fragmente um die Sinusoiden. *In vitro*-Studien an kultivierten MKn aus Zellen des Knochenmarks zeigten einen Polarisationsdefekt des Demarkationsmembransystems, welcher abhängig von der F-Aktin-Dynamik ist. ADAP-defiziente MKn wiesen nach *Spreading* auf Kollagen und Fibronektin einen reduzierten F-Aktin Gehalt und eine geringere Dichte von Podosomen in der untersten konfokalen Ebene auf. Zusätzlich zeigten ADAP-defiziente MKn beim *Spreading* Versuch eine verminderte Kapazität sich an Horm Kollagen anzuhaften, und die Aktivierung von β1-Integrinen war in der untersten konfokalen Ebene von MKn reduziert. Diese Ergebnisse deuten darauf hin, dass ADAP ein wichtiges Protein im terminalen Schritt der Thrombozytenproduktion ist.

Neben ADAP-defizienten Mäusen existieren drei weitere Knockout-Mausmodelle (für die Proteine: Profilin1 (PFN1), Wiskott-Aldrich-Syndrom-Protein (WASP) und *Actin-related protein 2/3 complex subunit 2* (ARPC2)), die eine ektopische Freisetzung von Proplättchen-ähnlichen Partikeln zeigen. Wie im letzten Teil der Arbeit gezeigt, war das Muster der ektopischen Freisetzung von Proplättchen-ähnlichen Partikeln in diesen

genetisch veränderten Mäusen (PFN1 und WASP) zu den ADAP-defizienten Mäusen vergleichbar. Darüber hinaus zeigten die MKn von den knockout Mäusen einen Adhäsionsdefekt sowie eine reduzierte Podosomendichte auf Horm Kollagen. Diese Ergebnisse deuten darauf hin, dass ähnliche Mechanismen für die Freisetzung von Proplättchen-ähnlichen Partikeln in das Knochenmark verantwortlich sein könnten.

CONTENTS

1. INTRODUCTION

1.1. Megakaryocytes

1.1.1. Megakaryopoiesis

Megakaryocytes (MKs) originate from hematopoietic stem cells (HSCs) and are the largest cells found in the bone marrow (BM), which is the main site of platelet production. Besides the BM, MKs are also found in the yolk sac, fetal liver and spleen during early development in mice.[1,2] Very recently, the lung was also suggested to be a site of platelet production in mice with a reservoir for hematopoietic progenitors.[3] Only 0.1% of cells in the BM are MKs and because of this extreme rarity many aspects of MK biology are understudied.[4] It was postulated that MKs migrate from the HSC osteoblastic niche to the vascular niche, where they mature and extend long, branching processes, so called proplatelets, into the vessel lumen, from which platelets are shed.[5,6] However, a revised model suggests, that MKs at sinusoids are replenished by sinusoidal precursors rather than cells from a distant periostic niche.[7] The fate and differentiation of HSCs is tightly regulated by transcription factors (such as GATA-1, GATA-2 and RUNX1), signaling pathways (such as PI3K, Akt, MAPK and ERK1/ERK2 pathways, reviewed in [8]), adhesion molecules, cytokines and chemokines. A breakthrough in MK research was in 1994, when several groups identified and cloned c-Mpl as the receptor that promotes the growth and development of MKs from HSCs.[9-16] This discovery was seminal for the development of *in vitro* culture systems and facilitated to study MK differentiation, maturation, platelet production and the molecular mechanisms that regulate these processes. The most important mediator of megakaryopoiesis is thrombopoietin (Thpo), the ligand of the c-Mpl receptor.[11] Loss of Mpl- or Thpo in mice and congenital *MPL* deficiency in humans leads to a severe thrombocytopenia, thus highlighting the importance of Thpo and its receptor c-Mpl in platelet production.[17,18]

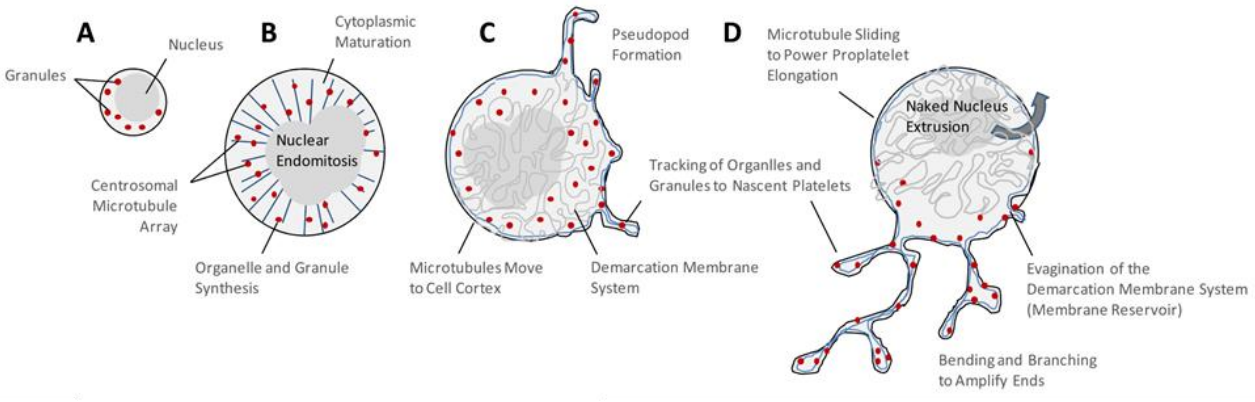

Figure 1: MK maturation including cytoskeletal rearrangements during megakaryopoiesis. A systematic series of events occurs during differentiation from immature progenitor cells (**A**) to mature MKs (**D**). These events include endomitosis (resulting in a polyploid nucleus), cytoplasmic maturation (**B**), development of an invaginated membrane system (demarcation membrane system) and reorganization of the cytoskeleton (**C**). Figure adapted from Thon and Italiano, 2010.[19]

During development, MKs increase in size, produce granules in their cytoplasm and become polyploid (up to 128n) (Figure 1).[6] This is the result of a process, designated endomitosis, characterized by repeated incomplete cell cycles with failure of both karyokinesis and cytokinesis.[20] In addition, MKs expand their content of cytoskeletal proteins and develop a highly invaginated membrane system (demarcation membrane system, DMS) during maturation (Figure 2), which serves as membrane reservoir for future platelets.[6] *In vitro* studies of cultured murine MKs by beam/scanning electron microscopy revealed that DMS biogenesis starts with focal membrane assembly at the cell periphery, followed by plasma membrane invagination and expansion through membrane delivery from Golgi complexes and ER-mediated lipid transfer.[21] Developing of the DMS in different stages relies on F-actin dynamics to polarize membranes and nuclei territories, and requires the activation of the guanosine triphosphate hydrolase Cdc42 and its p21-activated kinase effectors (Pak1/2/3).[22,23]

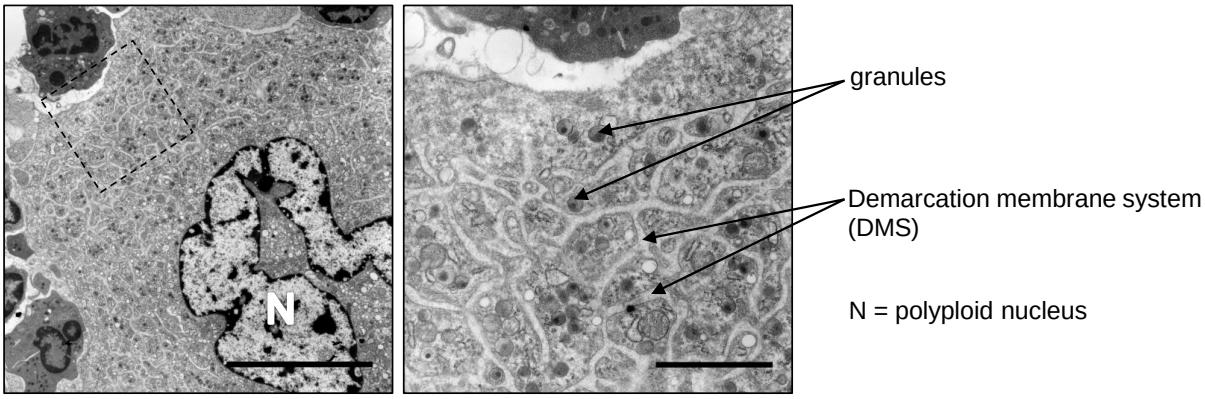

Figure 2: Transmission electron micrograph of a mature MK in the BM. The nucleus (N) is clearly visible as a white multilobular structure surrounded by electron dense material. The demarcation membrane system separates the cytoplasm, resulting in platelet territories packed with granules. Images from this work. Scale bars represent 5 µm (left) and 2 µm (right).

1.1.2. Thrombopoiesis

Fully developed, mature MKs extend long protrusions, designated proplatelets, into sinusoidal blood vessel of the BM.[24,25] However, terminal platelet production, with final sizing of the platelets occurs in the blood stream in shear-dependent manner (Figure 3).[25]

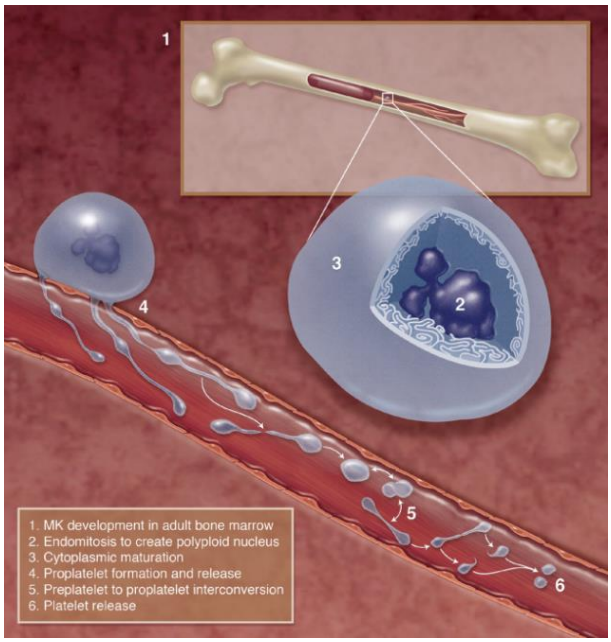

Figure 3: Scheme of platelet production *in vivo*. HSCs in the BM (1) differentiate into MKs in a Thpo-dependent manner. During maturation they undergo endomitosis resulting in large nuclei ranging in DNA content from 2n to 128n (2). In addition, MKs develop by invaginations of the plasma membrane, the demarcation membrane system, which serves as membrane reservoir for future platelets (3). Finally, MKs extend and release preplatelets into the blood stream (4). Once in the blood stream, preplatelets interconvert into proplatelets (5) and then into platelets with their final size (6). Figure adapted from Machlus and Italiano, 2013.[26]

In vitro proplatelet production studies of murine MKs derived from fetal liver stem cells (proplatelet yield about 60%, reviewed in [19]), revealed a morphological highly complex transformation process of the entire MK cytoplasm into platelet-sized particles, which have the appearance of beads linked by thin cytoplasmic bridges.[4] However, murine MKs derived from BM cells cultured with Thpo and human MKs derived from BM, fetal cord blood, mobilized peripheral blood progenitor cells and hESC H9 cells hardly produced proplatelets in culture, which hindered extensive proplatelet studies *in vitro* (reviewed in [19]). It was recently discovered that the addition of hirudin or heparin to the culture medium and cultivation of MK progenitors in 2% methylcellulose hydrogels improves the development of the DMS and dramatically increases the proplatelet yield in MKs derived from murine BM cells.[27,28] Based on *in vitro* MK culture methods it was shown that platelet biogenesis, including the elongation, the release and the package of proplatelets with cargo (e.g. granules, mitochondria) is highly cytoskeleton dependent.[6,26] Improvements of imaging techniques in the last decades have made it even possible to study proplatelet formation *in vivo* by two-photon intravital microscopy.[29,30]

1.1.3. Role of extracellular matrix proteins in platelet production

MKs can form proplatelets in cell culture implicating that for the process of platelet biogenesis the interplay between MKs and the microenvironment in the BM is not necessarily required. Nevertheless, the efficiency of platelet production in culture is dramatically decreased relative to that observed *in vivo*, suggesting a stimulating and enhancing role of the BM microenvironment on platelet biogenesis.[26] The BM contains a variety of cells, which together with extracellular matrix proteins (ECM), the vasculature and the bone cortex build up a complex architecture. Molecules and cells in this 3D environment have specific locations instead of being randomly distributed. The presence of a complex vascular system creates gradients of blood-derived molecules as well as oxygen tension.[31] ECM proteins are major components of the vascular niche, which

comprise collagens (type I, III, IV), fibrinogen, laminins, fibronectin and von Willebrand factor (vWF) in mice.[32] For human MKs from cord blood-derived $CD34^+$ cells it is described that adhesion to fibrinogen, fibronectin or vWF accelerate the development of proplatelets, but dramatically limits both amplitude and duration of the process, whereas type I collagen totally suppressed proplatelet extension.[33] The inhibitory impact of collagen I on proplatelet formation was also shown for murine fetal liver-derived MKs to be specifically controlled by GPVI, whereas collagen types III and IV as well as laminins and fibronectin had no influence on proplatelet formation in these assays.[32] However, using primary murine MKs from BM aspirates, Larson and Watson could show that fibrinogen supports proplatelet formation, whereas they observed no proplatelets on collagen or BSA, confirming the inhibitory effect of collagen on platelet biogenesis.[34]

1.2. Platelets

1.2.1. Platelet morphology and function

Blood platelets are crucial players in hemostasis. Platelet activation and aggregation are required to limit blood loss at sites of vessel damage. Under pathological conditions excessive platelet aggregation can lead to uncontrolled thrombus formation. Therefore, platelet activation requires a tight regulation. To this end platelets express a variety of receptor proteins responsible for adhesion, activation and aggregation at sites of exposed subendothelial ECM proteins.[35] Platelets are, with about 1-2 µm diameter (8-9 fl platelet volume) in humans and only 0.5 µm diameter (3-6 fl platelet volume) in mice, the smallest cells in the blood and exhibit a discoid shape under resting conditions.[36,37] Mouse platelets are similar to human platelets but have a greater granule heterogeneity and they differ in expression and function of several proteins, such as that they express the thrombin receptor PAR3 instead of PAR1.[38,39] One microliter of murine blood contains about 1-1.5 x 10^6 platelets, which circulate in the body for about 3-4 days, compared to only 150-400 x 10^3 platelets/µl in humans with a platelet lifespan of 8-12 days.[36] However, despite these differences between platelets from mice and humans,

genetically modified mice are still a valuable model system to study general aspects of platelet biology and function.[38,40]

Platelets are densely packed with granules (Figure 4), which are released upon activation. Three major granules types have been described in platelets: α-granules, δ-granules (dense granules) and lysosomes, with δ-granules and α-granules being the best–studied ones.[41] Over 300 proteins are stored in α-granules, such as membrane-associated receptors (e.g. P-selectin and αIIbβ3) and soluble cargo (e.g. platelet factor 4 [PF4], fibrinogen, vWF), whereas δ–granules contain bioactive amines (e.g. serotonin, histamine), adenine nucleotides, poly- and pyrophosphates as well as high concentrations of cations, particularly calcium.[41]

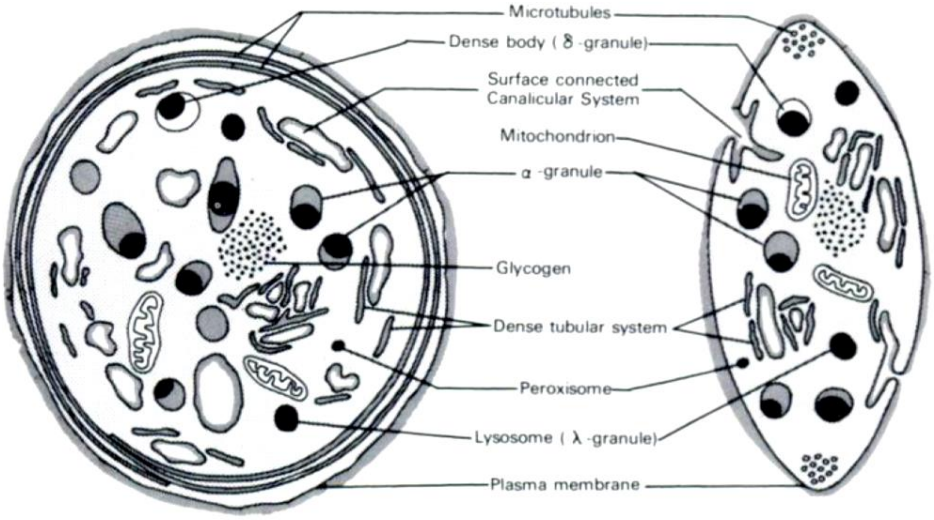

Figure 4: Diagram of a human platelet depicting cellular components based on electron micrographs. The round shape (left) results of sectioning along the marginal band (ring of microtubules in the periphery of the cell), whereas the elongated ellipse (right) is the result of a section in a 90-degree angle. Beside the major granules (α- and δ-granules), platelets also contain peroxisomes and lysosomes as storage organelles and mitochondria for energy production. Figure adapted from Bentfeld-Barker and Bainton, 1982.[42]

The adhesion and activation of platelets is a multistep process involving numerous platelet receptor-ligand interactions (Figure 5).[35] Upon injury of the vessel wall and the exposure of ECM proteins, GPIb-V-IX complexes interact with exposed vWF and induce tethering of platelets at sites of injury. Once the platelet is decelerated via GPIb-vWF

interaction, GPVI can bind to collagen and cellular activation including inside-out activation of β1- and β3-integrins leads to firm adhesion. Released ADP and TxA_2 amplify integrin activation of adherent platelets and mediate thrombus growth by recruiting and activating adjacent platelets.[35] Although platelets are best known for their role in hemostasis, there are several studies emphasizing the role of platelets in development, for the immune system and tissue repair.[43]

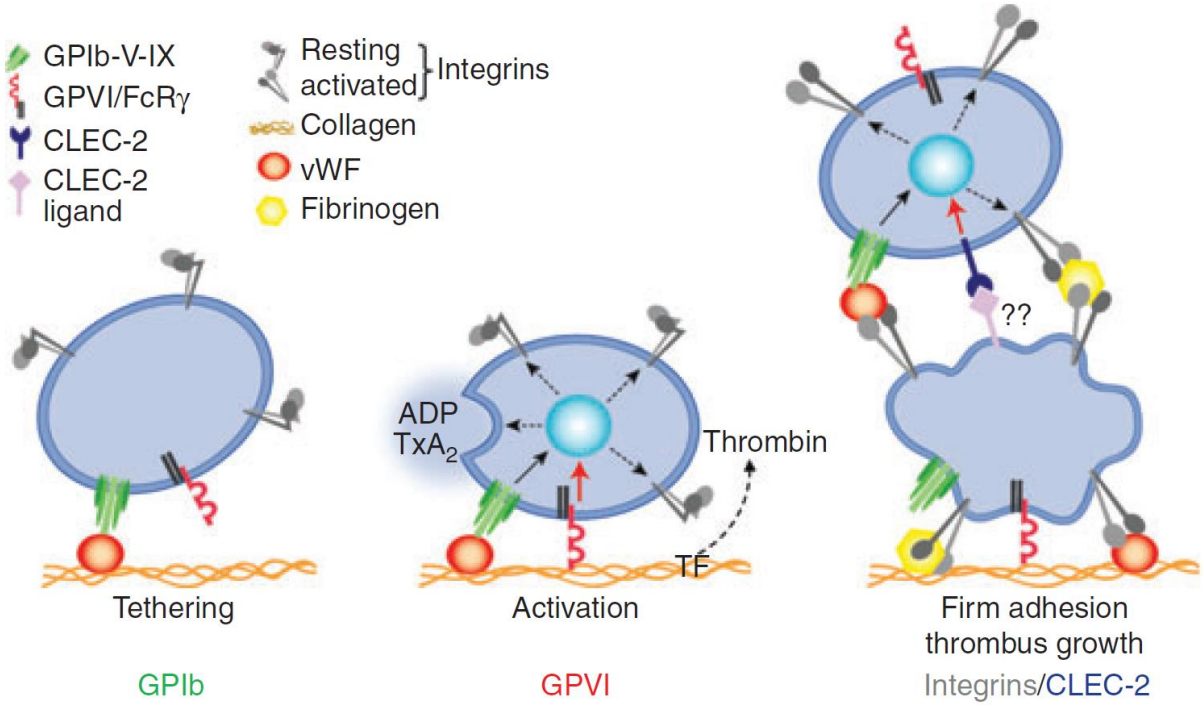

Figure 5: Model of adhesion receptor involvement in thrombus formation. Shown is a simplified model of major steps in thrombus formation (tethering, activation and firm adhesion/thrombus growth) and involved receptor proteins. Figure adapted from Nieswandt *et al*., 2011.[35]

1.2.2. Inherited microthrombocytopenia

Although there are many causes for a low platelet count, thrombocytopenias can be class-divided. There are thrombocytopenias which are acquired and mainly caused by an autoimmune reaction and such which are inherited. Inherited thrombocytopenias are a heterogeneous group of disorders characterized by a sustained reduction in platelet count manifesting as a bleeding diathesis.[44] Underlying mutations responsible for

thrombocytopenia are found in genes encoding proteins important for MK differentiation, maturation, proplatelet formation, platelet release or platelet clearance.[31,44,45] Most thrombocytopenias are associated with large or giant platelets, so called marcothrombocytopenias. In contrast, microthrombocytopenias (smaller and fewer platelets in the circulation) in humans are rare and predominantly associated with mutations in genes encoding for direct or indirect interaction partners of the F-actin cytoskeleton (*WAS*[46], *ARPC1B*[47]).

Recently, the congenital autosomal-recessive small-platelet thrombocytopenia (CARST[48,49]) was described as a platelet disorder with a low platelet count and a decreased mean platelet volume (MPV). Although some CARST patients have a severe thrombocytopenia, other display moderately reduced or variable platelet counts over time.[49,50] So far, eight patients in two families have been described, suffering from mild bleeding episodes to heavy menstrual bleeding. None of the patients had growth defects, immune defects, or unusual infections.[48-50] This is in contrast to microthrombocytopenic patients with Wiskott-Aldrich syndrome (mutation in *WAS*) or patients carrying mutations in the *ARPC1B* gene, which are characterized, among others, by immunodeficiency.[46,47] Genomic analyses revealed that mutations in the gene encoding the adhesion and degranulation-promoting adaptor protein (*ADAP*; synonyms: *FYB*, *SLAP-120/130*) are the underlying cause for CARST in humans. Two mutations have been reported (point mutation 393G>A: W131X; 2-bp deletion 1385_1386delAT:Y462) leading to a frameshift and/or the insertion of a premature stop codon, presumably resulting in a truncated gene product and no functional ADAP protein (Figure 6).[48,49]

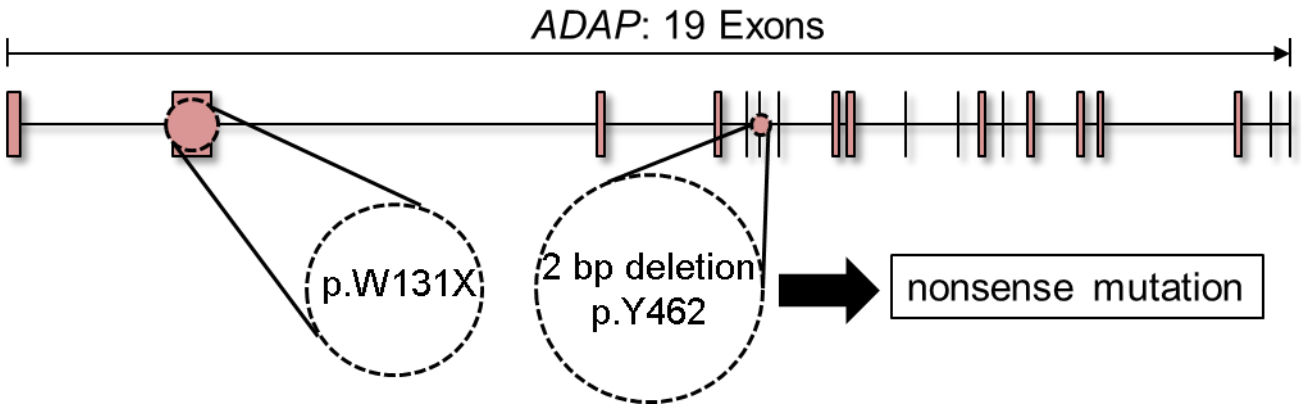

Figure 6: Schematic genetic map of the *ADAP* gene with mutations found in CARST patients. Two mutations are described. One point mutation in the 2nd exon results in an amino acid exchange in the polypeptide chain (W131X) and a 2 bp deletion in the 6th exon (p.Y462). Both mutations are nonsense mutations leading to a frameshift and the insertion of a premature stop codon.

1.3. The cytoskeleton of megakaryocytes and platelets

The cytoskeleton is highly important for cellular organization and a variety of cellular processes like motility, adhesion to the ECM or other cells, intracellular trafficking of cargo, cytokinesis, growth, polarization events and the maintenance of the cell shape. There are three major components of the cytoskeleton in platelets: microtubules, the actin-based cytoskeleton and the spectrin-based membrane skeleton. During proplatelet formation, protrusions from MKs become filled with thick bundles of microtubules that undergo a thinning phase down to approximately 20 microtubules.[25] In the finally released platelets the microtubules form the marginal band, an array of multiple highly dynamic microtubules of mixed polarity, which are responsible for the maintenance of the discoid shape of resting blood platelets (Figure 7).[51,52] F-actin, however, is found in the cytoplasm of platelets as well as in MKs and is important for DMS polarization[22] and during the terminal steps of platelet production.[53]

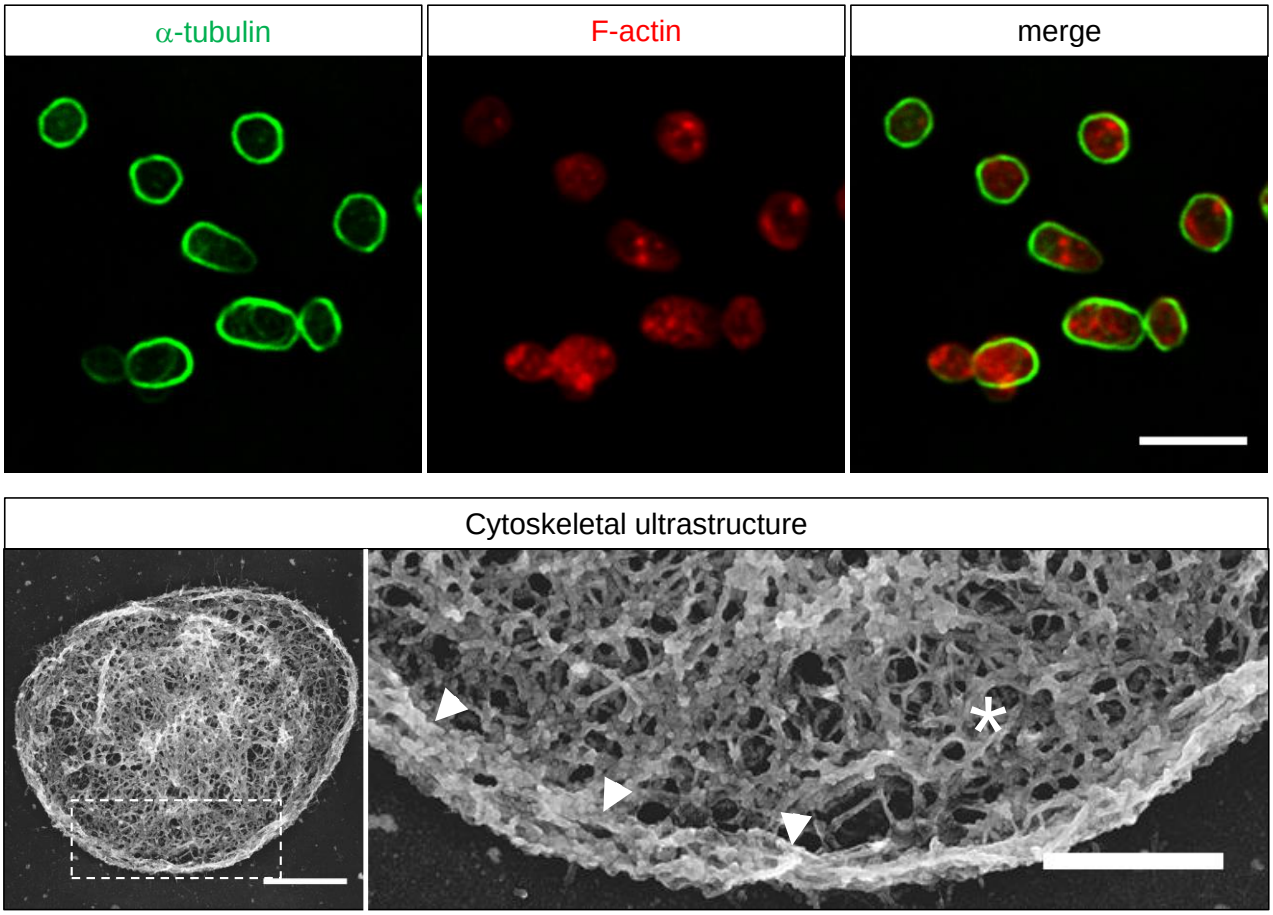

Figure 7: Organization of the cytoskeleton in platelets under resting conditions. Upper panel: Confocal microscopy image of immunostained resting platelets on poly-L-lysine. The array of microtubules in the marginal band was visualized by α-tubulin staining (left and right, green). F-actin was stained with fluorophore-coupled phalloidin (middle and right, red). Scale bar represents 5 µm. **Lower panel:** Transmission electron micrograph of the cytoskeletal ultrastructure of a resting platelet on poly-L-lysine. **Left:** overview image. Scale bar represents 1 µm. **Right:** Magnification of the marked region (rectangle with dotted lines) in the overview image. Microtubules are visible in the marginal band (arrowheads) and are connected to the branched F-actin network (asterisk). Scale bars represent 1 µm (left) and 0.5 µm (right). Images from this work.

1.3.1. The microtubule cytoskeleton

Microtubules are hollow, polarized tubes that dynamically assemble from heterodimers of α- and β-tubulin.[54] The strict regulation of dynamics and stability is of key importance for microtubule function and is thus controlled by several complementary mechanisms, like post-translational modifications (PTMs) of tubulin subunits, the expression of different tubulin isoforms and the expression of regulatory microtubule-associated

proteins and molecular motors.[54-56] In mammals, nine α-tubulin and nine β-tubulin genes have been identified. The corresponding proteins mainly differ in the C-terminus, in which most of the PTMs occur. PTMs of tubulin (e.g. polyglycylation, methylation, acetylation, detyrosination and polyglutamylation) together with the expression of different isoforms of α- and β-tubulin give rise to the so-called 'tubulin code' a regulatory mechanism to control the specialization of the microtubule cytoskeleton.[56]

MKs and platelets exhibit microtubules, which are selectively enriched in the specific β1-tubulin[52,56-58] and α4A-tubulin isotype.[59] This might be in part responsible for the specific functions of these microtubules in platelet production and function, which is supported by the appearance of (macro-) thrombocytopenias in the absence of either β1-tubulin or α4A-tubulin in the MK lineage in mice and humans.[52,58,59] Beside this, the marginal band of mouse platelets exhibits modified tubulin forms (most prominently detyrosinated, tyrosinated, acetylated and polyglutamylated ones), which may also in part contribute to microtubule dynamics and proplatelet formation.[51,60,61] Polymerization of microtubules is necessary to support the enlarging proplatelet mass, but the dynein-dependent sliding of overlapping microtubules drives proplatelet elongation and is a vital component of this process.[62,63]

1.3.2. The actin-based cytoskeleton

Monomeric globular-actin (G-actin) can polymerize into filamentous actin (F-actin), a right-handed F-actin helix, which can be further organized into higher-order structures by an array of actin-binding and -regulatory proteins.[64] Actin filaments are polar structures, whose two ends are referred to as the 'barbed end' and the 'pointed end'. Briefly, G-actin-ADP subunits are charged by polymerization factors such as profilin1 (PFN1), forming G-actin-ATP, and added to the growing end ('barbed end') of the filament. During F-actin aging, actin associated ATP decays to ADP + P_i and then to ADP. Effectors such as ADF or cofilin cause the severing and depolymerization of actin near

the pointed end, and release G-actin-ADP back into the uncharged pool, ready for another round of polymerization.[65]

The dynamic interplay between polymerization and depolymerization of F-actin in platelets and MKs is essential for their function. Upon platelet activation, cytoskeletal rearrangements result in a dramatic increase in the proportion of polymerized actin, manifesting as shape change of the platelet.[66] About 40-50% of total actin is present as F-actin in unstimulated platelets, whereas after short stimulation with thrombin (final concentration 0.1 NIH U/ml, 20-60 sec) this rapidly increases to 70%, thus underlining the fast response of the platelet activation machinery including the cytoskeleton to extracellular stimuli.[67,68]

Some inherited thrombocytopenias are associated with defects in proplatelet formation and platelet release. Interestingly, the underlying mutations in many of these inherited thrombocytopenias are found in genes coding for direct or indirect interaction partners of the F-actin cytoskeleton (e.g. *MYH9*-related disease,[69] *ACTN1*-related disease,[70] WASP-related disease [Wiskott-Aldrich-syndrome][71] and *FLNA*-related thrombocytopenia[72]). Moreover, genetically modified knockout mice of F-actin regulatory proteins also display platelet production defects (e.g. RAC1/CDC42,[73] ADF/Cofilin,[53] and PFN1[74]), thus emphasizing the importance of the F-actin cytoskeleton and its proper regulation in platelet biogenesis.

1.3.3. Podosomes in megakaryocytes

Cells can interact with the ECM through a variety of specialized structures. One of these cell-matrix contacts are podosomes. These cellular structures contain membrane proteins such as integrins, which via different linker proteins connect the membrane to the F-actin cytoskeleton.[75] Podosomes manifest as dot-like matrix contacts, with a two-part architecture: they consist of an F-actin rich core and actin-associated proteins (e.g. WASP, Arp2/3 and cortactin) that is surrounded by a ring structure consisting of plaque proteins (e.g. talin, vinculin, paxillin and Pyk2/FAK) and integrins (Figure 8).[75] The main

functions of podosomes are adhesion and matrix degradation by metalloproteases, but they also enable cell migration across substrates, and physical barriers, such as basement membranes, and are involved in cell-cell contacts.[75,76]

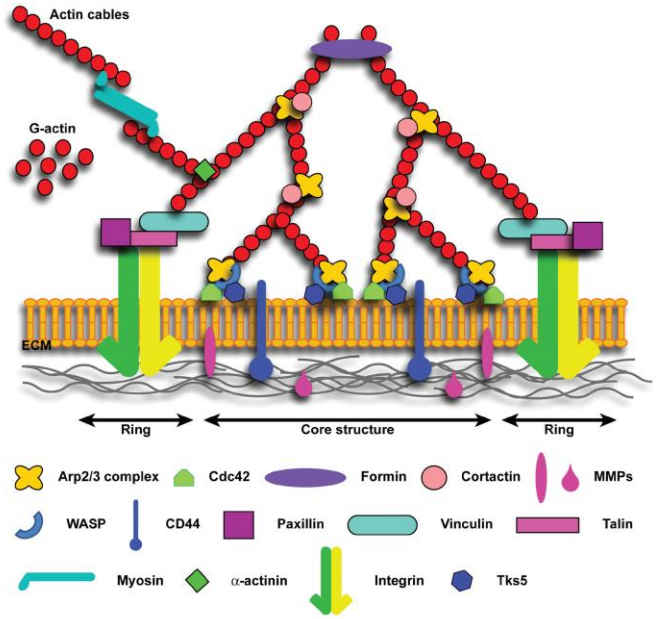

Figure 8: Molecular intracellular structure of podosomes. Podosomes exhibit an F-actin rich core which is packed with F-actin-associated proteins like Arp2/3 complex, WASP, cortactin and Formin. The core is typically surrounded by integrins, which enable the adhesion to the ECM. Podosomes are highly dynamic structures with a half-life of 2-12 min and are motile within a certain radius. Matrix-metalloproteases (MMPs) degrade the ECM and are associated with podosomes. Figure adapted from Schachtner, 2013.[76]

Podosomes are abundant in primary murine MKs, adherent on multiple ECM substrates, including native basement membrane and are suggested to play a role in proplatelet arm extension or penetration of the basement membrane.[77] This is supported by the study of knockout mice (WASP and PFN1) with platelet production defects whose mutant MKs show defective podosome formation.[74,78]

1.4. Actin interacting/modulating proteins

1.4.1. Profilin1 (PFN1)

Profilin (Pfn) is a small (15 kDa), ubiquitously expressed, cytosolic protein and was one of the first identified actin-binding proteins. Its main functions are to sequester actin monomers in a 1:1 complex and to promote the assembly of G-actin monomers into F-actin.[79-82] Four isoforms of Profilin have been described (PFN1-4), with PFN1 being the

most prominent isoform. PFN1 can interact with a variety of proteins besides actin, e.g. survival of motor neuron protein (SMN), partner of profilin (p42POP), Wiskott-Aldrich syndrome protein (WASP)-family verprolin-homologous protein (WAVE), mDia, vascular endothelial growth factor (VEGF) and Vasodilator-stimulated phosphoprotein (VASP).[82] In addition, PFN1 contains two PIP_2 binding sites, which are important for the PIP_2-Profilin-actin complex formation and the release of G-actin from this complex.[82-84] Interestingly, *in vitro* studies could show that PFN1 catalyzes actin polymerization in a concentration-dependent manner, serving as a catalyst at low concentration and as an inhibitor at higher levels.[85,86] Diseases, which are linked to PFN1, range from neurological disorders, like amyotrophic lateral sclerosis[87,88] and fragile X-syndrome,[89] to cancer (e.g. breast cancer,[90,91] Renal cell carcinoma [RCC],[92] bladder cancer[93] and pancreatic cancer[94]) as well as vascular defects, like hyperpermeability[95] and atherosclerosis.[96]

Deletion of PFN1 in MKs and platelets leads to a microthrombocytopenia in mice, which is caused by reduced platelet life span in the circulation and the ectopic release of platelet-like particles into the BM compartment.[74] Furthermore, PFN1-deficient platelets exhibit an increased number of microtubules in their marginal band, probably contributing to the reduced platelet size.[74] The impaired inside-out as well as outside-in signaling *in vitro* leads to an altered hemostatic function with prolonged bleeding times and impaired thrombosis due to thrombus embolization in these mice.[97]

1.4.2. Wiskott-Aldrich syndrome protein (WASP)

Wiskott-Aldrich syndrome protein (WASP) belongs to the WASP protein family consisting of five subfamilies (*WASP*, *N-WASP*, *WAVE1/SCAR1*, *WAVE2* and *WAVE3*). They share the WCA (WH2, connecting and acidic) domain, which enables Arp2/3 activation and F-actin nucleation. Members of this protein family are involved in different cytoskeleton-dependent cellular processes like autophagy, membrane tubulation, vesicle transport between Golgi and endoplasmatic reticulum (ER), regulation of receptor trafficking, endocytosis, lamellipodia formation and cell migration.[98] WASP is

ubiquitously expressed in non-erythroid hematopoietic cells and has an estimated molecular weight of 52.9 kDa.[99] Since the discovery of the WAS gene in 1994 by Derry J. and colleagues, approximately 300 different mutations were described, leading to a remarkably variable clinical phenotype including immunodeficiency, inflammatory symptoms, bleeding diathesis, autoimmunity and malignant potential.[99] Wiskott-Aldrich syndrome patients also display a microthrombocytopenia, which is the most consistent hallmark finding at diagnosis.[100]

WASP-deficient mice do not fully recapitulate the clinical features of WAS patients and only display a mild thrombocytopenia with normally sized platelets.[78] However, WASP-deficient mice, like PFN1-deficient mice, also display ectopically released platelets into the BM compartment and, in addition, a loss of collagen I-mediated inhibition of proplatelet formation.[78]

1.4.3. Adhesion and degranulation promoting adaptor protein (ADAP)

Adhesion and degranulation promoting adaptor protein (*ADAP*; synonyms: *FYB*, *SLAP-130/120*) is a cytosolic protein and primarily expressed in hematopoietic cells, except for B cells. Two isoforms of ADAP are described with an estimated molecular weight of 120 and 130 kDa.[101] The 130 kDa isoform contains an extra insertion of 46 amino acids and is preferentially expressed in peripheral T-cells,[102] but also in platelets.[103] Most of the studies regarding the cellular function of ADAP were performed in T-cells. The ADAP protein contains a proline-rich region and a Src homology 3 (SH3)-like domain, of which both bind to Src-kinase-associated phosphoprotein of 55 kDa (Skap55), phosphotyrosine sites that bind the SH2 domains of the Src family kinase Fyn and the adapter protein SLP-76, and an Ena/VASP-homology 1 (EVH1)-binding domain, which binds Ena/VASP family proteins.[104-109] ADAP is required for T-cell activation and proliferation *in vitro* and for proper immune responses *in vivo*, and for β1/β2 integrin clustering and adhesion through the T-cell receptor (TCR).[110,111] TCR stimulation leads to the phosphorylation of two Tyr-Asp-Asp-Val (YDDV) motifs in ADAP, which serve as binding sites for SLP-76. Mutations in these motifs lead to impaired T-cell activation.[109]

ADAP phosphorylation is followed by integrin activation (LFA-1) on the cell surface (inside-out signaling). Molecules activated downstream of LFA-1 engagement include FAK, ERK1/2, JNK, PLCγ1 (outside-in signaling). In addition, LFA-1 activation also induced F-actin polymerization via Vav-mediated Rac1, Cdc42, WASP and WAVE activation.[112] ADAP is therefore present in T-cells in an active complex with SLP-76, Nck and Vav1, taking part in inside-out as well as in outside-in signaling resulting in cell spreading, sustained adhesion, formation of actin foci/invadopodia-like protrusions, signaling microcluster assembly and formation of mature immunological synapses (Figure 9).[112]

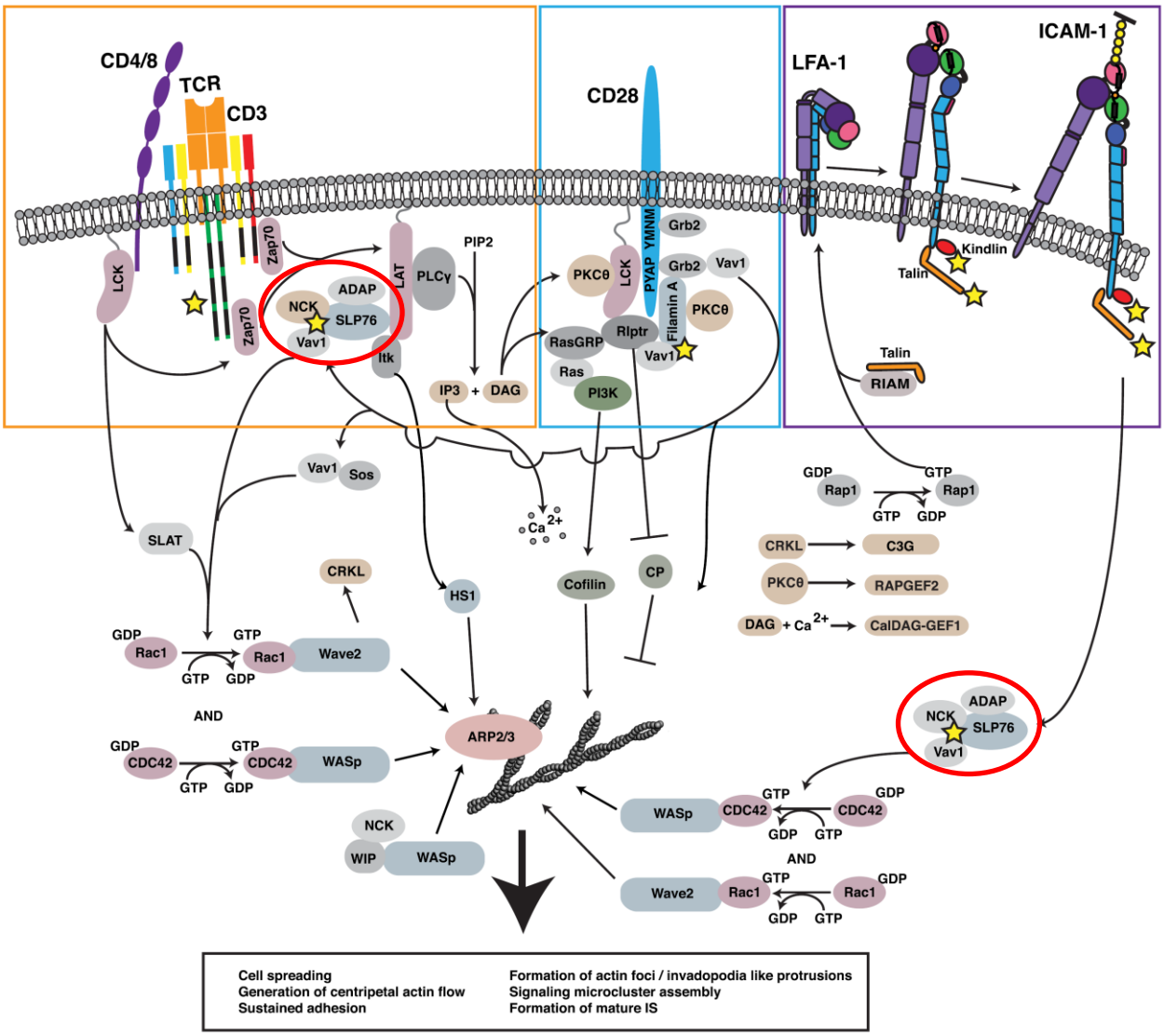

Figure 9: Regulation of the F-actin cytoskeleton in the immunological synapse in T-cells. Ligation of multiple receptors, including the TCR, the costimulatory molecule CD28, and the adhesion molecule LFA-

1, results in the induction of robust actin polymerization at the immunological synapse. The pathways that mediate F-actin polymerization are highly interdependent. The complex consisting of ADAP, Nck, SLP76 and Vav1 is marked with a red cycle. Figure adapted from Comrie and Burkhardt, 2016.[112]

Several studies have investigated the role of ADAP in murine platelet function. It has been shown that ADAP is involved in vWF/GP-Ib-IX-V signaling (leading to αIIbβ3 activation *in vitro*), promoting fibrinogen binding to αIIbβ3 (through interaction with talin and kindlin-3) and is an essential component of integrin-mediated mechano-transduction (thereby promoting F-actin assembly and thrombus stabilization).[113-116] Another group demonstrated that ADAP plays a role in mediating platelet activation via the collagen-binding integrin α2β1.[117,118] It is further described that the constitutive loss of ADAP in mice leads to a thrombocytopenia.[111]

2. AIM OF THIS STUDY

Although ADAP-deficient mice were generated and characterized in 2001, the mechanism responsible for the observed thrombocytopenia in those mice has remained unknown. So far, all studies have focused on studying platelet function in ADAP-deficient mice. However, nothing is known about the role of ADAP in MK biology. This is of high importance, since mutations in the *ADAP* gene in humans result in a microthrombocytopenia with increased bleeding tendency. Therefore, the first aim of this study was to investigate the role of ADAP in MKs and in platelet production.

The number of knockout mouse lines displaying ectopically released platelet-like particles into the BM compartment is rising. So far, three genetically-modified, thrombocytopenic mouse lines, namely PFN1-, WASP- and recently also ARPC2-deficient mice were described with such platelet production defects. However, it is unclear whether the mechanisms underlying the release of (pro)platelet-like particles into the bone marrow are comparable between these mutant mouse strains. Therefore, the second aim of this study was to gain new insights into mechanisms underlying ectopic platelet release analyzing the above-mentioned genetically-modified, (micro)thrombocytopenic mouse strains.

3. MATERIAL AND METHODS

3.1. Materials

3.1.1. Devices

Table 1: List of devices used in this study.

Device	Company
Cryotom CM1900	Leica (Wetzlar, Germany)
Eppendorf centrifuge 5415C	Eppendorf AG (Hamburg, Germany)
Eppendorf centrifuge 5427R	Eppendorf AG (Hamburg, Germany)
FACS Calibur	BD Biosciences (Heidelberg, Germany)
FACS Celesta	BD Biosciences (Heidelberg, Germany)
Gene Touch Thermal Cycler	Biozym Scientific GmbH (Oldenburg, Germany)
Herolab	Herolab GmbH (Wiesloch, Germany)
Leica EM ACE600	Leica (Wetzlar, Germany)
Leica EM CPD300	Leica (Wetzlar, Germany)
MultiImage II FC Light Cabinet	Alpha Innotech corporation (San Leandro, USA)
Nikon ECLIPSE TS 100	Nikon GmbH (Düsseldorf, Germany)
scil Vet abc Plus+	scil animal care company GmbH (Viernheim, Germany)
Sysmex KX 21N	Sysmex GmbH (Norderstedt, Germany)
TCS SP5 CLSM	Leica (Wetzlar, Germany)
TCS SP8 CLSM	Leica (Wetzlar, Germany)
VWR MEGA STAR 1.6R	VWR part of avantor (Darmstadt, Germany)
Zeiss EM 900	Carl Zeiss (Oberkochen, Germany)

3.1.2. Material

Table 2: List of materials used in this study.

Material	Company
Adhesive cryo films 2C/9	Section lab (Hiroshima, Japan)
Canula (18G, 20G, 22G)	BD Biosciences (Heidelberg, Germany)
TC dish 60 Standard	Sarsted (Nümbrecht, Germany)
Cell strainer 100/70 µm	Corning GmbH (Kaiserslautern, Germany)
Coverslips #1.5	Thermo fisher scientific (Dreieich, Germany)
Dynabeads™ Untouched™ Mouse CD4 Cells Kit	Thermo fisher scientific (Dreieich, Germany)
EDTA tubes	Sarsted (Nümbrecht, Germany)
Formvar-carbon-coated grids	Ted Pella Inc. (Redding, US)
Glass slide Superfrost Plus	Thermo fisher scientific (Dreieich, Germany)
Heparinized capillaries (100 µl)	Hartenstein (Würzburg, Germany)
Microcapillaries (50 µl)	Hartenstein (Würzburg, Germany)
PVDF membrane	GE Healthcare (Penzberg, Germany)
Round coverslips Ø18mm #1	Roth (Karlsruhe, Germany)
Syringe filters (70 µm)	Roth (Karlsruhe, Germany)
Syringes (1 ml)	Dispomed (Gelnhausen, Germany)
Well plates (96-well, 24-well, 6-well)	Greiner (Frickenhausen, Germany)

3.1.3. Chemical/reagent

Table 3: List of chemicals/reagents used in this study.

Chemical/reagent	Company
Acetone	Roth (Karlsruhe, Germany)
Adenosine diphosphate (ADP)	Sigma-Aldrich (Schnelldorf, Germany)
Agarose	Roth (Karlsruhe, Germany)
Ammonium peroxidsulfate (APS)	Roth (Karlsruhe, Germany)
Annexin V-FITC	provided by Jonathan F. Tait (Medical Center Washington, USA)
Apyrase (grade III)	Sigma-Aldrich (Schnelldorf, Germany)
Benzyl alcohol	Sigma-Aldrich (Schnelldorf, Germany)
Benzyl benzoate	Sigma-Aldrich (Schnelldorf, Germany)
Bovine serum albumin (BSA)	AppliChem (Darmstadt, Germany)
Clodronate/PBS encapsulated liposomes	Clodronate Liposomes (Haarlem, The Netherlands)
Collagen related peptide (CRP)	CRB Cambridge Research Biochemicals (Billingham, UK)
Collagen type I (human placenta)	Sigma-Aldrich (Schnelldorf, Germany)
Collagen type IV (human placenta)	Sigma-Aldrich (Schnelldorf, Germany)
Convulxin (CVX)	Axxora (Lörrach, Germany)
dNTP	Fermentas (St. Leon-Rot, Germany)
Dream Taq Polymerase	Fermentas (St. Leon-Rot, Germany)
Dream Taq Polymerase 10x buffer	Fermentas (St. Leon-Rot, Germany)
Eosin	Roth (Karlsruhe, Germany)
Ethanol	Roth (Karlsruhe, Germany)
Ethylene glycol-bis(2-aminoethylether)-N,N,N',N'-tetraacetic acid (EGTA)	Sigma-Aldrich (Schnelldorf, Germany)
Ethylenediaminetetraacetic acid (EDTA)	AppliChem (Darmstadt, Germany)

Eukitt	Sigma-Aldrich (Schnelldorf, Germany)
Fat-free dry milk	AppliChem (Darmstadt, Germany)
Fibrinogen	Sigma-Aldrich (Schnelldorf, Germany)
Fibronectin	Sigma-Aldrich (Schnelldorf, Germany)
Fluoroshield mounting medium with DAPI	Sigma-Aldrich (Schnelldorf, Germany)
GeneRuler 100 bp DNA Ladder	Fermentas (St. Leon-Rot, Germany)
Glutaraldehyde	Merck (Darmstadt, Germany)
Hematoxylin	Sigma-Aldrich (Schnelldorf, Germany)
Heparin sodium	Ratiopharm (Ulm, Germany)
Hirudin	CoaChrom Diagnostica GmbH (Maria Enzersdorf, Austria)
Horm collagen	Takeda (Linz, Austria)
IGEPAL CA-630	Roth (Karlsruhe, Germany)
Isofluran CP	cp-pharma (Burgdorf, Germany)
Isopropanol	Roth (Karlsruhe, Germany)
Midori Green DNA stain	Nippon Genetics (Düren, Germany)
Neuraminidase	Sigma-Aldrich (Schnelldorf, Germany)
Osmium tetraoxide	Merck (Darmstadt, Germany)
PageRuler prestained protein ladder	Fermentas (St. Leon-Rot, Germany)
Paraffine	Roth (Karlsruhe, Germany)
Paraformaldehyde (PFA)	Sigma-Aldrich (Schnelldorf, Germany)
Penicillin	PAN (Aidenbach, Germany)
Phalloidin-Alexa647N	Sigma-Aldrich (Schnelldorf, Germany)
Phalloidin-FITC	Enzo Life Sciences (New York, USA)
Phenol/Chloroform	Roth (Karlsruhe, Germany)
Poly-L-lysine	Sigma-Aldrich (Schnelldorf, Germany)
Prostacyclin (PGI_2)	Sigma-Aldrich (Schnelldorf, Germany)

Protease inhibitor cocktail	Sigma-Aldrich (Schnelldorf, Germany)
Proteinase K	Fermentas (St. Leon-Rot, Germany)
Rat serum	Sigma-Aldrich (Schnelldorf, Germany)
Rhodocytin	J. Eble (University Hospital Frankfurt, Germany).
Roti Lumin plus ECL solution	Roth (Karlsruhe, Germany)
Rotiphorese gel 30 acrylamide	Roth (Karlsruhe, Germany)
Sodium orthovanadate	Sigma-Aldrich (Schnelldorf, Germany)
Stem cell factor (SCF)	BioLegend (San Diego, USA)
Streptomycin	PAN (Aidenbach, Germany)
Sucrose	Roth (Karlsruhe, Germany)
Super cryo embedding medium (SCEM)	Section lab (Hiroshima, Japan)
Tannic acid	Merck (Darmstadt, Germany)
Tetramethylethylenediamine (TEMED)	Roth (Karlsruhe, Germany)
Thiazole orange	Sigma-Aldrich (Schnelldorf, Germany)
Thrombin	Roche Diagnostics (Mannheim, Germany)
Thpo (conditioned medium)	Nieswandt laboratory (Würzburg, Germany)
Triton X-100	AppliChem (Darmstadt, Germany)
Tween 20	Roth (Karlsruhe, Germany)
U46619	Enzo Lifesciences (Lörrach, Germany)
Uranyl acetate	EMS (Hatfield, USA)
Xylol	Roth (Karlsruhe, Germany)

If not stated otherwise above, all other reagents/chemicals for buffer solutions were obtained from Roth (Karlsruhe, Germany) or Sigma-Aldrich (Schnelldorf, Germany). Primers were obtained from Biomers (Ulm, Germany).

3.1.4. Primer

Table 4: List of primer used in this study.

Primer	Sequence
ADAP 5’	5’ CCG TGG GGC CAA AGT CAG GAG AA 3’
ADAP 3’	5’ CCC ACC CCA AGG TCC TTT CTT AC 3’
Neo 3’	5’ GCG CTA CCG GTG GAT GTG GAA TGT 3’
PF4_for	5’ CTC TGA CAG ATG CCA GGA CA 3’
PF4_rev	5’ TCT CTG CCC AGA TCA TCC T 3’
Pfn1_i2_f2	5’ TTC TGA CTC TGG CTC CCC AG 3’
Pfn1_i2_r2	5’ GCT AGG AAC GGC TGT GAT GC 3’

3.1.5. Antibodies

3.1.5.1. Monoclonal antibodies

Table 5: List of monoclonal antibodies used in this study.

Antigen	Clone	Isotype	Conjugate	Application	Reference/ Manufacturer
CD105 (endoglin)	MJ7/18	IgG2a	Alexa Fluor 647	Immuno-fluorescence (IF)	eBioscience, San Diego, USA
CD105 (endoglin)	MJ7/18	IgG2a	Alexa Fluor 594	IF	eBioscience, San Diego, USA
CD11b	M1/70	IgG2bκ	-	cell culture, Lin^- depletion	BioLegend (San Diego, USA)

CD16/CD32	2.4G2	IgG2b	-	blocking antibody, FC	BD Bioscience (Heidelberg, Germany)
CD3	17A2	IgG2bκ	-	cell culture, Lin^- depletion	BioLegend (San Diego, USA)
CD45R/B220	RA3-6B2	IgG2aκ	-	cell culture, Lin^- depletion	BioLegend (San Diego, USA)
CD9	96H10	-	FITC	FC	Nieswandt laboratory (Würzbrug, Germany)
CLEC-2	11E9	-	FITC	FC	Nieswandt laboratory (Würzbrug, Germany)
GPIbα-45	15E2	IgG2b	FITC	FC	Nieswandt laboratory (Würzbrug, Germany)
GPIX	56F8	IgG2b	Dylight488	FC	Nieswandt laboratory (Würzbrug, Germany)
GPIX	56F8	IgG2b	FITC	FC	Nieswandt laboratory (Würzbrug, Germany)
GPIX	56F8	IgG2b	Alexa Fluor 488	IF	Nieswandt laboratory (Würzbrug, Germany)
GPIX	56F8	IgG2b	Alexa Fluor 647	IF	Nieswandt laboratory (Würzbrug, Germany)
GPV	89H11	IgG2a	FITC	FC	Nieswandt laboratory (Würzbrug, Germany)
GPVI	98A3	IgG2a	FITC	FC	Nieswandt laboratory (Würzbrug, Germany)

Ly-6G/Ly-6C	RB6-8C5	IgG2bκ	-	cell culture, Lin$^-$ depletion	BioLegend (San Diego, USA)
P-selectin	5C8	-	FITC	FC	Nieswandt laboratory (Würzbrug, Germany)
Ter119	TER-119	IgG2bκ	-	cell culture, Lin$^-$ depletion	BioLegend (San Diego, USA)
α2	12C6	-	FITC	FC	Nieswandt laboratory (Würzbrug, Germany)
αIIbβ3	14A3	IgG2b	PE	FC	Nieswandt laboratory (Würzbrug, Germany)
αIIbβ3	14A3	IgG2b	FITC	FC	Nieswandt laboratory (Würzbrug, Germany)
αIIbβ3	5D7	IgG1	Alexa Fluor 649	FC	Nieswandt laboratory (Würzbrug, Germany)
αIIbβ3	5D7	IgG1	FITC	FC	Nieswandt laboratory (Würzbrug, Germany)
αIIbβ3	4H5	IgG2b	PE	FC	Nieswandt laboratory (Würzbrug, Germany)
α-tubulin	B-5-1-2	IgG1	Alexa Fluor 488	IF	Abcam (Cambridge, UK)
β1-integrin	(HMβ1-1)	IgG	FITC	Flow cytometry (FC)	BioLegend (San Diego, USA)
β1-integrin [active]	9EG7	IgG2a	FITC	IF	BD Bioscience (Heidelberg, Germany)

3.1.5.2. Polyclonal antibodies

Table 6: List of polyclonal antibodies used in this study.

Antigen	Host	Conjugate	Application	Reference/ Manufacture
ADAP	rabbit	-	WB, IF	Invitrogen (Karlsruhe, Germany)
Collagen type I	rabbit	-	IF	Abcam (Cambridge, UK)
GAPDH	rabbit	-	WB	Sigma-Aldrich (Schnelldorf, Germany)
GPIbα	rat	-	platelet depletion	emfret Analytics
rabbit IgG	goat	Horseradish peroxidase (HRP)	Western Blot (WB)	Cell Signaling (Denver, USA)
rabbit IgG	donkey	Cy3	IF	Invitrogen (Karlsruhe, Germany)
β1-tubulin	rabbit	-	IF	Biozol, Eching, Germany

3.1.6. Buffers and solutions

All buffers used for this thesis were prepared with H_2O from a MilliQ purification System. To adjust the pH HCl or NaOH was used.

- **CATCH buffer**

PBS	-
HEPES	25 mM
EDTA	3 mM
BSA	3.5%

- **Karnovsky fixative, pH 7.2**

Paraformaldehyde	2%
Glutaraldehyde	2.5%,
Cacodylate buffer	0.1 M

- **Cacodylate buffer, pH 7.2**

Sodium cacodylate	0.1 M

- **Dulbecco´s phosphate buffered saline (Sigma-Aldrich)**
  Endotoxin free

- **Phosphate buffered saline, pH 7.14**

NaCl	137 mM
KCl	2.7 mM
KH_2PO_4	1.5 mM
Na_2HPO_4	8.0 mM

- **Platelet buffer, pH 7.4**

Hepes	10 mM
NaCl	140 mM
KCl	3 mM

$MgCl_2$	0.5 mM
$NaHCO_3$	5 mM
Glucose	10 mM

- **Hepes-Tyrode-buffer without Ca^{2+}**

NaCl	137 mM
KCl	2.7 mM
$NaHCO_3$	12 mM
NaH_2PO_4	0.43 mM
$MgCl_2$	1 mM
HEPES	5 mM
BSA	0.35%
Glucose	1%

- **Hepes-Tyrode-buffer with Ca^{2+}**

NaCl	137 mM
KCl	2.7 mM
$NaHCO_3$	12 mM
NaH_2PO_4	0.43 mM
$CaCl_2$	2 mM
$MgCl_2$	1 mM
HEPES	5 mM
BSA	0.35%
Glucose	1%

- **Protein lysis buffer, 2x, pH 7.4**

HEPES	15 mM
NaCl	150 mM
EGTA	10 mM
Triton X-100	2%
(Protease inhibitor cocktail)	1:100

- **PHEM buffer, pH 7.2**

PIPES	60 mM
HEPES	25 mM
EGTA	10 mM
$MgSO_4$	2 mM

- **Separation gel buffer, pH 8.8**

Tris-HCl	1.5 M

- **Stacking gel buffer, pH 6.8**

Tris-HCl	0.5 M

- **SDS sample buffer, 4x reducing**

Tris-HCl	200 mM
Glycerol	40%
SDS	8%
Bromophenol blue	0.04%
β-Mercaptoethanol	20%

- **SDS PAGE buffer**

TRIS	40 mM
Glycine	0.95 mM
SDS	0.5%

- **Transfer buffer**

$NaHCO_3$	10 mM
Na_2CO_3	3 mM

- **Tris buffered saline (TBS), pH 7.3**

NaCl	137 mM
Tris-HCl	20 mM

- **Washing buffer (TBS-T)**

TBS (1x)	-
Tween 20	0.1%

- **Blocking buffer**

TBS-T	-
fat-free dry milk	5%

- **DNA-lysis buffer**

TRIS base	100 mM
EDTA	5 mM
NaCl	200 mM
SDS	0.2%
added Proteinase K	100 µg/ml

- **TAE buffer, 50x, pH 8.0**

TRIS	200 mM
Acetic acid	5.7%
EDTA	50 mM

- **Orange G, loading dye 6x**

Tris-HCl	10 mM, pH 7.6
Glycerol	60%
EDTA	60 mM
Orange G	0.15%

3.1.7. Cell culture media

- **FLC-derived MK cell culture medium**

DMEM + GlutaMAX (Gibco)	-
FCS	10%
Penicillin/streptomycin	100 U/ml

- **BM-derived MK cell culture medium**

StemPro (Gibco)	-
StemPro suppl. (40x) (Gibco)	2.6% (v/v)
Penicillin/streptomycin	100 U/ml
L-glutamine	20 mM
SCF	50 ng/ml
Thpo (conditioned)	1:1000

- **BM-derived MK cell culture medium (Lin^- depletion)**

DMEM + GlutaMAX (Gibco)	-
Penicillin/streptomycin	100 U/ml
Hirudin	100 U/ml
Thpo (conditioned)	1:1000

- **Lin^- depletion medium**

DMEM + GlutaMAX (Gibco)	-
Penicillin/streptomycin	100 U/ml

3.2. Methods

3.2.1. Molecular biology methods

3.2.1.1. Isolation and purification of murine genomic DNA from ear punches

Ear punches from mice were lysed in 500 µl DNA-lysis buffer supplemented with Proteinase K for at least 3 h at 56°C and 1400 rpm on a thermocycler. Next, the samples were mixed with 500 µl Phenol/Chloroform and centrifuged at 4°C, 14000 rpm for 10 min. The upper phase was transferred into new reaction tubes and mixed with 500 µl isopropanol. After centrifugation at 4°C, 14000 rpm for 10 min, the supernatant was discarded and pelletized DNA was washed with 70% ethanol and subsequently centrifuged at 4°C, 14000 rpm for 10 min. DNA was dried by leaving reaction tubes on on a thermocycler (40°C for 30-60 min) and solved in TE-buffer for at least 30 min. The isolated DNA was stored at -20°C.

3.2.1.2. Polymerase chain reaction (PCR) for genotyping

Genotype specific DNA-fragments were amplified form isolated murine DNA by polymerase chain reaction.

- ADAP-KO (constitutive)

Primer:

ADAP 5’

5’ CCG TGG GGC CAA AGT CAG GAG AA 3’

ADAP 3’

5’ CCC ACC CCA AGG TCC TTT CTT AC 3’

Neo 3’

5’ GCG CTA CCG GTG GAT GTG GAA TGT 3’

PCR-Mix:

1 µl	ADAP 5’ (10 pmol/µl)
1 µl	ADAP 3’ (10 pmol/µl)
1 µl	Neo 3’ (10 pmol/µl)
2.5 µl	10x DreamTaq buffer
1 µl	dNTPs (10 mM)
0.2 µl	Taq polymerase
17.3 µl	H_2O
1 µl	Template DNA
25 µl	

PCR-program

94°C	3 min	1 cycle
94°C	30 sec	35 cycles
60°C	45 sec	
72°C	1 min	
72°C	10 min	1 cycle
4°C	∞	

Expected bands

~550 bp	knock-out
~350 bp	wild-type
Both bands	heterozygous

- PF4-Cre

Primer:

PF4_for

5’ CTC TGA CAG ATG CCA GGA CA 3’

PF4_rev

5’ TCT CTG CCC AGA TCA TCC T 3’

PCR-Mix:

1 µl	PF4_for (10 pmol/µl)
1 µl	PF4_rev (10 pmol/µl)
2.5 µl	10x DreamTaq buffer
1 µl	dNTPs (10 mM)
0.2 µl	Taq polymerase
18.3 µl	H_2O
1 µl	Template DNA
25 µl	

PCR-program

96°C	3 min	1 cycle
94°C	30 sec	35 cycles
60°C	30 sec	
72°C	45 sec	
72°C	3 min	1 cycle
4°C	∞	1 cycle

Expected band

~450 bp

- floxed *Pfn1* allele

Primer:

Pfn1_i2_f2

5’ TTC TGA CTC TGG CTC CCC AG 3’

Pfn1_i2_r2

5’ GCT AGG AAC GGC TGT GAT GC 3’

PCR-Mix:

1 µl	Pfn1_i2_f2 (10 pmol/µl)
1 µl	Pfn1_i2_r2 (10 pmol/µl)
2.5 µl	10x DreamTaq buffer
1 µl	dNTPs (10 mM)
0.2 µl	Taq polymerase
18.3 µl	H_2O
1 µl	Template DNA
25 µl	

PCR-program

96°C	3 min	
94°C	30 sec	35 cycles
55.5°C	30 sec	
72°C	60 sec	
72°C	5 min	
4°C	∞	

Expected band

~187 bp	wildtype *Pfn1* allele
~221 bp	floxed *Pfn1* allele

3.2.1.3. Agarose gel electrophoresis and DNA detection

PCR samples and DNA ladder were loaded on a 1.5% (w/v) agarose gel (agarose solved in TAE-buffer) containing midori green and separated in an electrical field (constant voltage: 100 V) for 30-45 min. DNA amplicons were detected in a Herolab using UV light.

3.2.2. Animals

Constitutive ADAP-deficient mice (*Adap*$^{-/-}$) were generated as described previously.[111] Conditional ADAP-deficient as well as PFN1-deficient mice were generated by intercrossing *Adap*$^{fl/fl}$ (HEPD0569_8_D07 EUCOMM European Conditional Mouse Mutagenesis Program; exon 2 flanked by loxP sites) or *Pfn1*$^{fl/fl}$ (EUCOMM, Strain ID EM:03711; exon 2 flanked by loxP sites) with mice carrying the Cre-recombinase under the platelet factor 4 (PF4) promoter.[74,119] The WASP-deficient mice as well as respective control mice were kindly provided by Theresia E.B. Stradal, Braunschweig. All mice used in this study were 6 to 14 weeks old. All animal experiments were approved by the district government of Lower Frankonia (Bezirksregierung Unterfranken).

3.2.3. Protein biochemical and immunological methods

3.2.3.1. Isolation and purification of murine platelets for *in vitro* studies

Mouse blood (>700 µl) was collected in a reaction tube containing 20 U/ml heparin in TBS, pH 7.3 (300 µl). Blood-heparin mixture was centrifuged at 800 rpm (~300 *xg*, Eppendorf centrifuge 5415C) for 5 min. Supernatant (platelet rich plasma, PRP) with little of the red phase (mainly red blood cells) was transferred into new reaction tubes containing 300 µl heparin 20 U/ml in TBS. After centrifugation at 800 rpm (~300 *xg*, Eppendorf centrifuge 5415C) for 5 min the supernatant (PRP) was transferred without red blood cells into new reaction tubes and supplemented with prostaglandin (PGI_2; final

concentration 50 nM) and apyrase (final concentration 0.02 U/ml). To wash the platelets, samples were centrifuged at 2800 rpm (~800 *xg*, Eppendorf centrifuge 5427R) for 5 min and platelet pellet was resuspended in 1 ml Tyrode`s buffer without Ca^{2+}, containing 50 nM PGI_2 and 0.02 U/ml apyrase. This washing step was repeated, and platelet count was adjusted by measuring the platelet concentration with a hematological analyzer (Sysmex KX 21N). Desired platelet concentration was adjusted by centrifugation at 2800 rpm (~800 *xg*, Eppendorf centrifuge 5427R) for 5 min and subsequent resuspension of the pellet in calculated volume with Tyrode`s buffer with or without Ca^{2+} (depending on the experiment) and with 0.02 U/ml apyrase. The washed platelets were incubated for 30 min at 37°C before they were used for experiments.

3.2.3.2. Platelet lysate

Washed platelets were adjusted to 2 x 10^6 cells per µl in Tyrode`s buffer without Ca^{2+} and BSA and lysed by adding 1:1 ready to use 2x lysis buffer containing IGEPAL CA-630, protease inhibitor cocktail and Na_2VO_3. Platelet lysates were incubated for 20 min on ice and centrifuged for 1 min at 14000 rpm. Supernatant was mixed 1:1 with 2x sample buffer (reducing conditions) and boiled for 5 min at 95°C. Samples were stored at -20°C before they were separated by electrophoresis.

3.2.3.3. Sodium dodecyl sulfate polyacrylamide gel electrophoresis (SDS-PAGE) of platelet lysates

10% sodium dodecyl sulfate polyacrylamide gels were produced and the platelet lysate samples were loaded and separated at ~15 mA per gel for about 90 min in a electrophoresis chamber containing SDS-PAGE buffer.

3.2.3.4. Immunoblotting

Platelet lysates separated by SDS-PAGE were blotted onto polyvinylidene difluoride membranes using wet blot transfer (transfer buffer; 100 V for about 75 min). Blots were blocked with 5% (w/v) milk powder in TBS-T and probed for ADAP (Invitrogen) or GAPDH (Sigma-Aldrich). Horseradish peroxidase-conjugated secondary antibodies (Cell Signaling) and enhanced chemiluminescence solution (MoBiTec) were used for visualization. Images were recorded using a MultiImage II FC Light Cabinet device. As loading control, GAPDH levels were determined.

3.2.4. Flow cytometry

For measurements of platelet glycoprotein expression, activation, reticulated platelets (thiazole orange), glycosylation (lectin binding) and phosphatidylserine (PS)-exposure on platelets, 50 µl blood was mixed with 300 µl heparin (20 U/ml) and 650 µl Tyrode`s buffer without Ca^{2+} to obtain diluted blood, which was further processed depending on the experiment.

3.2.4.1. Measurements of reticulated platelets

50 µl of diluted blood was stained with thiazole orange (1 µg/ml; Sigma-Aldrich) and phycoerythrin (PE) coupled antibodies against αIIbβ3 (1 µg/ml; clone 14A3) for 30 min at room temperature (RT). After adding 500 µl PBS, the sample was analyzed by flow cytometry on a FACS Calibur (BD Biosciences). The analysis of reticulated (thiazole orange positive) platelets in the whole platelet population (αIIbβ3 positive) was performed with FlowJo.

3.2.4.2. Detection of the ECL (*Erythrina cristagalli* Lectin) binding capacity of platelets (glycosylation)

Diluted blood was centrifuged at 2800 rpm for 5 min at RT and the cell pellet was resuspended in 1 ml Tyrode`s buffer without Ca^{2+}. 50 µl were used for resting samples and neuraminidase treated samples respectively. Neuraminidase treated samples were incubated with 2.5 µl neuraminidase (0.017 U/ml; from *Vibrio cholera*, Boehringer Mannheim) at 37°C and 400 rpm for 15 min on a thermocycler. Glycosylation was analyzed after incubation with fluorescein isothiocyanate (FITC)-conjugated *Erythrina cristagalli* Lectin (ECL) (10 µg/ml; Vector) for 20 min on a flow cytometer. In neuraminidase treated samples, signal for ECL-FITC was set to 100%.

3.2.4.3. Ca^{2+} stress-induced phosphatidyl serine (PS) exposure on platelets

Diluted blood was centrifuged at 2800 rpm for 5 min on RT and cell pellet was resuspended in 1 ml Tyrode`s buffer without $Ca^{2+}$. After repeated centrifugation at 2800 rpm for 5 min at RT, the blood cell pellet was resuspended in Tyrode`s buffer containing 4 mM $CaCl_2$ and stored at 37°C for 60 min. Every 15 min a 50 µl sample was incubated with DyLight649-labeled anti-αIIbβ3 antibodies (0.1 µg per sample; clone 5D7) to gate for platelets and Dylight488-conjugated Annexin V proteins (0.1 µg per sample) for 15 min to analyze PS exposure. Analyses were performed on a FACS Calibur (BD Biosciences).

3.2.4.4. Surface glycoprotein expression on platelets

50 µl of diluted blood were incubated for 15 min at RT with FITC-conjugated antibodies (2 µg/ml) directed against major platelet surface glycoproteins (GPIb, GPV, GPIX, GPVI, CLEC2, CD9, α2, β1 and αIIbβ3). After adding 500 µl PBS, each sample was analyzed by flow cytometry on a FACS Calibur (BD Biosciences).

3.2.4.5. Analysis of platelet integrin activation and P-selectin

Diluted blood was centrifuged at 2800 rpm for 5 min at RT and pellet was resuspended in 1 ml Tyrode`s without $Ca^{2+}$. To obtain washed blood, the centrifugation and resuspension step were repeated. The samples were incubated for 5 min at 37°C on a thermocycler and finally centrifuged at 2800 rpm for 5 min at RT. Cell pellets were resuspended in Tyrode`s buffer containing 2 mM $CaCl_2$ (in case of β1-integrin activation, buffer contained 1 mM $MgCl_2$ in addition). 50 µl of washed blood were incubated with specific fluorophore coupled antibodies (active αIIbβ3 integrin: 4H5-PE; active β1 integrin: 9EG7-FITC, anti-P-selectin: 5C8-FITC) and agonists (ADP, U46619 [U46, thromboxane analogue], thrombin [Thr], collagen related peptide [CRP], convulxin [CVX] and rhodocytin [Rhod]) for 7 min at RT and 7 min at 37°C. Afterwards, reaction was stopped by adding 500 µl PBS and platelet integrin activation and P-selectin exposure were analyzed by flow cytometry on a FACS Calibur (BD Biosciences).

3.2.4.6. F-actin content and assembly

Washed platelets (concentration: 500.000 plt/µl) were diluted 1:1 with Tyrode`s with Ca^{2+} (at least 100 µl: 50 µl resting + 50 µl activated sample). Platelet suspension was incubated with 10 µl Dylight-649-coupled anti-GPXI antibody derivative (clone 56F8) for 3 min at 37°C and 400 rpm on a thermocycler. Per condition, 50 µl of the sample were either incubated for 2 min at 37°C and 400 rpm on a thermocycler with different concentrations of thrombin or left unstimulated (resting condition). Platelets were fixed with 0.55 volume of the sample with 10% PFA in PHEM buffer for 10 min at 37°C and 400 rpm on a thermocycler. Fixed platelets were centrifuged at 2800 rpm for 5 min at RT and resuspended in 55 µl Tyrode`s with Ca^{2+} containing 0.1% Triton X-100. 50 µl of the sample were directly transferred into a FACS tube already containing 10 µM phalloidin-FITC and incubated for 30 min at RT in the dark. To stop the reaction, 500 µl PBS was added and the samples were centrifuged at 2800 rpm for 5 min at RT. The platelet pellet was resuspended in 500 µl PBS and the samples were incubated on ice and measured immediately by flow cytometry.

3.2.4.7. Measurements of glycoprotein expression on BM-MKs

For determination of surface glycoprotein expression on MKs and (pro)platelet-like particles, femoral BM from one mouse was flushed out in 1 ml PBS. Single cell suspensions were obtained by pipetting the BM suspension up and down using a syringe and needles with different gauge (18G, 22G, and finally 26G). The suspension was passed through a cell strainer (100 µm) into a 50 ml canonical tube to remove bone and other solid tissue parts. Unspecific binding sites were blocked with anti-CD16/CD32 antibodies (0.02 µg/µl; clone 2.4G2) for at least 20 min at RT. 200 µl/condition (single staining, double staining) of the cell suspension were incubated either with Alexa649-labeled anti-αIIbβ3 antibodies (0.1 µg per sample; clone 5D7) or with FITC-labeled specific antibodies to analyze glycoprotein expression (GPIb, GPV, GPIX, GPVI, CLEC2, αIIbβ3, α2β1 for MKs and GPIb, GPV, GPIX, αIIbβ3 for (pro)platelet-like particles) or both antibodies (anti-αIIbβ3 antibodies used as MK marker and FITC-labeled antibodies to detect the expression of glycoproteins). Analysis was performed on a FACSCelesta (BD Biosciences).

3.2.4.8. Determination of MK ploidy levels (BM-MKs and MKs in culture)

For determination of BM-MK ploidy levels, mice were sacrificed and femoral bone marrows were flushed out in 2 ml CATCH buffer. Single cell suspension was obtained by pipetting the BM suspension up and down using a syringe and needles with different gauge (18G, 22G, finally 26G). The suspension was passed through a cell strainer (100 µm) into a 50 ml canonical tube to remove bone and other solid tissue parts. For BM cell-derived MKs in culture, cells were centrifuged for 5 min at 200 *xg* at RT and washed once with 1 ml PBS. 200 µl of this suspension were used to obtain one sample per condition. The samples were centrifuged at 1200 rpm for 5 min at RT and the cell pellet was resuspended in 400 µl 1:1 mixture CATCH/PBS + 5% FCS. All samples were incubated for 15 min on ice with anti-CD16/CD32 antibodies (0.02 µg/µl; clone 2.4G2). All samples except control samples (pooled samples from each genotype without MK staining) were incubated for 20 min on ice with FITC-labeled anti-αIIbβ3 antibodies

(clone 5D7) to stain the MK population. After adding 1 ml 1:1 mixture CATCH/PBS + 5% FCS per sample and centrifugation at 1200 rpm for 5 min at RT, the cell pellet was resuspended in 250 µl PBS with 0.1% EDTA and fixed with 250 µl PBS/1% PFA per sample for 10 min on ice. To remove the fixative, cell suspension was washed with 3 ml PBS per sample and after centrifugation at 1200 rpm for 10 min the cell pellet was resuspended in 500 µl PBS/0.1% Tween for 10 min on ice to permeabilize the cells. The washing step with 3 ml PBS was repeated and the DNA was stained using propidium iodide (PI) (final concentration: 25 µg/ml) in H_2O supplemented with RNase (final concentration: 100 µg/ml) over night at 4°C in the dark. Analysis was performed on a FACS Calibur (BD Bioscience).

3.2.5. Cell culture

3.2.5.1. Fetal liver cell (FLC)-derived MKs

Pregnant ADAP-deficient and control mice were sacrificed and embryos (Day: E13.5-E14.5) were isolated. The fetal liver was removed and placed in DMEM medium containing 10% FCS, 1% streptomycin/penicillin. To obtain a single cell suspension, fetal liver cells were isolated by pipetting up and down with syringes and needles of different gauge (18G, 22G, and finally 26G). Next, cell suspension was passed through a cell strainer (70 µm) to remove connective tissue. Cell suspension was centrifuged at 200 g for 5 min at RT and cell pellet was resuspended in DMEM medium containing 10% FCS, 1% streptomycin/penicillin and Thpo (1:1000, Thpo conditioned medium). The cells were cultured for 3 days at 37°C and 5% CO_2. On day 3, the MKs were isolated via a BSA gradient. Therefore, cell suspension was added on top of the pre-warmed BSA gradient (3% BSA in PBS overlaid with 1.5% BSA in PBS) and incubated for 30 min at RT. After removing the BSA, the MK pellet was resuspended in DMEM medium containing 10% FCS, 1% streptomycin/penicillin and Thpo (1:1000 of Thpo conditioned).

3.2.5.2. Proplatelet formation of FLC-derived MKs

Analysis of proplatelet forming MKs was performed on day 4 of culture (day one after BSA gradient) in 6-well culture plates. Therefore 5 visual fields per fetal liver with a MK density of about 10 MKs per visual field were analyzed. Proplatelet forming MKs were defined as MKs with at least on (proplatelet-sized) protrusion with a clearly visible tip.

3.2.5.3. BM cell-derived MKs – culture in the presence of SCF

Mice were sacrificed and femoral BMs were flushed out in 2 ml completed StemPro medium. Single cell suspension was obtained by pipetting the BM suspension up and down using a syringe and needles with different gauge (18G, 22G, and finally 26G). The suspension was passed through a cell strainer (100 µm) into a 50 ml canonical tube to remove bone and other solid tissue parts. Cell suspension was centrifuged at 200 *xg* for 5 min at RT and the cell pellet was resuspended in complete StemPro medium supplemented with SCF (final concentration 50 ng/ml) and cultured for 2 days at 37°C and 5% CO_2. After two days, medium was replaced by fresh StemPro medium containing Thpo (1:1000, Thpo conditioned medium). After two additional cultivation days, medium was replaced with fresh StemPro medium containing only Thpo and no SCF. On day 5, a BSA gradient was performed to obtain a pure MK fraction. The MKs after BSA gradient were cultured for on additional day in complete StemPro medium containing Thpo. Analysis of MKs was on day 6 if not stated otherwise. For the analysis of the DMS (Figure 21), adhesion and spreading (Figure 22-24) of constitutive ADAP-deficient MKs, cultured MKs according to this cultivation protocol were used.

3.2.5.4. BM cell-derived MKs – Lin^- depletion and hirudin treatment

Mice were sacrificed and femoral BMs were flushed out in 2 ml Lin^- medium. Single cell suspension was obtained by pipetting the BM suspension up and down using a syringe and needles with different gauge (18G, 22G, and finally 26G). The suspension was passed through a cell strainer (100 µm) into a 50 ml canonical tube to remove bone and

other solid tissue parts. Cells were centrifuged for 7 min at 300 *xg* and cell pellet was resuspended in 1 ml Lin^- medium. 50 µl rat serum were added and incubated for 10 min at RT. After this blocking step, antibodies were added against CD11b, Ly-6G/Ly-6C, CD3, TER-119, CD45R/B220 (final concentration 3 µg/ml, Biolegend) and incubated for 1 h at RT. Magnetic beads were washed with equal amount of Lin^- medium (200 µl beads per mouse) and resuspended in 200 µl Lin^- medium. The magnetic beads were added to the cell suspension and incubated for 20 min at RT under gentle rotation. The magnetic beads together with bound cells were removed with a magnetic holder and the remaining cells were cultured in DMEM medium containing 10% FCS, 1% streptomycin/penicillin, Thpo (1:100, Thpo conditioned medium) and hirudin (100 U/ml) for 3 days (37°C, 5% CO_2). On day 3, BSA gradient was performed to remove undesired small cells and MKs were cultivated for one additional day in DMEM medium containing 10% FCS, 1% streptomycin/penicillin, Thpo (1:100, Thpo conditioned medium) and hirudin (100 U/ml). The analysis of adhesion and spreading (Figure 26) of ADAP-, PFN1- and WASP-deficient MKs, was carried out with cells obtained according to this cultivation protocol.

3.2.5.5. MK adhesion assay on ECM

Wells of a 96-well plate were coated with Horm collagen (5 µg), fibrinogen (10 µg) or fibronectin (10 µg) over night at 4°C and blocked with either StemPro medium or DMEM medium for 1 h at 37°C. 100-200 MKs were seeded per well and manually counted with a Nikon ECLIPSE TS 100 microscope (= 100% initial MK number). The cells were allowed to adhere and spread for 3 h at 37°C and 5% CO_2. After three washing steps to remove non-adhesive cells, MKs were fixed with 4% PFA in PHEM. Remaining MKs, which adhered and spread, were counted manually (= X% adherend MKs after 3 h).

3.2.6. Transmission electron microscopy (TEM)

3.2.6.1. Washed platelets – ultrastructure

To analyze platelet ultrastructure, washed platelets were fixed with a final concentration of 2.5% glutaraldehyde in 50 mM cacodylate buffer (pH 7.2). After embedding in epon 812, ultra-thin sections were generated and stained with 2% uranyl acetate and lead citrate. Images were taken on a Zeiss EM900.

3.2.6.2. Washed platelets – cytoskeleton

To prepare the cytoskeleton of resting platelets, washed platelets were spun onto poly-L-lysine (PLL)-coated coverslips, treated as previously described[74] and then sequentially incubated with 1% glutaraldehyde, 0.1% tannic acid and 0.2% uranyl acetate. Dehydration was performed by transferring samples through graded acetone. Critical point drying was done in a Leica EM CPD300. Samples were finally coated with 1.2 nm of platinum with rotation at 45°C and 3 nm of carbon at 90°C without rotation under high vacuum in a Leica EM ACE600. Replicas were floated, picked up on formvar-carbon-coated grids and examined on a Zeiss EM900.

3.2.6.3. TEM of BM MKs

For TEM of MKs, femora were prepared and the BM was fixed overnight at 4°C using Karnovsky fixative (2% PFA, 2.5% glutaraldehyde in 0.1 M cacodylate buffer). Subsequently, the samples were post-fixed with 2% osmium tetroxide in 50 mM sodium cacodylate (pH 7.2), stained with 0.5% aqueous uranyl acetate, dehydrated with a graded ethanol series and embedded in epon 812. Ultra-thin sections were stained with 2% uranyl acetate followed by lead citrate. Images were taken on a Zeiss EM900.

3.2.7. Immunofluorescence

3.2.7.1. Proplatelet forming MKs and released platelets in culture

Round coverslips (Ø18mm) were coated with PLL in a 24-well plate for 20 min at RT and covered with prewarmed 0.5 ml platelet buffer. Proplatelet forming MK culture (FLC-derived MKs day 4 of cultivation) was added and centrifuged for 4 min at 200 *xg*. Cells were fixed by adding 4% PFA in PHEM supplemented with 0.1% Triton-X-100 (final conc. 2% PFA, 0.05% Triton-X-100). After blockage with 5% BSA in PBS, α-tubulin was stained using Alexa488-conjugated anti-α-tubulin antibodies (1 µg/ml, clone B-5-1-2, Thermo Fisher). Samples were visualized with a TCS SP5 CLSM.

3.2.7.2. Cryosections

Femora were isolated, fixed for 1 h at RT (4% PFA, 5 mM sucrose in PBS), transferred into 10% sucrose in PBS and dehydrated using a graded sucrose series (10%, 20% and 30% for 24h each). Subsequently, the samples were embedded in Cryo-Gel (Section lab) and frozen at -20°C. Seven-micrometer-thick cryosections were generated using the Kawamoto method[120] and probed with Alexa488-or Alexa647-conjugated anti-GPIX antibodies (1.33 µg/ml; clone 56F8) to label platelets and MKs, Alexa647-conjugated anti-CD105 antibodies (3.33 µg/ml; MJ7/18) to stain the endothelium and FITC-conjugated anti-β1 integrin antibodies (9EG7, BD Pharmingen) to visualize active β1-integrin. For α-tubulin/β1-tubulin stainings, cryosections were treated with 0.1% Triton-X-100 in PBS to permeabilize the cells. α-tubulin was stained using Alexa488-conjugated anti-α-tubulin antibodies (1 µg/ml, clone B-5-1-2, Thermo Fisher). β1-tubulin was stained using polyclonal anti-β1-tubulin (20 µg/ml, Biozol) and Cy3-conjugated anti-rabbit IgG (Jackson immune research). Nuclei were stained using Fluoroshield with DAPI (Sigma-Aldrich). Samples were visualized with a Leica TCS SP5 and a Leica TCS SP8 confocal microscope.

3.2.7.3. Visualization of cleared whole sternum

BM vasculature was visualized by injection of Alexa594-conjugated anti-CD105 antibodies (0.4 µg per g body weight). Platelets and MKs were stained with Alexa647-conjugated anti-GPIX antibody derivatives (0.6 µg per g body weight). After *in vivo* labelling of target proteins, mice were perfusion-fixed with 4% PFA, the sternum was isolated and decalcified for 4 days in 10% EDTA. After dehydration with a methanol-series (50%, 70%, 95%, 100% methanol 30 min each; 100% methanol overnight at 4°C), the sternum was cleared by BABB solution (1 part benzyl alcohol and 2 parts benzyl benzoate) overnight as described previously.[7] Images were acquired with a Leica TCS SP8 confocal microscope.

3.2.7.4. Resting platelets

Washed platelets were fixed and permeabilized with 2% PFA and 0.1% IGEPAL CA-630 in PHEM-Buffer and immobilized on poly-L-lysine coated surface. F-actin was stained using phalloidin-Atto647N (0.075 pg/µl, Sigma-Aldrich) and α-tubulin using Alexa488-conjugated anti-α-tubulin antibodies (1 µg/ml, Thermo Fisher). ADAP was stained using anti-ADAP antibodies (20 µg/ml, PA5-20400, Invitrogen) and Cy3-conjugated goat anti-rabbit IgG (1:400, Sigma-Aldrich). Samples were visualized with a Leica TCS SP5 confocal microscope.

3.2.7.5. Demarcation membrane system of megakaryocytes

To visualize the DMS, cultured MKs (untreated or daily treated with 50 µg/ml p0p/B or IgG) were fixed and permeabilized with 4% PFA and 0.1% Triton-X-100 in PHEM-buffer and stained using phalloidin-Atto647N (0.075 pg/µl, Sigma-Aldrich) and Alexa488-conjugated anti-GPIX antibodies (1.33 µg/ml, clone 56F8). Nuclei were stained using Fluoroshield with DAPI (Sigma-Aldrich).

3.2.7.6. Cold-induced microtubule disassembly

Microtubules were depolymerized by incubation of washed platelets at 4°C for 3.5 h; reassembly was allowed by subsequent rewarming of the sample at 37°C for 30 min. Samples maintained at 4°C and 37°C, as well as rewarmed platelets were fixed and permeabilized in PHEM buffer supplemented with 1.5% PFA and 0.075% IGEPAL CA-630 and allowed to adhere to a poly-L-lysine-coated coverslip. Samples were immunostained using Alexa488-conjugated anti-α-tubulin antibodies (1 µg/ml, Thermo Fisher) and visualized using a Leica TCS SP5 confocal microscope.

3.2.7.7. Megakaryocyte spreading

In vitro cultivated BM cell-derived MKs were allowed to adhere and spread at 37°C/5% CO_2 on coverslips coated with fibrillar Horm collagen (5 µg; Takeda), non-fibrillar human collagen I (5 µg; Sigma-Aldrich), non-fibrillar human collagen IV (5 µg; Sigma-Aldrich), fibronectin (10 µg; Sigma-Aldrich) or fibrinogen (10 µg; Sigma-Aldrich) for 3 h. MK spreading was stopped by fixation and permeabilization using PHEM buffer supplemented with 4% PFA and 0.1% Triton-X-100. Samples were blocked with 5% BSA in PBS for one hour at RT. F-actin was stained using phalloidin-Atto647N (0.075 pg/µl, Sigma-Aldrich). Active β1-integrin was stained with FITC-conjugated anti-β1-integrin antibodies (9EG7, BD Pharmingen). Collagen I was stained with Rb pAb to collagen I (20 µg/ml, Abcam) and Cy3-conjugated goat anti-rabbit IgG (1:400, Sigma-Aldrich). Nuclei were stained using Fluoroshield with DAPI (Sigma-Aldrich). Visualization was performed with a Leica TCS SP8 confocal microscope (Leica Microsystems).

3.2.8. Histology of the spleen

Five-micrometer-thick sections of formalin-fixed paraffin-embedded spleens of male and female mice were prepared, deparaffinized and stained with hematoxylin and eosin. Number of MKs was analyzed with an inverted Leica DMI 4000 B microscope.

3.2.9. *In vivo* methods

3.2.9.1. Two-photon intravital microscopy

Mice of 12 weeks age were anaesthetized, and a 1-cm incision was made along the midline to expose the frontoparietal skull, while carefully avoiding damage of the bone tissue. The mouse was placed on a customized metal stage equipped with a stereotactic holder to immobilize its head. BM vasculature was visualized by injection of tetramethylrhodamine dextran (8 µg/g body weight, 2MDa, Molecular Probes) and Alexa594-conjugated anti-CD105 antibodies (0.4 µg/g body weight). Platelets and MKs were antibody stained (0.6 µg/g body weight anti-GPIX-Alexa Fluor 488). Images were acquired with a fluorescence microscope equipped with a 20x water objective (numerical aperture: 0.95) and a TriM Scope II multiphoton system (LaVision, BioTec), controlled by ImSpector Pro-V380 software (LaVision, BioTec). Emission was detected with HQ535/50-nm and ET605/70-nm filters. A tunable broad-band Ti:Sa laser (Chameleon, Coherent) was used at 760 nm to capture Alexa Fluor 488 and rhodamine dextran fluorescence. ImageJ software (NIH) was used to generate movies.

3.2.9.2. Measurement of platelet life span

Platelet life span was determined by injection of 5 µg DyLight488-labeled anti-GPIX antibody derivative (clone 56F8) into mice. Labeled platelet population was monitored over five days by daily blood collection and analysis by flow cytometry on a FACSCalibur (BD Biosciences).

3.2.9.3. Splenectomy

Platelet count of female and male mice was determined by flow cytometry before surgical splenectomy. The surgical site on anaesthetized mice was sterilely prepared and a 1-cm paramedian incision over the left upper quadrant was made. After the spleen was identified, blood supply was stopped by ligation of vascular pedicles with surgical

suture material and the spleen was removed. Wounds were closed with surgical suture material and surgical braces. Mice were monitored for two weeks regarding signs of internal bleeding and infection. After a recovery period of 6 days, platelet counts were followed for 8 days by flow cytometry.

3.2.9.4. Macrophage depletion

Anaesthetized mice were injected with clodronate-encapsulated or PBS-encapsulated liposomes (2 µl/g body weight). Platelet count was monitored for 4 days by daily blood collection and subsequent analysis by flow cytometry.

3.2.9.5. Platelet depletion

Platelets were depleted by injection of polyclonal anti-GPIb antibodies (R300, emfret Analytics, 2µg/g body weight). Platelet count recovery was monitored for eight days by daily blood drawings and determination of platelet counts by flow cytometry.

3.2.9.6. Blood count analysis by a hematological analyzer

Mice were anesthetized with isoflurane and bled from the retroorbital plexus. Blood was collected with heparinized capillaries in EDTA coated sample tubes (Sarsted, Nümbrecht) and blood parameters were analyzed by a hematological analyzer (scil Vet abc Plus+, scil animal care company GmbH, Viernheim).

3.2.10. Image processing and analysis

Adjustments of brightness/contrast and pseudo flat-field correction (cryosections: DAPI channel) of images as well as analysis of mean fluorescent intensities/number of podosomes/area of spread MKs of unmodified images were performed using ImageJ. Adjustments made were linearly applied to the whole image.

3.2.11. Data analysis

Results are mean ± s.d. from at least three independent experiments per group, if not otherwise stated. Differences between control and knockout mice were statistically analyzed using the Mann-Whitney-U test. P-values<0.05 were considered as statistically significant: *P<0.05; **P<0.01; ***P<0.001. Results with a P-value>0.05 were considered as not significant.

4. RESULTS

4.1. Characterization of ADAP-deficient mice

4.1.1. ADAP-deficient mice recapitulate the microthrombocytopenia of CARST patients

To investigate the role of ADAP in platelet production, we capitalized on constitutive (*Adap*$^{-/-}$) as well as conditional (*Adap*$^{fl/fl}$PF4-cre) ADAP knockout mice and confirmed the absence of the ADAP protein in ADAP-deficient platelets by western blot analysis, whereas we detected ADAP with an apparent molecular weight of 130 kDa in control samples (Figure 10A). Constitutive and conditional ADAP-deficient mice displayed a significantly reduced platelet count (Figure 10B, left) and mean platelet volume (MPV) in the peripheral blood compared to controls (Figure 10B, right). This observation was confirmed by analyzing the area as well as length and width of *Adap*$^{+/+}$ and *Adap*$^{-/-}$ platelets from transmission electron micrographs (Figure 10C-G), thus clearly demonstrating the microthrombocytopenia in ADAP-deficient mice. These data point to an important role of ADAP in maintaining normal peripheral platelet counts and indicate that ADAP-deficient mice recapitulate the microthrombocytopenia observed in CARST patients.

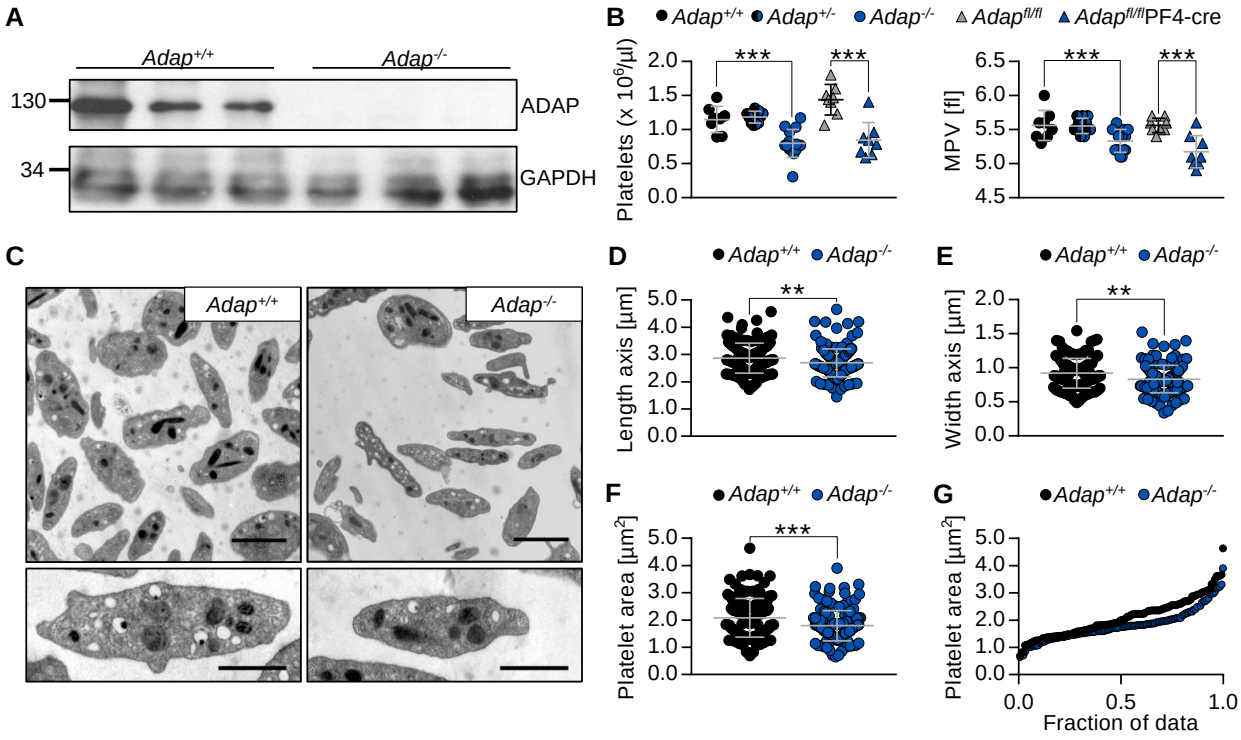

Figure 10: ADAP-deficient mice display a microthrombocytopenia. (A) Immunoblot of platelet lysates from three control and three ADAP-deficient mice. Glyceraldehyde 3-phosphate dehydrogenase (GAPDH) served as loading control. **(B)** Platelet count per microliter (left) and MPV (right) were determined from constitutive knockout mice (*Adap*$^{-/-}$, *Adap*$^{+/-}$ and control mice) as well as conditional knockout mice (*Adap*$^{fl/fl}$ and *Adap*$^{fl/fl}$PF4-cre) using a hematology analyzer. Values are mean ± standard deviation (s.d.; n ≥ 8) ***P<.001. **(C)** Transmission electron micrographs from *Adap*$^{+/+}$ and *Adap*$^{-/-}$ platelets; scale bars represent 2 µm (top panel) and 1 µm (bottom panel). Determination of platelet length **(D)**, platelet width **(E)**, platelet area **(F)** and area distribution **(G)** of control and *Adap*$^{-/-}$ platelets. (**D-G**) Analyses are based on transmission electron micrographs **(C)**. Values are mean ± s.d. (at least 126 platelets per genotype were analyzed). ***P<.001; **P<.01.

4.1.2. Lack of ADAP in platelets leads to mildly impaired integrin activation and P-selectin exposure

Platelets from CARST patients display a higher basal expression of P-selectin and αIIbβ3 integrin activation, whereas stimulation with ADP leads to reduced P-selectin exposure and integrin activation compared to control samples.[48] However, we could not detect preactivated platelets in ADAP-deficient mice under resting conditions measured by P-selectin exposure and the level of active αIIbβ3- as well as β1-integrins with

specific antibodies in flow cytometry (Figure 11A) which is in agreement with the literature.[115] Upon platelet activation with commonly used agonists, ADAP-deficient platelets exhibited mildly reduced integrin activation (αIIbβ3 and β1 integrins) as well as diminished P-selectin exposure (Figure 11A). Glycoprotein surface expression analysis from control and mutant platelets revealed an unaltered copy number of αIIbβ3, GPVI and CLEC2 and an overall mildly reduced expression of GPIb, GPV, GPIX, α2, β1 as well as CD9, which is probably due to the smaller sized platelets (Figure 11B). In addition, the number of α– and δ-granules in mutant platelets was unaltered, based on analysis of transmission electron micrographs (Figure 11C), excluding reduced granule numbers to account for the observed P-selectin exposure defect. However, we did not analyze the content of granules in further detail. From these observations we conclude that the lack of ADAP moderately impairs integrin activation and P-selectin exposure in mutant platelets and mildly affects the expression of certain glycoproteins.

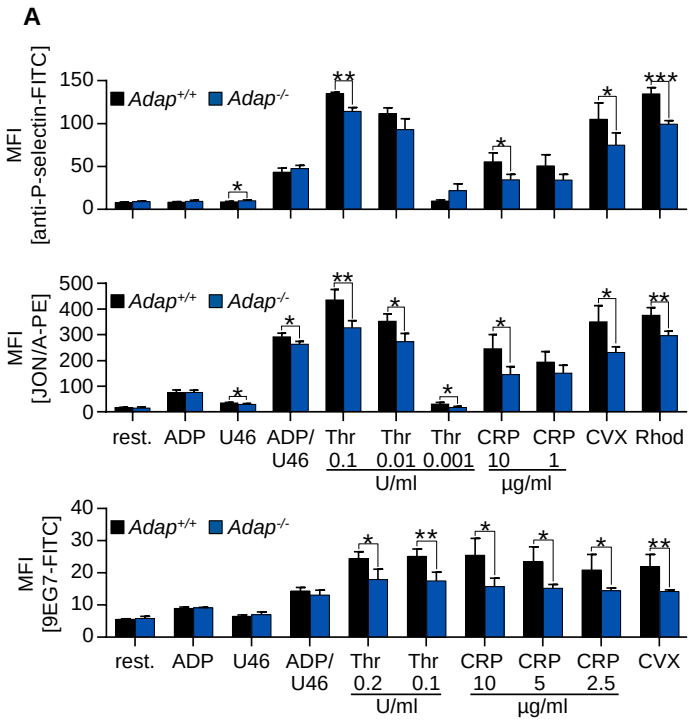

B

	Adap$^{+/+}$	*Adap*$^{-/-}$	*Significance*
GPIb	333.8 ± 5.8	247.8 ± 7.3	***
GPV	228.4 ± 7.2	184.2 ± 5.5	***
GPIX	392.8 ± 3.9	326.8 ± 9.6	***
GPVI	41.8 ± 0.4	42.0 ± 2.0	N.S.
α2	43.6 ± 1.9	40.2 ± 1.1	*
β1	146.8 ± 1.3	139.4 ± 2.5	**
αIIbβ3	461.4 ± 8.6	446.6 ± 27.2	N.S.
CD9	809.0 ± 12.7	704.6 ± 20.5	***
CLEC2	110.0 ± 7.3	101.8 ± 2.9	N.S.

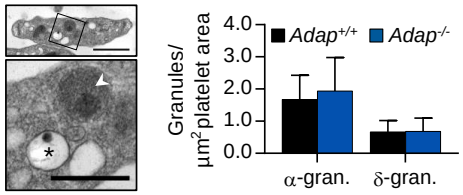

Figure 11: Slightly reduced glycoprotein surface expression and activation of ADAP-deficient platelets. (A) Determination of P-selectin exposure (upper panel), αIIbβ3 integrin activation (middle panel) and β1-integrin activation (lower panel) on the surface of resting platelets and upon stimulation with ADP, U46619 (U46, thromboxane analogue), thrombin (Thr), collagen related peptide (CRP), convulxin (CVX) and rhodocytin (Rhod) with specific antibodies. **(B)** Surface expression of major platelet glycoproteins measured by flow cytometry. **(A,B)** Values are mean ± s.d., n ≥ 4. ***P<.001; **P<.01; *P<.05; N.S. P>.05.

(C) Transmission electron micrographs of a control platelet showing clearly distinguishable α-graunles (white arrow head) and δ-granules (black asterisk); scale bars represent 1 µm (top panel) and 0.5 µm (bottom panel). Number of α– and δ–granules per μm^2 platelet area. Values are mean ± s.d. (n ≥ 126 platelets per genotype were analyzed).

4.1.3. ADAP is associated with the F-actin cytoskeleton

The size and shape of a cell is mainly determined by the cytoskeleton and terminal platelet sizing occurs in the bloodstream by conversion of barbell-shaped proplatelets into final platelets, a process regulated by the diameter and thickness of the peripheral marginal band (reviewed in Thon and Italiano[25]). Bender and colleagues could recently show that PFN1-deficient mice display a microthrombocytopenia and exhibit increased numbers of microtubules in the marginal band, which are cold- as well as colchicine-resistant, suggesting a correlation between increased microtubule stability and smaller-sized platelets.[74] To test whether this phenomenon also accounts for the observed microthrombocytopenia in ADAP-deficient mice, we analyzed the number of microtubules in the marginal band of ADAP-deficient platelets in transmission electron micrographs and observed no differences compared to control platelets (Figure 12A). Furthermore, the cold-induced disassembly of microtubules in the marginal band of *Adap*$^{-/-}$ platelets as well as the ability of the platelets to reassemble their microtubules and regain their original size was comparable to controls (Figure 12B,C,D). These data suggest, that increased cold-resistance of microtubule (cold-stable microtubules) is not the cause for the reduced platelet size in ADAP-deficient platelets.

ADAP can interact with actin-regulatory proteins in T-cells (reviewed in Wang and Rudd[101], Comrie and Burkhardt[112]) and it was shown that ADAP localizes to actin-rich structures, in which also other actin-regulatory proteins localize in murine platelets under flow[116] as well as in human platelets on fibrinogen under static conditions.[121] In line with this, we found, by using confocal microscopy, that ADAP in control platelets is rather associated with F-actin than with microtubules under resting conditions (Figure 12E). Ultrastructural analysis of mutant resting platelets revealed a partly fragmented and incomplete F-actin network, indicating a role for ADAP in F-actin dynamics and

maintenance of F-actin structures under steady state conditions (Figure 12F). Flow cytometric analysis of fixed platelets revealed a normal F-actin content under resting conditions, whereas after platelet activation with low doses of thrombin we detected a mild decrease of F-actin content in mutant platelets (Figure 12G), indicating only minor consequences of ADAP deficiency for F-actin dynamics under stimulating conditions.

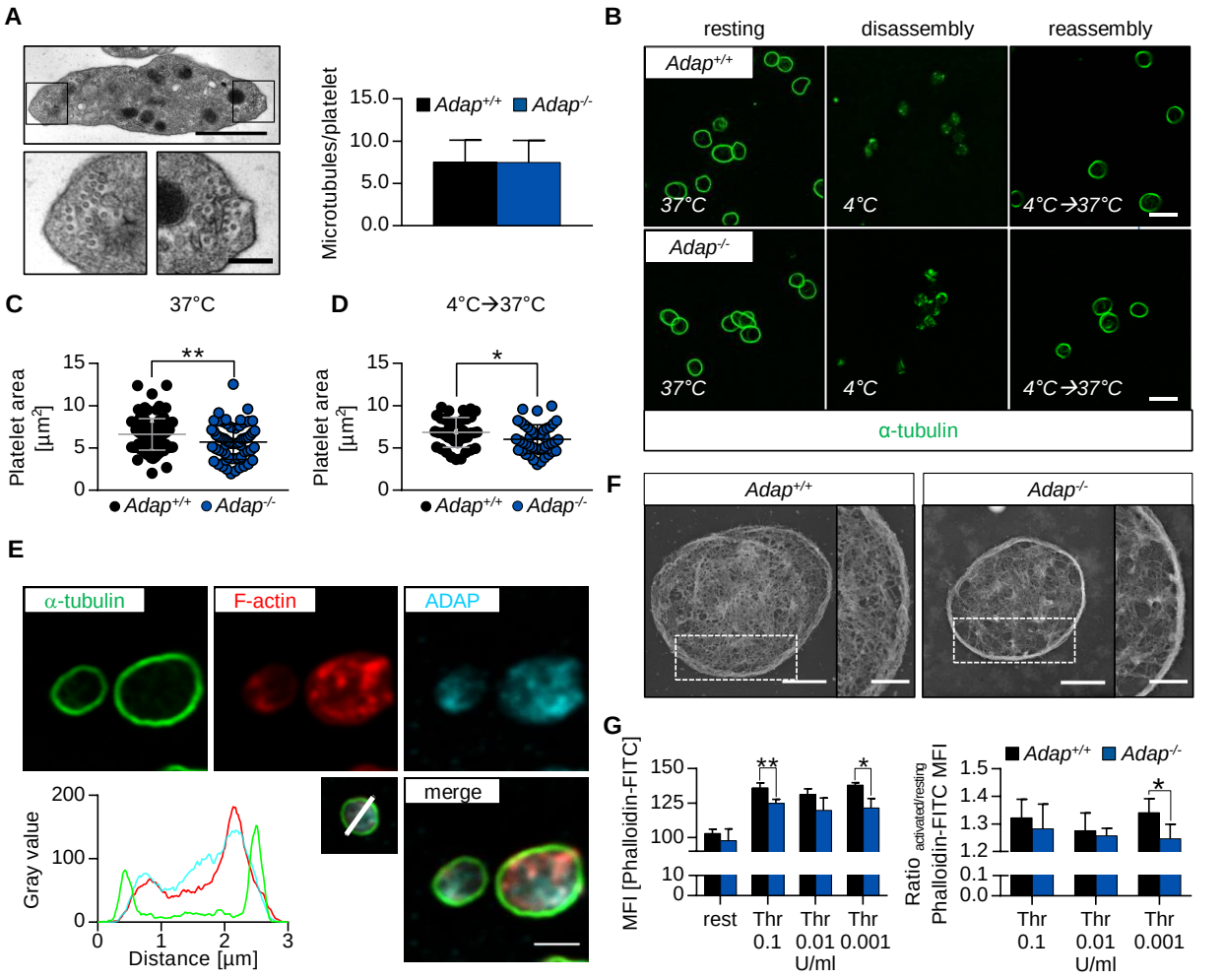

Figure 12: ADAP deficiency affects the F-actin cytoskeleton, but not microtubules. (A) Representative transmission electron micrographs of a control platelet (left) and quantitative analysis of microtubule number per platelet in the marginal band (right) based on transmission electron micrographs. Values are mean ± s.d. (n ≥ 87 platelets per genotype were analyzed). Microtubules are visible as rings at the end; scale bars represent 1 µm (top panel) and 200 nm (bottom panel). **(B)** Representative confocal microscopy images of immunostained resting platelets on poly-L-lysine (PLL). Washed platelets were fixed either after 3.5 h at 37°C (resting), after 3.5 h at 4°C (disassembly) or after 3.5 h at 4°C followed by 30 min at 37°C (reassembly). Scale bar represents 5 µm. Platelet area of control and *Adap*$^{-/-}$ platelets under resting conditions **(C)** and after reassembly **(D)** based on α-tubulin staining in **(B)**; n ≥ 39 platelets per genotype were analyzed. Values are mean ± s.d.**P<.01; *P<.05. **(E)** ADAP localization in resting control platelets was assessed by confocal microcopy; scale bar represents 2 µm. Line plot histogram of

the marked platelet in the upper right corner of the graph. **(F)** Images of the platelet cytoskeleton ultrastructure on PLL. Scale bars represent 1 µm (overview, left) and 0.5 µm (inset, right). **(G)** F-actin content under resting conditions and upon stimulation with 0.1, 0.01 and 0.001 U/ml thrombin (Thr) was assessed by measuring the mean fluorescence intensity (MFI) of bound FITC-labeled phalloidin in flow cytometry (left). Ratio of MFI of activated vs. resting samples reflecting F-actin polymerization rates (right). Values are mean ± s.d. (n=4). **P<.01; *P<.05.

4.1.4. Faster clearance of ADAP-deficient platelets is macrophage-driven

Low platelet counts can be caused by an increased platelet clearance on the one hand or on the other hand by an impaired platelet production. To test, whether an accelerated platelet turnover is the cause for the observed thrombocytopenia in ADAP-deficient mice, we analyzed platelet life span by flow cytometry and detected a decrease in the labeled platelet population in constitutive as well as in conditional ADAP-deficient mice already after 24 h, which was consistent over 5 days, indicating enhanced removal of platelets from the circulation (Figure 13A). This resulted in a reduced platelet half life span (*Adap*$^{+/+}$ t½: 41.3 ± 2.3 h vs. *Adap*$^{-/-}$ t½: 29.3 ± 2.9 h and *Adap*$^{fl/fl}$ t½: 40.6 ± 2.6 h vs. *Adap*$^{fl/fl}$PF4-cre t½: 31.2 ± 2.8 h). In contrast to CARST patients,[48] flow cytometric analysis of αIIbβ3 activation under resting conditions and after stimulation with epinephrine, adenosine 5'-diphosphate (ADP), or the thromboxane analog U46619 (U46) revealed no preactivated platelets in ADAP-deficient mice (Figure 13B, Figure 11A). Although the spleen can function as a site of platelet sequestration and subsequent removal, we observed no splenomegaly and only a moderate increase in MK numbers in spleens of mutant mice (Figure 13C,D). Of note, splenectomy in control and knockout mice had no long-term effects on platelet counts (Figure 13E). Since the platelet life span is also determined by a continuous loss of sialic acids from surface-exposed glycoproteins, which triggers platelet removal by interaction of exposed galactose residues with the hepatic Ashwell-Morell receptor,[122] we analyzed platelet desialylation by flow cytometry. Platelets from *Adap*$^{-/-}$ mice displayed a small, but significant decrease in *Erythrina cristagalli lectin* (ECL) binding to exposed galactose (Figure 13F). However, the ratio of platelets treated with neuraminidase (100% desialylation) vs. untreated ones was comparable between control and knockout

samples (Figure 13G), indicating no major alteration in terminal galactose levels. Of note, the proportion of circulating young, reticulated (RNA rich) platelets in blood samples of ADAP-deficient mice stained with thiazole orange was not increased, but rather decreased, strongly suggesting that the increased clearing occurred independent of platelet age (Figure 13H). Moreover, ADAP-deficient platelets displayed an increased tendency of Ca^{2+} stress-induced phosphatidylserine (PS) exposure during storage *in vitro* (Figure 13I). Interestingly, macrophage depletion in constitutive and conditional ADAP-deficient mice resulted in a continuous increase of the platelet count almost reaching control levels after 4 days (Figure 13J,K). These data suggest that the increased clearance of platelets in ADAP-deficient mice is mainly triggered by increased PS exposure on platelets, which may lead to enhanced clearing by macrophages similar to observations made in microthrombocytopenic ARPC2-deficient mice.[123]

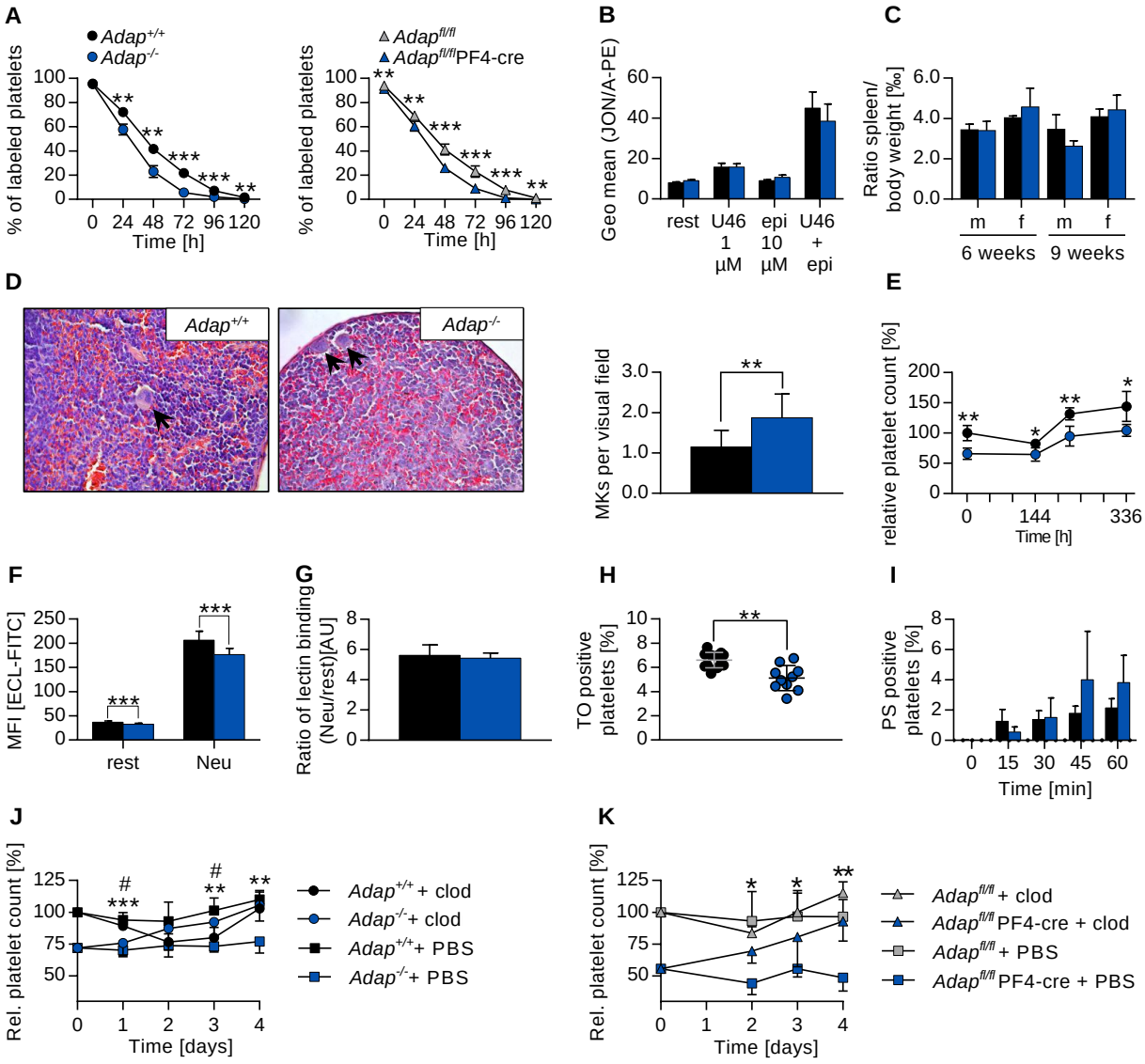

Figure 13: ADAP-deficient platelets display a reduced platelet life span and are removed from the circulation by macrophages. (A) Platelet life span of constitutive (left) and conditional (right) mice was analyzed by injection of a Dylight488 anti-GPIX antibody. The fluorescently labeled platelet population was measured over 5 days by flow cytometry. **(B)** αIIbβ3-integrin activation was analyzed by JON/A-PE binding under resting (rest) conditions and upon stimulation with 1 µM U46619 (U46; thromboxane analogue), 10 µM epinephrine (epi) alone and in combination. **(C)** Ratio of spleen to body weight. Six weeks or nine weeks old male and female mice were analyzed. Values are mean ± s.d. (n ≥ 3). **(D)** Representative images of hematoxylin and eosin stained paraffin embedded histological sections from spleens of *Adap*$^{+/+}$ and *Adap*$^{-/-}$ mice (left). MKs are marked with arrows. Quantitative analysis of the MK number per visual field in the spleen of control and ADAP-deficient mice. 20 images from one section of one spleen were analyzed; 12 spleens per genotype were analyzed. Values are mean ± s.d. **P<.01. Relative platelet count was determined after splenectomy **(E)** or macrophage depletion using clodronate (clod) **(J,K)** by flow cytometry. * significance between control groups; # significance between macrophage depletion groups. **(F)** Desialylation of *Adap*$^{+/+}$ and *Adap*$^{-/-}$ platelets in washed blood was determined by assessing FITC-labeled ECL binding by flow cytometry. Platelets were treated with neuraminidase (Neu) or left untreated (rest). **(G)** Ratio of lectin binding between neuraminidase treated and untreated samples.

(H) Reticulated platelets were determined by thiazole orange (TO) staining and analyzed by flow cytometry. Values are mean ± s.d. (n = 10-12). **P<.01. **(I)** Percentage of PS-positive platelets in whole blood was determined by DyLight488-conjugated Annexin-V-binding using flow cytometry. (n = 4).

4.1.5. *Adap*$^{-/-}$ MKs release (pro)platelet-like particles ectopically into the BM

The observed reduced platelet life span may in part explain the reduced platelet count in ADAP-deficient mice. However, we were interested, whether an additional platelet production defect accounts for the thrombocytopenia in *Adap*$^{-/-}$ mice. Therefore, we analyzed the capacity of platelet production in a model of antibody-mediated platelet depletion in order to synchronize platelet biogenesis, thereby increasing the population of young platelets in the circulation. Determining the kinetics of platelet recovery over 7 days after platelet depletion, we could not detect any differences between ADAP-deficient and control mice (Figure 14A). These results suggest that ADAP is required for normal platelet production at steady state *in vivo,* but not under conditions of acute elevated platelet demand. In addition, we analyzed the capability for proplatelet formation of fetal liver cell (FLC)-derived MKs from ADAP-deficient and control mice in culture under static conditions and could not observe any defects (Figure 14B). Interestingly, released platelets from ADAP-deficient MKs were also smaller, whereas tips of barbell-shaped proplatelets were increased in size (Figure 14C), strongly suggesting that a shear-independent, MK intrinsic mechanism leads to smaller-sized platelets in the circulation of ADAP-deficient mice.

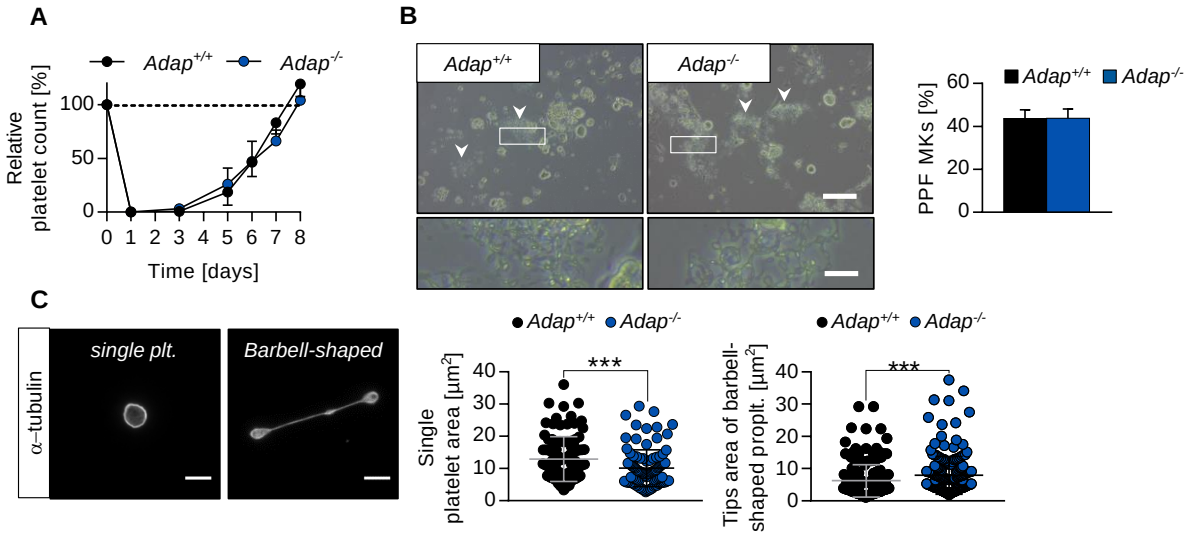

Figure 14: Normal platelet production capacity in ADAP-deficient mice under elevated platelet need and *in vitro* under static conditions. (A) Platelet count recovery after antibody-mediated platelet depletion was measured by flow cytometry over eight days. Values are mean ± s.d. (n = 6). **(B)** Representative images of FLC-derived MKs on day 4 in culture (left). Scale bars represent 100 µm (upper panel) and 20 µm (lower panel); white arrow heads point to proplatelet forming MKs. Relative quantitative analysis of proplatelet forming (PPF) FLC-derived MKs on day 4 in culture (right). Values are mean ± s.d. n = 11 per genotype. **(C)** Area analysis of single and barbell-shaped platelets produced under static conditions *in vitro* on day 4 of cultivation. The area was determined measuring the marginal band based on α-tubulin staining; scale bar represents 5 µm. Values are mean ± s.d., 100 single and barbell-shaped platelets per genotype were analyzed. ***P<.001.

Next, we analyzed the native BM from ADAP-deficient mice as major site of platelet production by confocal microscopy and detected, besides morphologically normal MKs, also fragmented MKs and, strikingly, a massive accumulation of platelet-like particles in the BM compartment (Figure 15A). The number and localization of morphologically normal MKs per visual field was comparable between control and ADAP-deficient BM (Figure 15B,C). The majority of MKs were in close proximity to vessels (vessel contact: *Adap*$^{+/+}$: 54.9 ± 1.5% vs. *Adap*$^{-/-}$: 55.9 ± 10.7%; BM compartment: *Adap*$^{+/+}$: 45.1 ± 1.5% vs. *Adap*$^{-/-}$: 44.1 ± 10.7% and inside vessel lumen: *Adap*$^{+/+}$: 0.5 ± 0.9% vs. *Adap*$^{-/-}$: 0 ± 0%), which is in line with a vessel-biased MK pool.[7] Since we also observed a massive accumulation of platelet-like particles in the BM of conditional ADAP-deficient mice (Figure 15D), this phenotype is very likely driven by ADAP-deficiency in MKs and not caused by ADAP-deficiency in other hematopoietic cells.

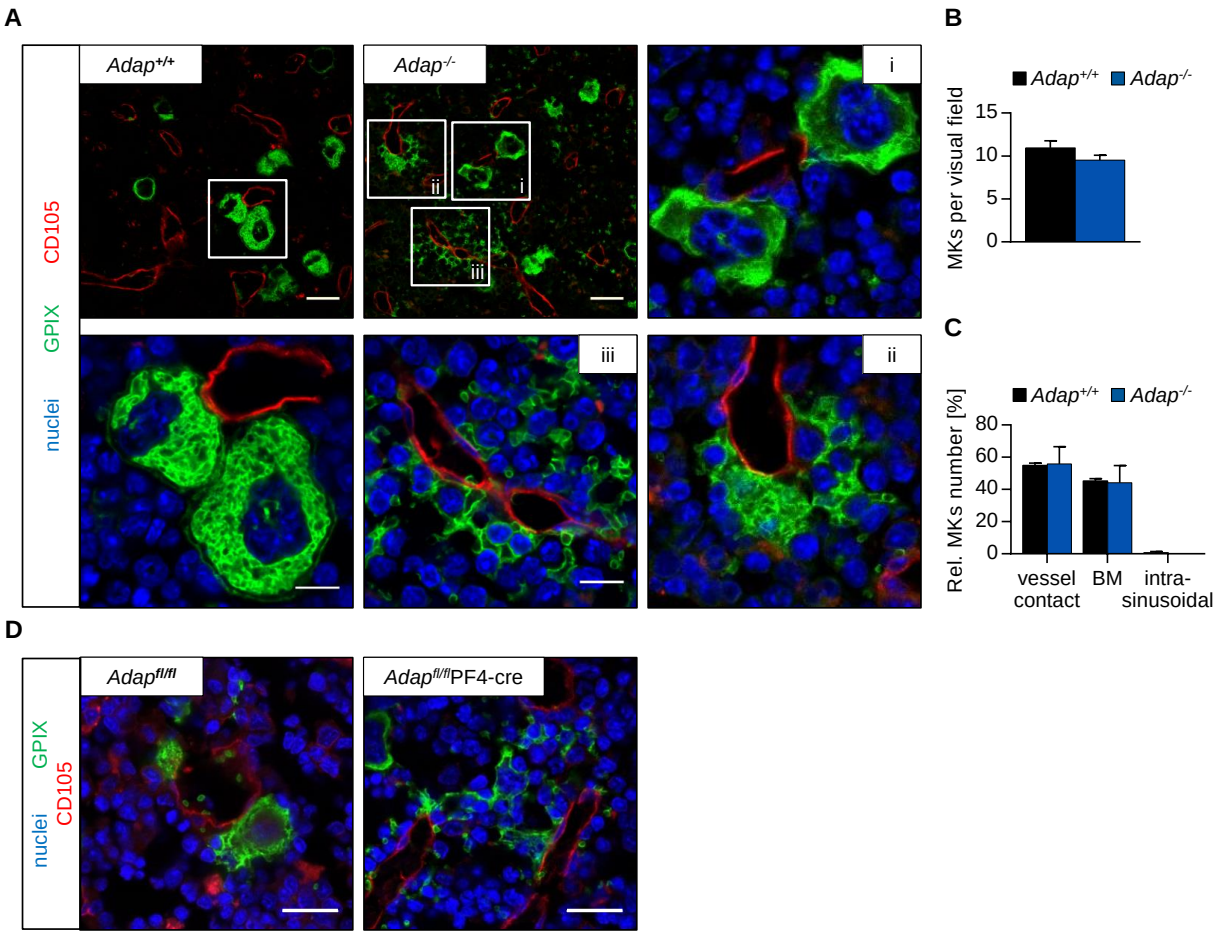

Figure 15: Detection of (pro)platelet-like particles in the BM compartment of *Adap*$^{-/-}$ mice. (A,D) Representative confocal microscopy images of immunostained cryosections from femora of control and ADAP-deficient mice (constitutive: **A** and conditional: **D**). Sinusoids are depicted in red (CD105), MKs in green (GPIX), and nuclei in blue (DAPI). Scale bars represent 30 µm and 10 µm (insets). **(B)** MK number per visual field was determined based on cryosection stainings **(A)**. **(C)** Localization of non-fragmented MKs in the BM based on cryosections in relative numbers. Three categories were defined: vessel contact (MKs with contact to sinusoids); BM (MKs in the BM compartment with no contact to sinusoids) and intrasinusoidal (MKs inside the sinusoid lumen). Values are mean ± s.d.. **(B,C)** Three cryosections per femora from each genotype (3 vs. 3 mice) and at least 5 images per cryosection were analyzed.

Quantitative analysis of BM by flow cytometry revealed a three-fold increase of αIIbβ3/GPIb/GPV/GPIX positive particles in mutant mice compared to controls, thus strongly suggesting that these fragments originated from MKs (Figure 16A). Interestingly, the size of these particles measured by the forward scatter signal (FSC) from flow cytometric analysis was increased in samples from ADAP-deficient mice

(Figure 16B). These data point to larger fragments and suggest the presence of pre- or proplatelets in BM compartment in ADAP-deficient mice.

We further analyzed the ectopically released (pro)platelet-like particles regarding the presence of a marginal band, a hallmark of platelets in circulation. To this end, we used cyrosections of ADAP-deficient and control femora and probed the sections with antibodies against α-tubulin after permeabilization. We visualized the BM in 10 µm z-stacks by confocal microcopy. The majority of the (pro)platelet-like particles (GPIX-positive particles) displayed a diffuse staining for α-tubulin, a phenomenon also observed in patients with mutations in the cytochrome c gene (Thrombocytopenia Cargeeg).[124] However, at times some (pro)platelet-like particles exhibited a marginal band comparable to control platelets in the vessel lumen (Figure 16C). Of note, we cannot exclude that all (pro)platelet-like particles display a marginal tubulin band shortly after their release into the BM and that it is quickly disassembled due to the permanent presence of collagen in the BM. Together, these data suggest that a mixture of pre-, pro- and platelets are present in the BM of ADAP-deficient mice and that some (pro)platelet-like particles exhibit a marginal tubulin band, which is a hallmark of platelets within the circulation.

To assess MK maturation, we analyzed ploidy levels as well as the expression of major glycoproteins receptors of mutant and control MKs from the BM by flow cytometry. We detected a slightly decreased percentage of >32n MKs (Figure 16D), which might be the result of fragmentation of mature MKs during sample preparation. Regarding the expression of major glycoproteins, an overall unaltered expression was found except for αIIbβ3, which was slightly reduced (Figure 16Ei+ii). Of note, we analyzed the native cells without fixation or permeabilization, therefore just the surface expression of the glycoproteins and not the internal pool was measured. From these data we conclude, that no massive maturation or expression defects of glycoproteins is responsible for the observed ectopic release of (pro)platelet-like particles into the BM compartment in ADAP-deficient mice. In summary, it can be suspected that ADAP plays a role in terminal and transendothelial proplatelet formation of mature MKs.

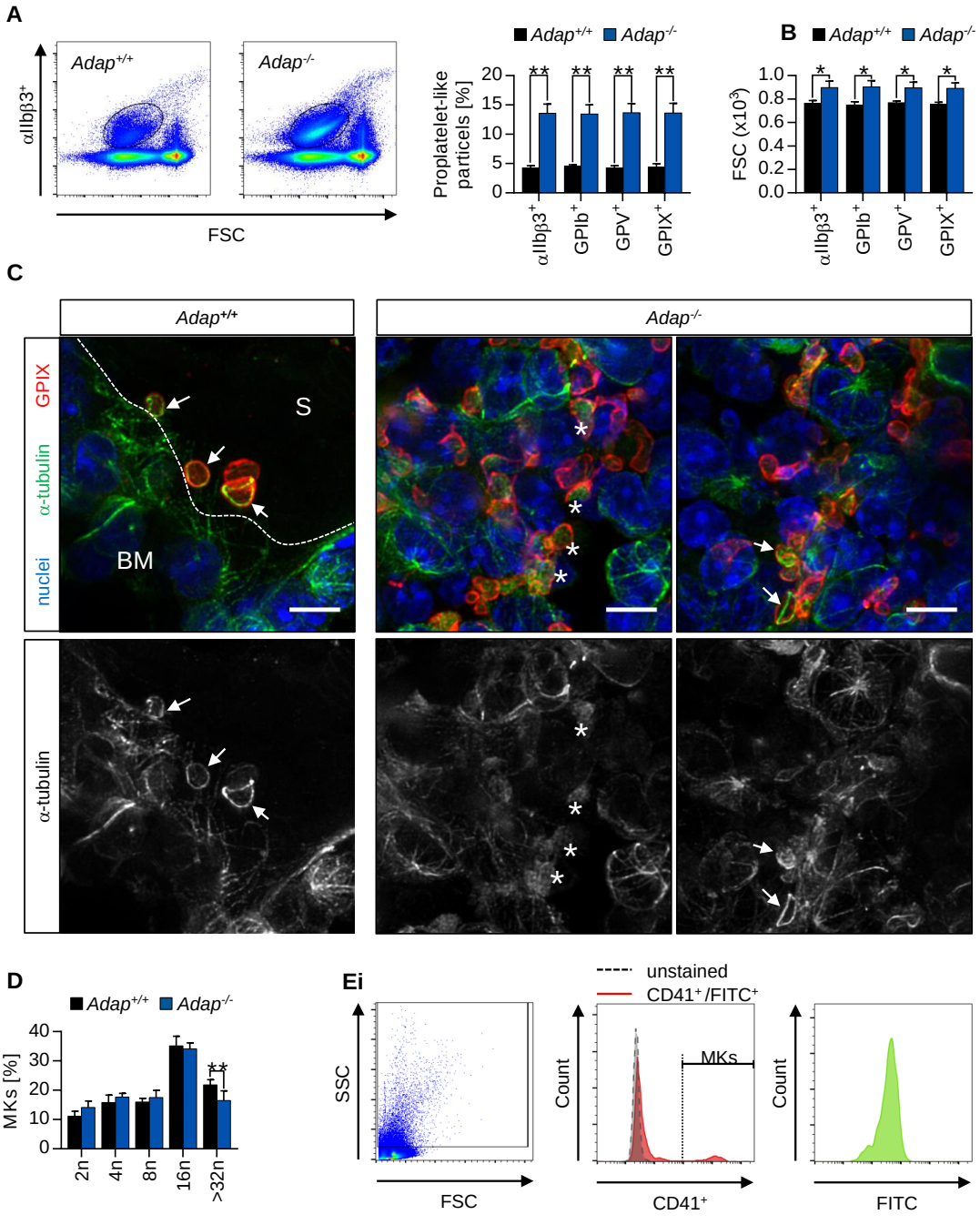

Eii

	GPIb	GPV	GPIX	GPVI	CLEC2	αIIbβ3	α2β1
Adap$^{+/+}$	314.3 ± 11.2	316.3 ± 3.21	424.3 ± 58.2	36.4 ± 1.8	266.3 ± 33.7	128.6 ± 7.6	122.0 ± 12.5
Adap$^{-/-}$	370.3 ± 39.1	341.0 ± 15.1	462.0 ± 40.1	37.0 ± 2.6	291.6 ± 24.8	109.0 ± 4.6	129.0 ± 3.0
P-value	N.S.	N.S.	N.S.	N.S.	N.S.	*	N.S.

Figure 16: (Pro)platelet-like particles in ADAP-deficient mice originate from MKs and some exhibit a marginal band. (A,B) Gating strategy (A, left) and analysis of platelet-like particles in the BM by flow cytometry using different MK markers (A, right) and forward scatter signal (B). Values are mean ± s.d. (n = 3). **P<.01; *P<.05. **(C)** Representative maximum projection of 10 µm z-stacks obtained by confocal

microscopy from femoral BM cryosections of control and ADAP-deficient mice. (Pro)platelet-like particles (red, GPIX), marginal band (green, α-tubulin) and nuclei (blue, DAPI). The border of a vascular sinus (S) is depicted as dotted line in *Adap*$^{+/+}$ cryosection. Scale bars represent 5 µm. Arrow indicates marginal band; * indicates diffuse staining of α-tubulin in ADAP-deficient mice. **(D)** Ploidy level of BM MKs was assessed by flow cytometry. Values are mean ± s.d. (n = 6; **P<.01). **(Ei)** Gating strategy of BM cells. **(Eii)** Surface expression of major glycoproteins on MKs in the BM measured with FITC-labeled specific antibodies by flow cytometry. Values are mean ± s.d. *P<.05.

A role of ADAP in transendothelial proplatelet formation by mature MKs is in addition supported by the fact that the (pro)platelet-like particles are positive for β1-tubulin (Figure 17), which is thought to be exclusively expressed by mature MKs and is necessary for proper platelet production. Loss of β1-tubulin in mice leads to a thrombocytopenia with spherical platelets in the circulation.[7,57,58] The presence of (pro)platelet-like particles (positive for β1-tubulin) strongly suggests that these particles are released by mature MKs during the terminal steps of platelet production. Interestingly, we could not observe β1-tubulin in the marginal band of ectopically released particles, whereas platelets in the circulation and proplatelets *in vitro* incorporate β1-tubulin in the marginal band.[57,125]

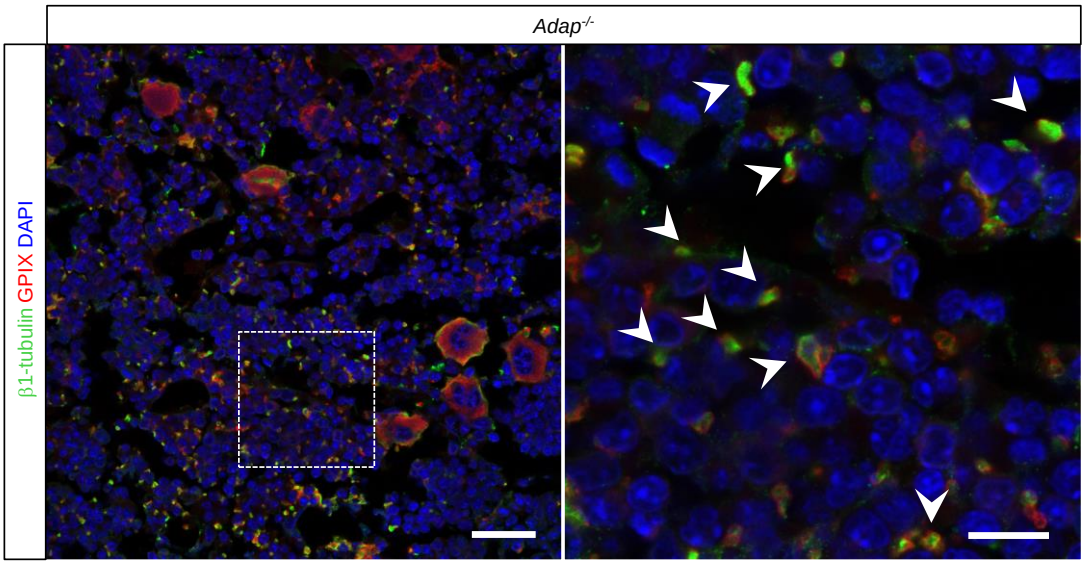

Figure 17: (Pro)platelet-like particles in BM of ADAP-deficient mice are positive for β1-tubulin. Representative images obtained by confocal microscopy from femoral BM cryosections of ADAP-deficient mice. White arrowheads point to GPIX positive (red) (pro)platelet-like particles with diffuse β1-tubulin staining (green). Scale bars represent 30 µm (left) and 10 µm (right).

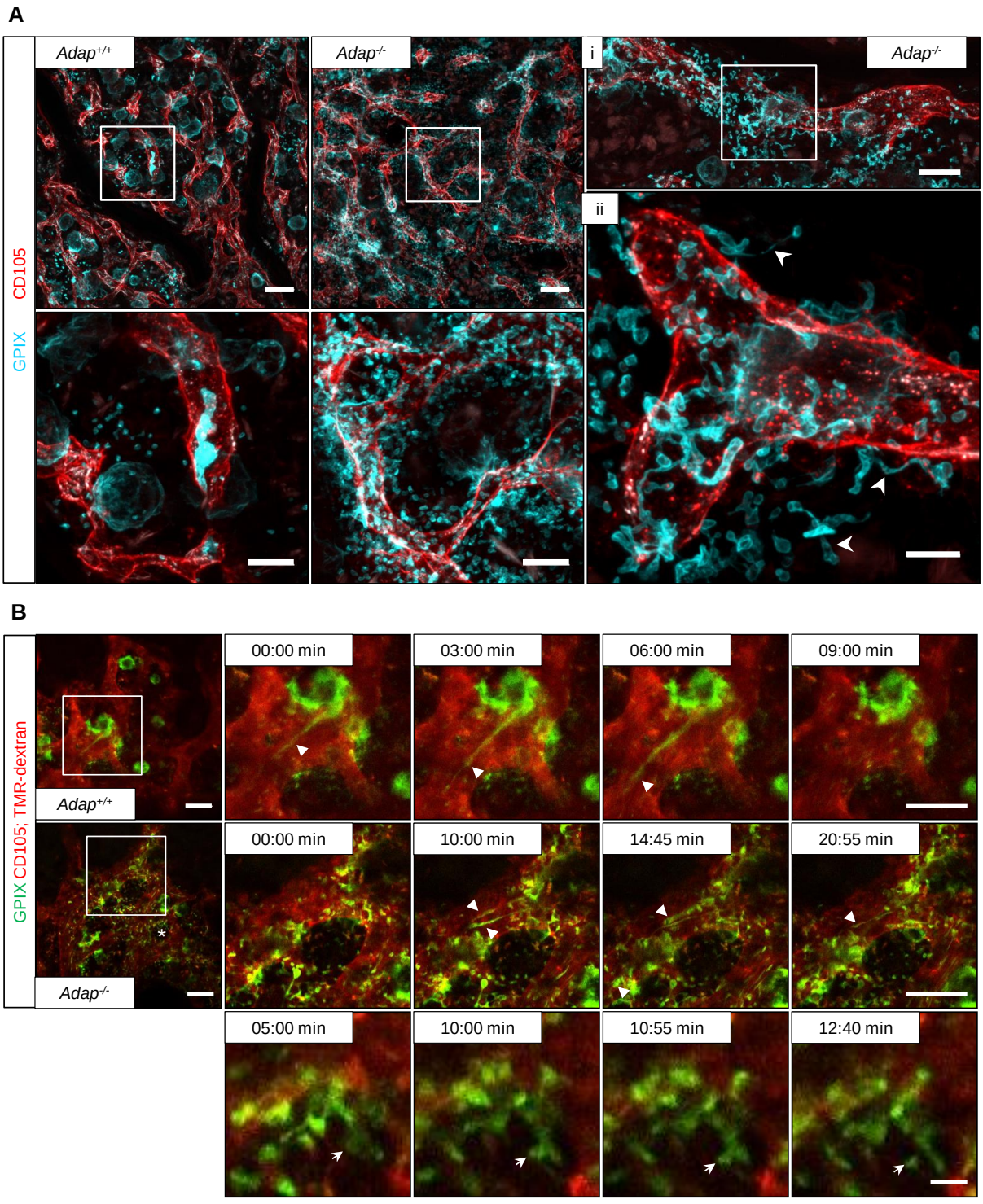

Figure 18: Release of (pro)platelet-like particles next to the vessels in ADAP-deficient mice. (A) Maximum projection of 60 µm z-stacks obtained by confocal microscopy from sternal BM of control and ADAP-deficient mice. Vessels are shown in red (CD105) and MKs in cyan (GPIX). Sternum was fixed and cleared for imaging. Scale bars represent 50 µm (top panel; left) and 20 µm (bottom panel; left). Bottom panel, digital magnification of the region marked in the top panel. **(i, ii)** Maximum projection of a 25 µm z-stack from a sternum of an ADAP-deficient mouse. Scale bars represent 30 µm (i) and 10 µm (ii). Arrowheads in (ii) point to proplatelets released into the BM compartment. **(B)** Intravital two-photon

microscopy of proplatelet formation in the skull at the indicated time points. Vessels were visualized by staining of CD105 and with tetramethylrhodamine-dextran (TMR-dextran; red); MKs/platelets are shown by GPIX staining (green). Scale bars represent 50 µm (top and middle panel) and 10 µm (bottom panel). Arrowheads point to proplatelets (top and middle panel), arrows point to platelet-like particles released into the BM compartment (bottom panel) in the region marked with an asterisk (middle panel, left).

Next, we analyzed the localization of the (pro)platelet-like particles in more detail. To this end, we stained vessels and MKs/platelets *in vivo* with respective fluorophore-coupled antibodies and cleared the whole sternum after fixation. Maximum projection of z-stacks from transparent *Adap*$^{-/-}$ sternae by confocal microcopy revealed MKs next to vessels with protrusions into the BM compartment, the accumulation of (pro)platelet-like particles next to sinusoids and the presence of barbell-shaped (pro)platelet-like fragments (Figure 18A,Ai+ii). We confirmed these data using intravital two-photon microscopy of the BM in the skull of ADAP-deficient mice, showing the release of (pro)platelet-like particles into the BM (Figure 18B). Surprisingly, intravital microscopy also revealed that ADAP-deficient MKs are in principle able to form protrusions into the vessel lumen (Figure 18B). Interestingly, we observed no obvious change in the amount of ectopically released (pro)platelet-like particles in macrophage-depleted animals on day 5 after depletion (Figure 19) neither in conditional nor constitutive ADAP-deficient mice, which could be a hint to a macrophage-independent clearing process within the BM, but further studies regarding the removal of ectopically released particles are required. Together, these data clearly demonstrate that the observed thrombocytopenia in ADAP-deficient mice is a consequence of enhanced clearing of platelets from the circulation as well as of an ectopic release of (pro)platelet-like particles into the BM compartment.

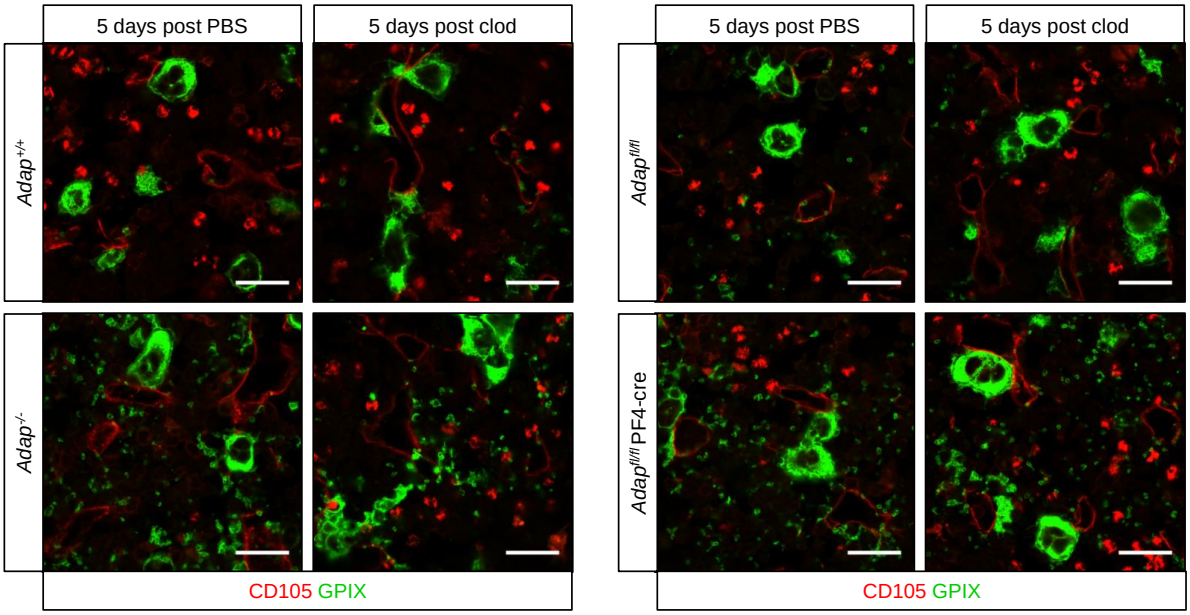

Figure 19: Ectopic release of (pro)platelet-like particles in constitutive and conditional ADAP-deficient mice persists 5 days after macrophage depletion with clodronate. Representative confocal microscopy images of immunostained cryosections from femora of control and ADAP-deficient mice 5 days after clodronate (clod) or PBS administration (constitutive: *Adap*$^{+/+}$, *Adap*$^{-/-}$; conditional: *Adap*$^{fl/fl}$, *Adap*$^{fl/fl}$PF4-cre). Sinusoids are shown in red (CD105) and MKs, (pro)platelet-like particles in green (GPIX). Scale bars represent 30 µm.

4.1.6. ADAP-deficient MKs display impaired polarization of the DMS *in vitro*

The DMS serves as a membrane reservoir for future platelets and develops during maturation of MKs. The ectopic release of (pro)platelet-like particles in the ADAP-deficient mice prompted us to examine the ultrastructure of BM MKs in these mice. Transmission electron microscopy revealed a normally developed DMS in ADAP-deficient MKs, albeit the occasional presence of MKs with a dilated DMS (Figure 20A), suggesting an abnormal anchorage of membranes to the cytoskeleton. In addition, we found fragmented MKs close to sinusoids and observed granules inside the ectopically released (pro)platelet-like particles (Figure 20B). These data point to a non-homogeneous maturation of the DMS or a defective coordination of cytoskeletal forces that drive DMS organization.

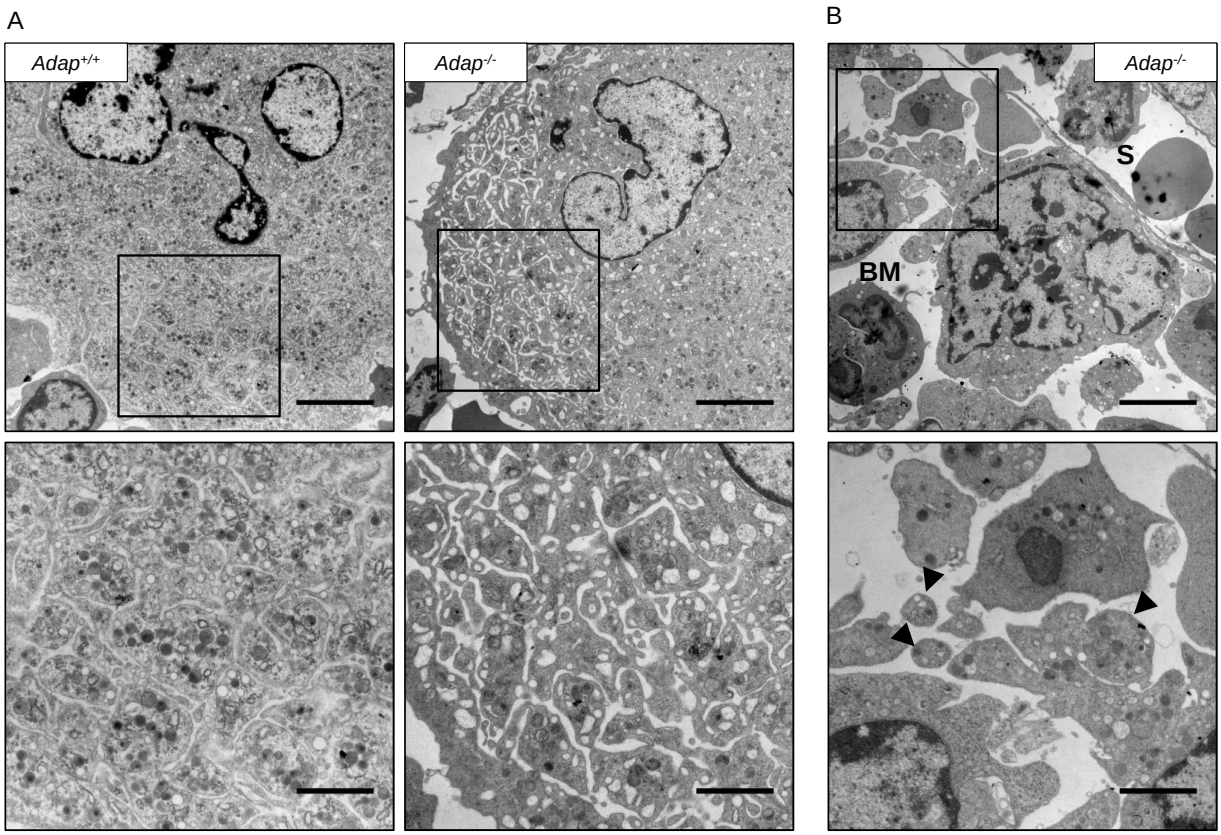

Figure 20: Defective DMS maturation of ADAP-deficient MKs *in vivo*. (A) Transmission electron micrographs from MKs with DMS in the BM of control and ADAP-deficient mice. Scale bars represent 5 µm (top panel) and 2 µm (bottom panel, inset). **(B)** Release of (pro)platelet-like particles into the BM compartment (BM) next to a sinusoid (S) (top panel). Higher magnification of released (pro)platelet-like particles (black arrowheads; bottom panel).

It has been demonstrated that the organization of the DMS relies on F-actin rearrangements necessary to polarize membranes and nuclei within MKs.[22,23] Given the involvement of ADAP for actin dynamics in platelets and coordinated proplatelet formation in the BM, we hypothesized that ADAP may influence DMS polarization. To test this, we cultured BM MKs *in vitro* (SCF treatment) and analyzed DMS polarization by confocal microscopy similar as it was described by Antkowiak and colleagues.[22] In addition, Dütting *et al*. showed that the DMS polarization in MKs is GPIb-dependent and blockade of GPIb in cultured MKs using the anti-GPIb antibody p0p/B results in reduced DMS polarization in control cells.[126] Cultured MKs from ADAP-deficient BM cells exhibited normal morphology after 5 days of culture independent of p0p/B or IgG $F(ab)_2$

treatment (Figure 21A). We classified MKs into different groups depending on the localization of the DMS (GPIX signal) and the nucleus (Figure 21B). MKs with a non-polarized DMS were grouped into class I and II, with only one peripheral signal for GPIX (class I) or more signals also between nuclear lobes (class II), whereas class III MKs displayed a polarized DMS cap on one side of the cell separated from the nucleus. Analysis of MK cultures on day 5 revealed a significant reduction of MK diameter in p0p/B-treated ADAP-deficient cultures with a polarized DMS cap (class III), whereas class I MKs were increased in size (Figure 21C, right middle). The overall MK diameter was comparable between the groups (Figure 21C, left). The polarization of the DMS in ADAP-deficient MKs was decreased on day 5 (Figure 21D, left), day 6 and 7 (Figure 21E) and p0p/B treatment showed no effect on DMS polarization under these settings (Figure 21D, middle). Of note, in contrast to Dütting *et al.*[126] we used a different MK cultivation protocol,[127] which included the cultivation of MKs from stem cell factor (SCF)-treated and -expanded HSCs. The ploidy of cultured *Adap*$^{+/+}$ and *Adap*$^{-/-}$ BM MKs was comparable (Figure 21F). Taken together, we conclude that the observed defect in DMS polarization *in vitro* is rather a consequence of defective cytoskeletal dynamics than impaired MK maturation, and that this defect might contribute to the ectopic release of (pro)platelet-like particles into the BM compartment *in vivo*.

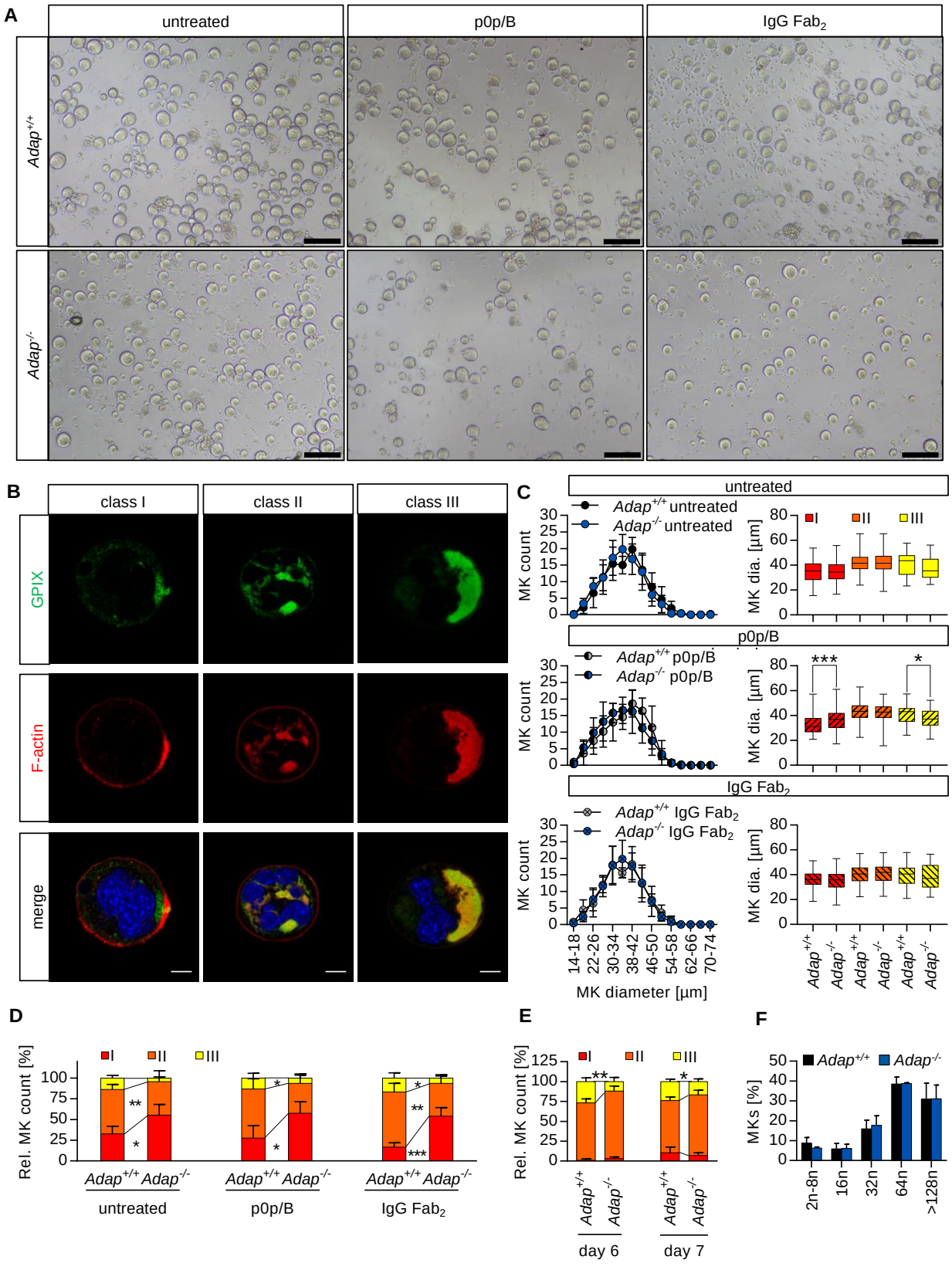
A
untreated
p0p/B
IgG Fab2
Adap+/+
Adap-/-
B
class I
class II
class III
GPIX
F-actin
merge
C
untreated
Adap+/+ untreated
Adap-/- untreated
p0p/B
Adap+/+ p0p/B
Adap-/- p0p/B
IgG Fab2
Adap+/+ IgG Fab2
Adap-/- IgG Fab2
MK count
MK dia. [µm]
MK diameter [µm]
14-18
22-26
30-34
38-42
46-50
54-58
62-66
70-74
D
Rel. MK count [%]
untreated
p0p/B
IgG Fab2
E
Rel. MK count [%]
day 6
day 7
F
MKs [%]
2n-8n
16n
32n
64n
>128n

Figure 21: Defective DMS polarization of ADAP-deficient MKs *in vitro*. (A) Representative images of MK cultures on day 5 of cultivation from control and ADAP-deficient MKs treated with p0p/B, IgG Fab_2 control or untreated. Scale bar represents 60 µm. **(B)** Representative confocal images of *Adap*$^{+/+}$ MKs cultured *in vitro* for 5 days and stained for F-actin (red), GPIX (green), and the nucleus (blue). According to the localization of GPIX and F-actin as well as the position of the nucleus three classes were defined (class I-III). Scale bar represents 10 µm. **(C)** Diameter distribution of BM-derived MKs was determined on day 5 of cultivation (left). Treatment is indicated (untreated: upper panel, p0p/B-treated: middle panel, IgG Fab_2: lower panel). Mean diameter of ADAP-deficient and control MKs of the three classes (right). **(D)** Quantitative analysis of the distribution of the 3 MK classes *in vitro* on day 5 of cultivation with or without treatment. **(C,D)** 500 MKs per genotype were analyzed. Values are mean ± s.d. (n = 5) (***P<.001; **P<.01; *P<.05). **(E)** Quantitative analysis of the distribution of the three MK classes *in vitro* on day 6 and 7 of cultivation without treatment. **(F)** Relative MK numbers of different maturation stages (ploidy) on day 6 of cultivation assessed by flow cytometry.

4.1.7. Spread *Adap*$^{-/-}$ MKs display defective F-actin organization and reduced β1-integrin activation on collagen

Podosomes have been proposed to be modulators of MK interactions with matrix proteins and to be important for proplatelet penetration through the basement membrane.[77] Podosomes consist of an actin-rich core structure and the surrounding ring is characterized by adhesion plaque proteins such as integrins and multiple adaptor proteins.[76] The stability and dynamics of podosomes were shown to be dependent on actin cytoskeletal dynamics.[77] Thus, we hypothesized that ADAP could be important for podosome formation, MK adhesion to the extracellular matrix and consequently directional proplatelet formation into the blood stream. Semeniak *et al*. showed that fibronectin, collagen IV and collagen I are present throughout the BM cavity. While collagen I is also found around larger arterioles and arteries, and subjacent to sinusoids, collagen IV is localized to basement membranes of sinusoids.[32] At first, a quantitative assessment of MK spreading on fibronectin, fibrinogen, non-fibrillar collagen I and non-fibrillar collagen IV was performed (Figure 22A). ADAP-deficient MKs displayed a reduced capacity to spread on all tested ECM proteins, reflected by a smaller spreading area (Figure 22B). These data indicate that the signaling machinery responsible for ECM recognition and F-actin dynamics is affected by the loss of ADAP. This defect is reflected by reduced F-actin content in the lowest plane of MKs spread on fibronectin and collagen I, measured by mean fluorescent intensity of Phalloidin-Atto647N (Figure

22C). In line with this, podosome formation was also reduced on these ECM proteins (Figure 22D), whereas on collagen IV and fibrinogen F-actin content and podosome density was comparable between ADAP-deficient and control MKs (Figure 22C,D).

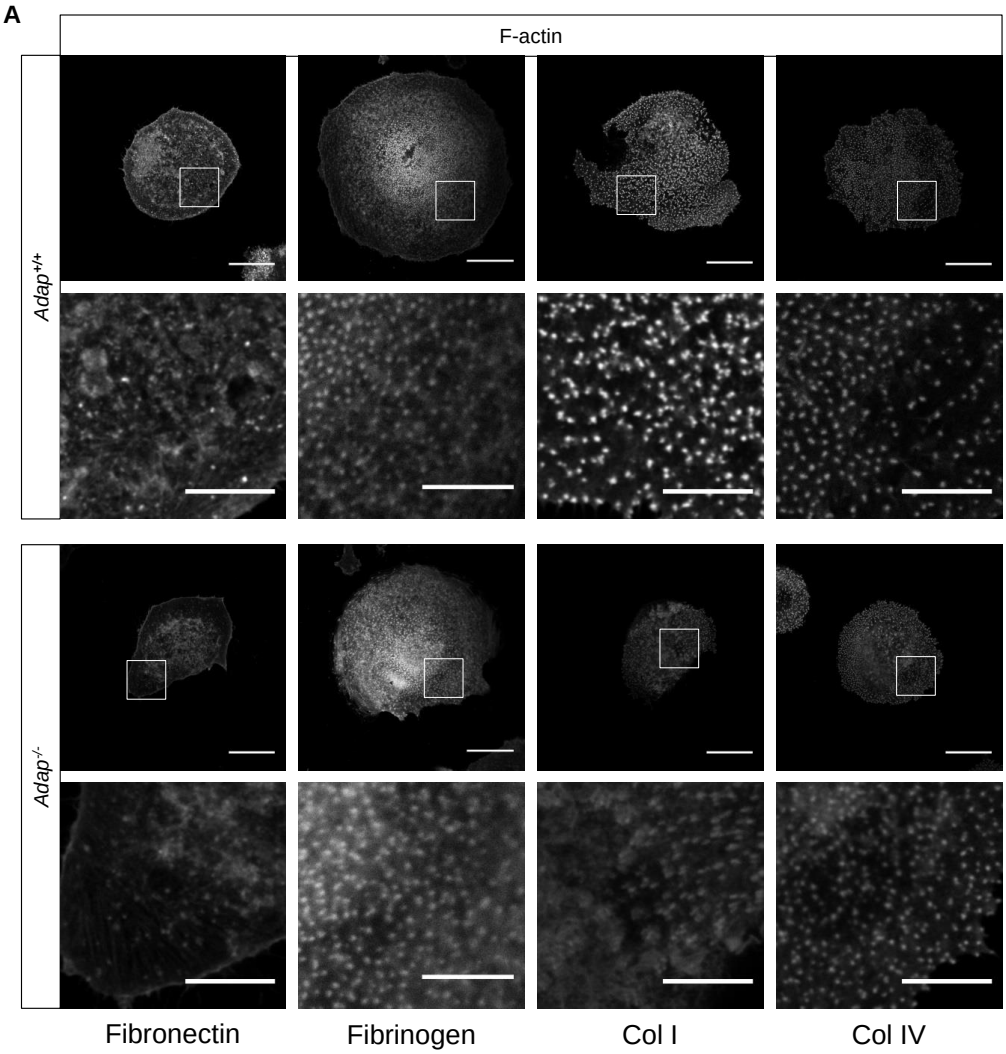
A
F-actin
Adap+/+
Adap-/-
Fibronectin
Fibrinogen
Col I
Col IV
B
Adap+/+ Adap-/-
Spread MK area [x10³µm²]
C
Normalized MFI [Phalloidin-Atto647N]
D
Normalized Podosomes/100 µm²
**
***

Figure 22: Defective F-actin organization in ADAP-deficient MKs upon spreading on collagen I and fibronectin. (A) Representative confocal images of cultured control and ADAP-deficient MKs 3h after spreading on fibronectin, fibrinogen, collagen I and collagen IV, and staining for F-actin. Scale bars represent 30 µm and 10 µm (zoom in). **(B)** Spread area, **(C)** mean fluorescence intensity of F-actin and **(D)** podosome density of ADAP-deficient and control MKs spread on fibronectin, fibrinogen, collagen I or collagen IV. **(B-D)** Analysis of images in the lowest optical section of spread MKs and normalized to the respective control. At least 50 MKs per genotype were analyzed. Each data point represents individual MK. ***P<.001; **P<.01.

Interestingly, MKs spread on Horm collagen (native type I fibrils from equine tendon) also displayed defective spreading capacity and actin polymerization as reflected by reduced spread area and a strongly decreased MFI when stained with Phalloidin-Atto647N (Figure 23A,B,C). This also translated into reduced podosome density of ADAP-deficient MKs on Horm collagen coated surfaces (Figure 23E).

The main integrins on MKs, which mediate binding to collagen and fibronectin, are α2β1- and α5β1-integrins, respectivley. Since loss of ADAP in platelets results in moderately reduced integrin activation (Figure 11A and ref.[115]), we investigated whether impaired actin arrangement in MKs causes altered integrin function. Indeed, β1-integrin activation on spread ADAP-deficient MKs was reduced as measured by MFI of fluorophore-coupled antibodies against active β1-integrin (Figure 23D). In line with this, adhesion of mutant MKs was impaired on Horm collagen (Figure 23F). In addition, approximately 60% of control MKs displayed an organized F-actin network along collagen fibers, whereas this was only seen in about 40% of ADAP-deficient MKs (Figure 24A,B). Of note, we also detected a distinct cellular staining pattern for active β1-integrin in the BM of control mice, which was reduced in ADAP-deficient BM (Figure 25). Collectively, these data show that *Adap*$^{-/-}$ MKs exhibit defective F-actin organization and impaired adhesion to the extracellular matrix protein collagen I. It further suggests that ADAP functions in MKs as an interface between integrin affinity and F-actin-dependent DMS polarization, and loss of ADAP results in ectopic, non-directional (pro)platelet release into the BM compartment.

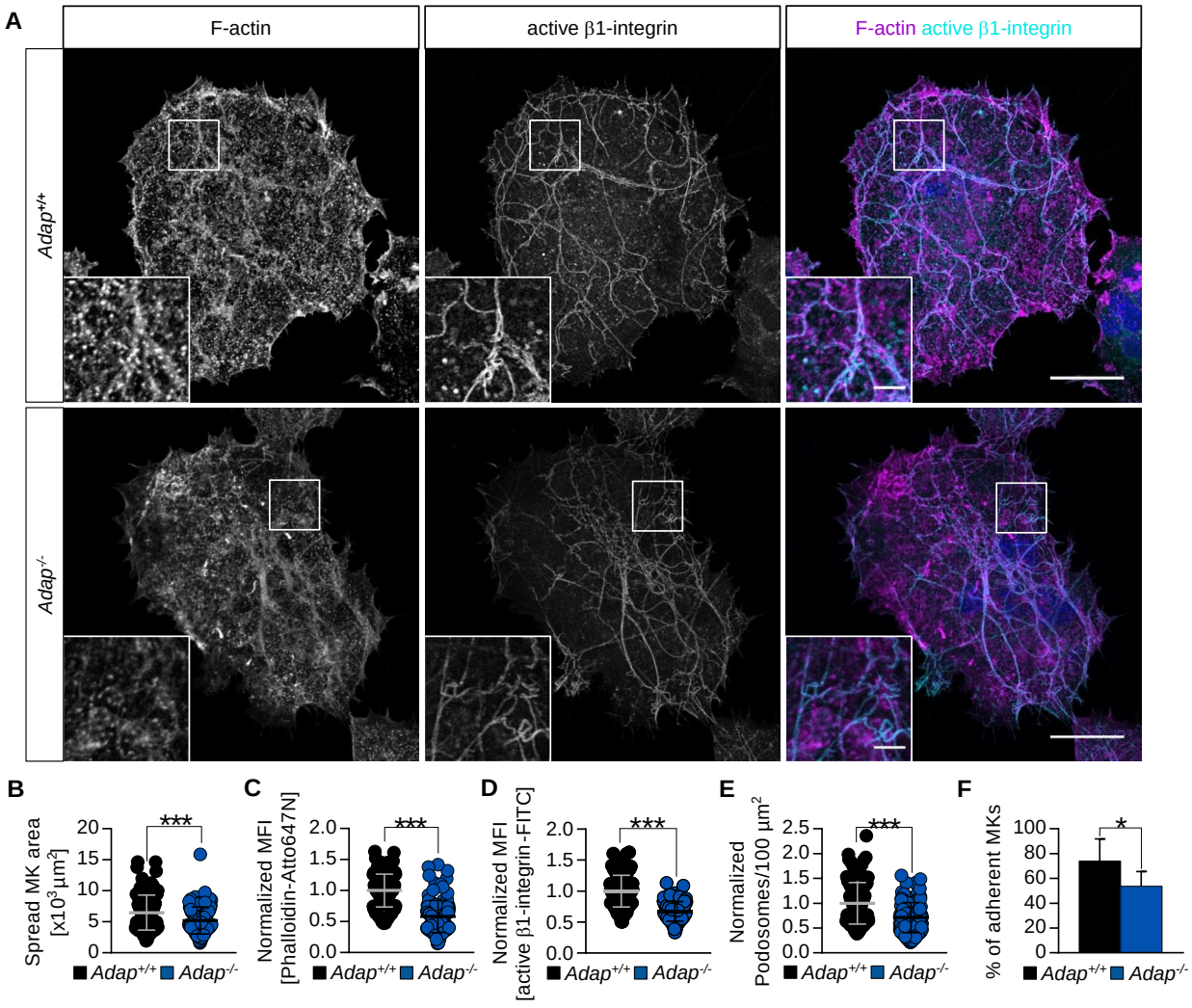

Figure 23: Defective F-actin organization and β1-integrin activation in ADAP-deficient MKs upon spreading on Horm collagen. (A) Representative confocal images of cultured control and ADAP-deficient MKs 3 h after spreading on Horm collagen and stained for F-actin and active β1-integrin. Scale bars represent 30 µm and 5 µm (inset). **(B)** Spread MK area 3 h after spreading. Mean fluorescence intensity of F-actin **(C)** and active β1-integrin **(D)** and density of podosomes **(E)** in the lowest optical section of spread MKs, normalized to respective control. **(B-E)** 100 MKs per genotype were analyzed. Data points display individual MKs. (***P<.001). **(F)** Relative adhesive MKs in percent after 3 h; representative graph from 2 independent experiments. Two biological replicates and 3 technical replicates were analyzed per experiments (*P<.05).

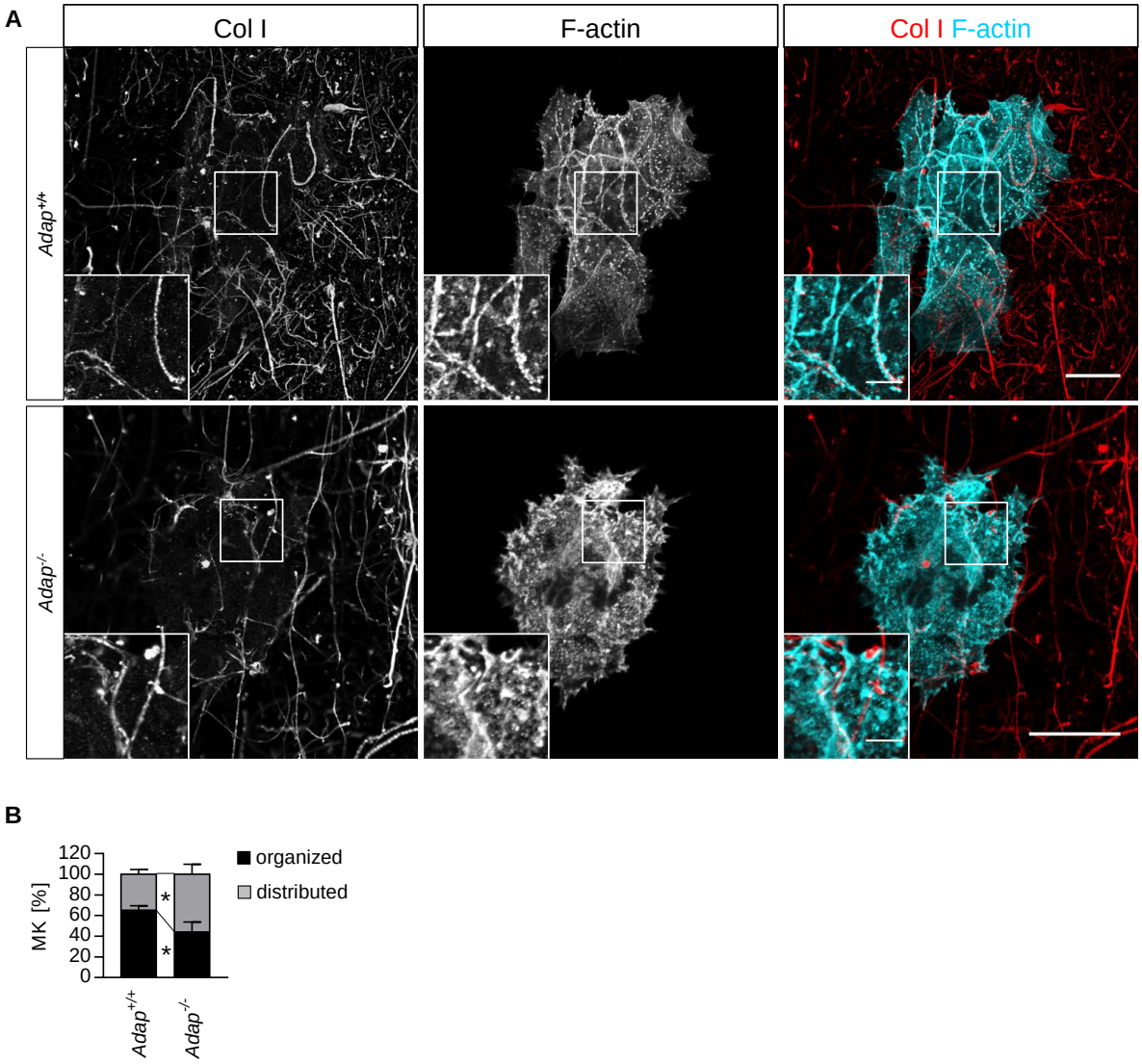

Figure 24: Altered F-actin organization in ADAP-deficient MKs. (A) Representative confocal images of cultured control and ADAP-deficient MKs 3 h after spreading on Horm collagen (Col I, red), and stained for F-actin (cyan). Scale bars represent 30 µm and 10 µm (inset). **(B)** F-actin organization along collagen fibers of spread MKs. 100 MKs per genotype were analyzed.

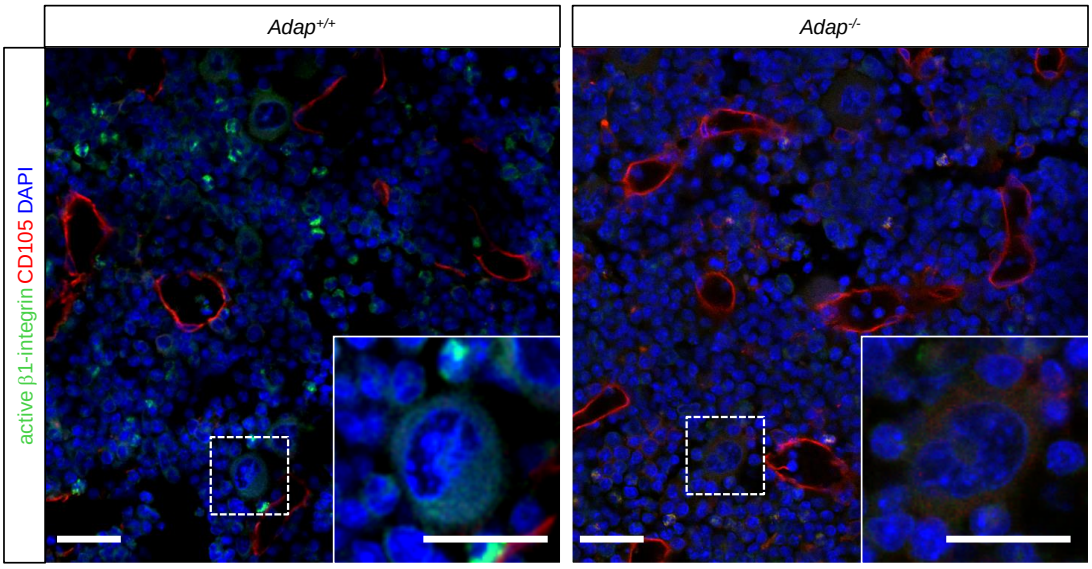

Figure 25: Reduced β1-integrin activation in ADAP-deficient BM. Representative images obtained by confocal microscopy from femoral BM cryosections of control and ADAP-deficient mice stained for vessels (CD105, red), active β1-integrin and nuclei (DAPI). Scale bars represent 30 µm and 20 µm (inset).

4.2. Knockout mouse models displaying ectopic (pro)platelet release

4.2.1. PFN1-, WASP- and ADAP-deficient mice display comparable ectopic release of (pro)platelet-like particles into the BM

Besides ADAP-deficient mice, three other knockout mouse lines (PFN1, WASP and ARPC2) have been reported to show a similar phenotype with release of platelet-like particles into the BM compartment.[74,78] All three proteins (PFN1, WASP and ARPC2) are well known actin-regulatory proteins, pointing to an important axis of actin-mediated directional proplatelet formation. However, the reason for ectopic release of (pro)platelet-like particles into the BM compartment in these mouse lines is still incompletely understood. We hypothesized that similar defects as we have described for the ADAP-deficient mice underlie the ectopic release. Therefore, we first analyzed the ectopically released particles in PFN1-, WASP- and ADAP-deficient mice by confocal microscopy of cryosections in a comparative analysis.

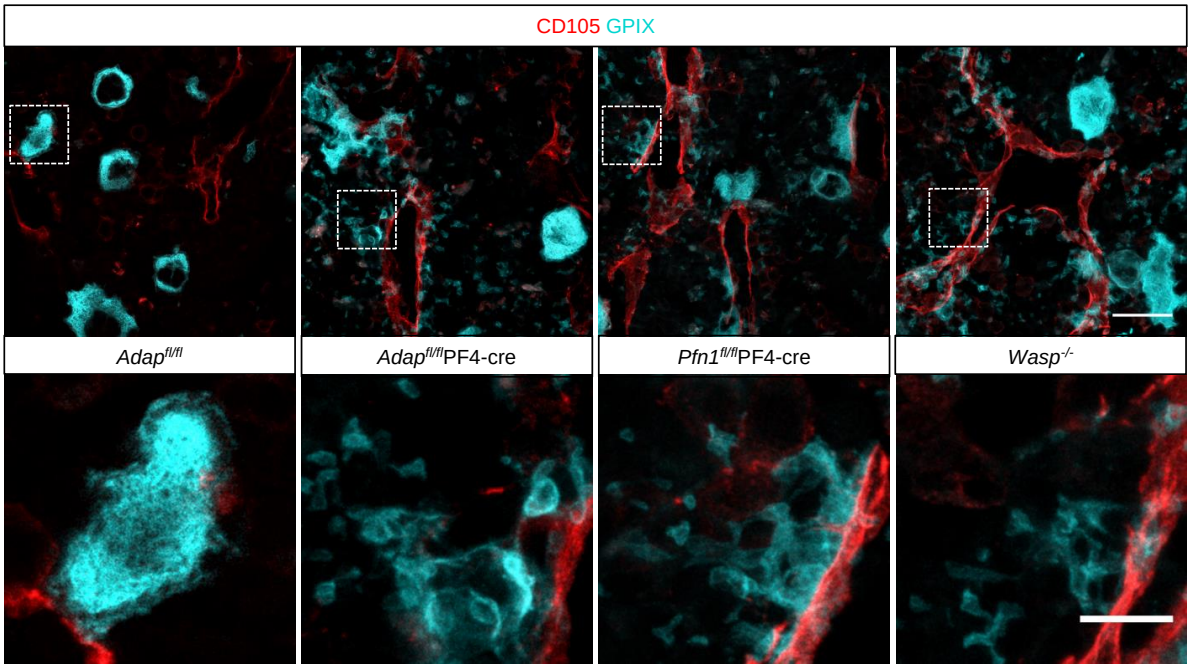

Figure 25: *In situ* analysis of sternal BM from ADAP, PFN1 and WASP-deficient mice reveals comparable release of (pro)platelet-like particles into the BM compartment. Representative confocal images of *Adap*$^{fl/fl}$ (control), *Adap*$^{fl/fl}$PF4-cre, *Pfn1*$^{fl/fl}$PF4-cre and *Wasp*$^{-/-}$ sternal BM. Respective control sternal BM from all tested genotypes gave comparable results to *Adap*$^{fl/fl}$ (data not shown). Scale bars represent 30 µm (top panel) and 10 µm (bottom panel, inset). Cyan: GPIX (MKs/platelets); red: CD105 (vessel).

Surprisingly, in all mutant mice (*Pfn1*$^{fl/fl}$PF4-cre and *Wasp*$^{-/-}$) we detected fragments in the BM in a pattern, which was similar to the ectopically released (pro)platelet-like particles in ADAP-deficient mice (Figure 25). These data indicate that PFN1, WASP and ADAP may be part of the same molecular machinery involved in transendothelial platelet production. Of note, MKs of WASP-deficient mice displayed ectopic (pro)platelet-like particle release to a lesser extent.

4.2.2. PFN1- and WASP-deficient MKs show reduced adhesion to Horm collagen

To test whether PFN1- and WASP-deficient MKs also exhibit a reduced capacity to adhere to Horm collagen as observed for ADAP-deficient MKs, we seeded mature MKs onto Horm collagen-, fibrinogen- and fibronectin-coated wells and incubated the cells for 3 h. PFN1, WASP as well as ADAP-deficient MKs displayed a selectively reduced adhesion to Horm collagen, whereas the relative number of adherent cells was unaltered or only slightly impaired on fibrinogen and fibronectin (Figure 26B,G,L).

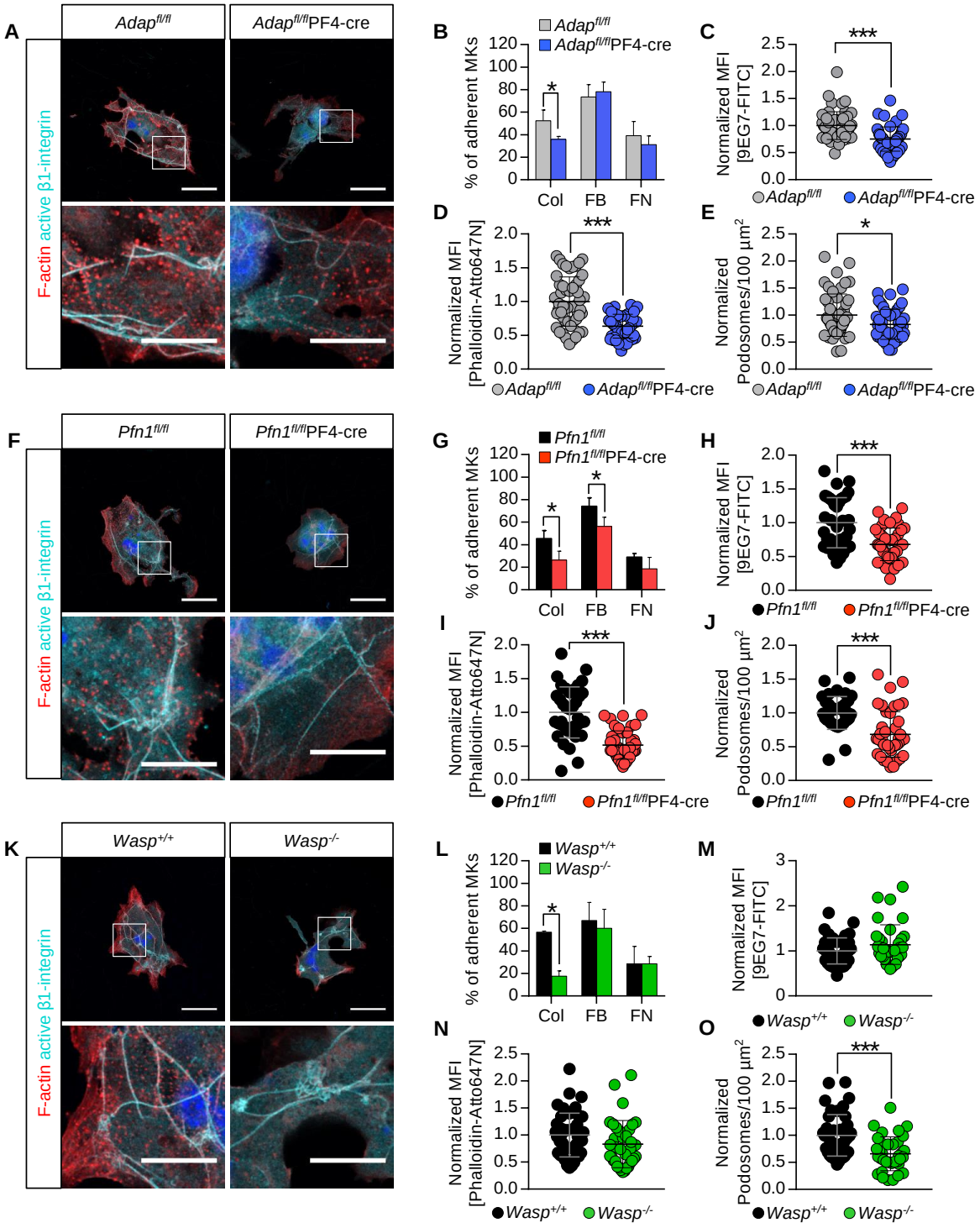

Figure 26: Reduced adhesion of and altered cytoskeletal rearrangements in MKs of ADAP-, PFN1- and WASP-deficient mice spread on Horm collagen. (A,F,K) Representative confocal images of cultured (Lin$^-$ depletion and hirudin treatment) control, ADAP-, PFN1- and WASP-deficient MKs 3 h after spreading on Horm collagen stained for F-actin and active β1-integrin. Scale bars represent 50 µm and 20

µm (inset). **(B,G,L)** Relative adhesive MKs in percent on Horm collagen (Col), fibrinogen (FB) and fibronectin (FN) after 3 h; representative graph from 2 independent experiments. At least two biological replicates and 6 technical replicates were analyzed per experiment (*P<.05). MFI of active β1-integrin (9EG7-FITC) **(C,H,M)** and F-actin **(D,I,N),** and density of podosomes **(E,J,O)** in the lowest optical section of spread MKs on Horm collagen, normalized to respective control. **(C-E,H-J,M-O)** n ≥ 40 MKs per genotype were analyzed. Data points display individual MKs. (***P<.001; *P<.05).

4.2.3. PFN1- and WASP-deficient spread MKs exhibit diminished podosome formation on Horm collagen

Since PFN1- and WASP-deficient mice displayed an ectopic release and MKs derived from these mice exhibited reduced adhesion to Horm collagen, we speculated whether β1-integrin activation was diminished as well. To this end, we let MKs adhere and spread on Horm collagen for 3 h and stained the F-actin cytoskeleton as well as active β1-integrin in spread MKs on Horm collagen (Figure 26A,F,K). Surprisingly, only PFN1- and ADAP-deficient MKs displayed a reduction in active β1-integrin staining and F-actin content (Figure 26C,H,M,D,I,N), whereas WASP-deficient MKs only assembled less podosomes per cell area (Figure 26E,J,O), latter is in line with the literature.[77] In WASP-deficient spread MKs on Horm collagen we could not detect a reduced β1-integrin activation, although we saw the strongest reduction of adherent MKs on Horm collagen for this genotype. It is possible that the few WASP-deficient MKs, which manage to adhere and spread, display normal integrin activation. Together with the results from the adhesion assay on ECM molecules these data point to a selective spreading defect of PFN1- and ADAP-deficient MKs on Horm collagen. In addition, in all tested genotypes we detected a reduced density of podosomes in the lowest plane of spread MKs on Horm collagen, suggesting altered F-actin dynamics.

Overall, these data point to an important role for β1-integrin activation during adhesion and spreading of MKs on Horm collagen and point out that β1-integrin activation may play an important role in the process of transendothelial proplatelet production in ADAP-, PFN1- and WASP-deficient mice. Further studies addressing this hypothesis are required.

5. DISCUSSION

So far, mutations in 36 human genes have been identified to cause different forms of inherited thrombocytopenia. Proteins translated from these genes are involved in different processes in MK and platelet biology, such as megakaryocyte differentiation and maturation, platelet formation/release and clearance.[31,44,45] The clinical manifestations of these inherited disorders are even more diverse ranging from mild/heavy bleedings, immunodeficiency, BM aplasia, hearing impairment or myelofibrosis to cardiac and facial defects.[45] Studies on and knowledge about these rare diseases have increased considerably over the last twenty years due to improved sequence technologies for the identification of mutations, the improvement in obtaining MKs differentiated *in vitro* from hematopoietic stem cells of patients and finally also because of the use of genetically modified mouse models. The latter has helped to better understand pathophysiological mechanism in patients and to provide new insights into fundamental biological processes.[40]

Recently, two mutations which are the underlying cause for mild to severe microthrombocytopenia with variable bleeding symptoms in CARST patients were described.[48,49] The mutations were found in the gene encoding ADAP (adhesion and degranulation promoting adapter protein), a protein which is predominantly expressed in cells of the hematopoietic system and its function has already been intensively investigated in T-cells.[111,128] Although ADAP-deficient mice were generated in the year 2001 by Peterson and colleagues, who also identified a reduced peripheral platelet count in those mice, nothing is known about the mechanism of how ADAP-deficiency influences platelet numbers.[111] We show for the first time that loss of ADAP does not only lead to a moderate thrombocytopenia in mice, but also to a reduced platelet size (Figure 10). The thrombocytopenia is caused on the one hand by a reduced platelet life span in the circulation (Figure 13), and on the other hand by an ectopic release of (pro)platelet-like particles into the BM compartment (Figure 15-20). MKs deficient for ADAP displayed an F-actin-dependent polarization defect of the DMS *in vitro* under static conditions (Figure 21) and an impaired adhesion to Horm collagen (Figure 24).

Furthermore, we could show that ADAP-deficient MKs spread on Horm collagen, collagen I and fibronectin exhibited F-actin defects, reflected by reduced podosome formation and reduced F-actin content in the lowest plane of spread cells (Figure 22-23). We could also demonstrate that reduced adhesion of MKs to Horm collagen is due to reduced β1-integrin activation of MKs deficient for ADAP. Based on that, we suggest that ADAP is required for proper MK adhesion to collagen and directed proplatelet formation into the vessel lumen.

5.1. ADAP-deficient mice as mouse model for CARST

CARST patients carrying homozygous nonsense mutations in the *ADAP* gene display a microthrombocytopenia. Both described mutations (point mutation 393G>A: p.W131X in exon 2; 2-bp deletion 1385_1386delAT:Y462 in exon 6) are predicted to lead to premature translation termination and to non-functional ADAP protein in all ADAP-expressing cells.[48,49] In constitutive ADAP-deficient mice the translational start site and first coding exon was replaced by a neomycin cassette also resulting in loss of the gene product.[111] The thrombocytopenia in CARST patients was explained by an increased basal expression of P-selectin and active integrin αIIbβ3 in platelets, which might lead to increased clearance of the platelets from the circulation.[48] In contrast, in ADAP-deficient mice we could not detect preactivated platelets in the circulation. However, ADAP-deficient platelets are cleared faster from the circulation by macrophages and an increased PS exposure on platelets might lead to the enhanced clearing similar to what was described for ARPC2-deficient mice.[123] In agreement with published data on platelet activation in patients and mutant mice, we found reduced β1- and αIIbβ3- integrin activation as well as P-selectin exposure upon stimulation with classical agonist.[48,114,115,117] In contrast to a previous report[117] we could not detect a splenomegaly in ADAP-deficient mice, which is also in line with data from CARST patients.[48,49] We could further demonstrate that there is a reduced percentage of mature MKs (>32n) in ADAP-deficient mice as measured by flow cytometry. Levin *et al.* detected normal number and size of MKs but a reduced number of multilobulated MKs

(three or more nuclear lobules, n ≥ 30 MKs) in BM aspirate from a CARST patient.[48] However, since different experimental setups were used (flow cytometry vs. microscopy), it is difficult to compare the obtained results. Interestingly, no (pro)platelet-like particles were observed in BM aspirates from patients, probably due to sample preparation. In this procedure BM aspirate is obtained by inserting a needle into the BM space followed by withdrawal of marrow in several different syringes. These samples are then transferred to evacuated blood collection tubes and a portion of liquid marrow is then smeared on a glass slide for subsequent staining and observation under a light microscope. However, the architecture of the BM is destroyed and (pro)platelet-like particles can be lost during sample preparation by this method. Moreover, it is difficult to detect (pro)platelet-like particles in a hematoxylin/eosin staining due to their small size. In order to assess whether CARST patients also display an ectopic release of (pro)platelet-like particles into the BM compartment it would therefore be necessary to analyze a BM biopsy using stainings for MK specific markers. Differences between ADAP-deficient mice and CARST patients can also be the result of truncated gene products in CARST patients. Although it is predicted that the mutations lead to premature termination of translation, truncated ADAP proteins might still be expressed, which then in turn could have additional effects on cellular behavior. Overall, since ADAP-deficient mice recapitulate the microthrombocytopenia as described in CARST patients, we suggest that these mice are a valuable model system to study the underlying mechanism.

5.2. Ectopic release and ECM

Interestingly, we identified that the pattern of ectopically released (pro)platelet-like particles into the BM compartment of PFN1- and WASP-deficient mice is similar to *Adap*$^{-/-}$ mice. Although proplatelet formation occurs in MK cultures *in vitro*, suggesting a cell autonomous driven process, there is evidence that ECM proteins like fibronectin, laminins and collagens can contribute to and modulate proplatelet formation. Collagen I is well-known to inhibit proplatelet formation[34,129] which occurs via Syk-dependent GPVI

signaling in FLC-derived MKs.[32] However, it was reported that proplatelet formation is inhibited upon engagement of α2β1 integrin, not upon GPVI activation, likely through activation of the Rho/ROCK pathway in human MKs.[129] It is tempting to speculate that ADAP, PFN1 and WASP are involved in an inhibitory signaling cascade, since MKs, deficient for the before mentioned proteins, exhibit cytoskeletal and adhesion defects on collagen I. The inability to recognize the inhibitory signal of collagen I could explain the ectopic release of (pro)platelet-like particles. Semeniak and colleagues postulated that an inhibitory signal via GPVI with a branchpoint downstream of Src family kinases Fyn and Lyn attenuates proplatelet formation.[32] Interestingly, in T-cells two YDDV motifs of ADAP were shown to be phosphorylated by Fyn,[101] suggesting a possible interaction of Fyn and ADAP also in MKs. A multi-molecular complex containing SLP-76, ADAP, Ena/VASP, Nck, and WASP has been identified in Raw264.7 macrophages, which mediates signaling between the Fcγ receptor and the actin cytoskeleton. SLP-76 might function as a central component in this complex, by binding both ADAP, which then recruits Ena/VASP and profilin, and Nck, which in turn recruits WASP and Arp2/3.[130] Similarly, in activated T-cells, ADAP associates with Ena/VASP family proteins and is present in complexes containing the proteins WASP, Nck, and SLP-76.[121] Interestingly, in human platelets, adhesion to fibrinogen stimulated the association of SLP-76 with ADAP and VASP, thereby enabling SLP-76 to relay signals from the αIIbβ3 integrin to cytoskeletal reorganization.[131] We speculate that this or a similar complex might also operate in MKs, but this hypothesis requires further investigation.

Despite the evidence for an inhibitory role of collagen I on proplatelet formation *in vitro* mediated via GPVI[32] or α2β1 integrin,[129] the respective knockout mice display normal peripheral platelet counts[132,133] and a reduced platelet volume was only observed in integrin α2-deficient mice.[134] Likewise, MKs in the BM of GPVI or α2-deficient mice are unaltered and show no sign of ectopically released (pro)platelet-like particles in the BM, suggesting that *in vivo* additional compensatory mechanism might lead to normal proplatelet formation in these mice.[32] There are additional collagen receptors expressed on MKs, which can potentially compensate for the lack of GPVI and α2β1. Collagen receptor discoidin domain receptor 1 (DDR1) was described to regulate human MK migration and was suggested to modulate MK-collagen interactions.[135] Mice lacking the

inhibitory collagen receptor leucocyte-associated immunoglobulin-like receptor 1 (LAIR-1) exhibit significantly increased platelet counts and increased proplatelet formation on fibrinogen *in vitro,* strongly suggesting that LAIR-1 mediates an inhibitory signal *in vivo*.[136] Although all of these findings suggest modulation of proplatelet formation by ECM proteins, these hypotheses still demand further verification. Recently, it was described that the activation of transient receptor potential cation channel subfamily V member 4 (TRPV4), a mechano-sensitive ion channel, is induced upon adhesion of human MKs on softer matrices like collagen IV, which promotes platelet production. Interestingly, this response is triggered by a cascade of events including β1-integrin activation, which is not found on stiffer matrices like collagen I. This emphasizes the role of β1-integrin in proplatelet formation.[137] According to this, it was observed that mimicking the BM stiffness using methylcellulose enhances the production of proplatelets from BM-cultured MKs *in vitro*.[28]

5.3. Ectopic release and podosomes

Podosomes are actin-based structures involved in cell adhesion, migration and ECM degradation. It has been proposed that altered podosome formation has an effect on proper transendothelial proplatelet formation and the delivery of platelets into the bloodstream.[77] In support of this, *Wasp*$^{-/-}$, *Pfn1*$^{-/-}$, *Arpc2*$^{-/-}$ and *Adap*$^{-/-}$ mice display a thrombocytopenia, ectopic release of (pro)platelet-like particles and a strong defect in MK podosome formation (this study and in [74,78,123]). These data suggest a possible link between impaired podosome formation *in vitro* and platelet production defects characterized by ectopic release of platelets into the BM compartment *in vivo*. However, it has to be noted that alternative mechanisms may exist since phospholipase D (Pld)-deficient MKs display abnormal actin rearrangement with almost abolished formation of podosomes, but normal platelet counts. Interestingly, in Pld2-deficient and Pld1/2-double-deficient mice signs of increased MK fragmentation, reminiscent of an ectopic platelet release within the BM, were observed.[138] In this study, we showed that ADAP-deficient MKs display severe defects in F-actin organization on collagen I and fibronectin

matrices and significantly reduced podosome formation, whereas unaltered F-actin organization was detectable on collagen IV.

It was suggested, that podosomes from MKs play a role in formation of protrusions across the basement membrane in a matrix-metalloprotease dependent manner.[77] However, it is still controversial debated whether podosomes in general are of relevance *in vivo*. Recently, Spuul *et al.* could show that, during angiogenesis in the retina, podosome-mediated degradation of the basement membrane is important for endothelial cell sprouting and anastomosis within the developing vasculature.[139] To prove that podosomes can degrade the basement membrane via matrix-metalloprotease dependent processes and are of physiological relevance also in MKs in the BM it is key to visualize podosomes in their native environment. This is challenging, since high quality sample preparation and an imaging system which allows a nanoscale spatial resolution combined with the opportunity for 3D imaging would be required. One possibility to solve this problem could be expansion microscopy, which can be used to perform scalable super-resolution microscopy with diffraction-limited microscopes.[140] One drawback is that podosomes are at least *in vitro* highly dynamic structures and for expansion microscopy it is necessary to fix the tissue, which makes dynamic analysis with this approach impossible.

5.4. Ectopic release and integrins

As shown before, ADAP can modulate integrin activation in platelets.[113-116] In addition, we observed a similar integrin modulating effect with diminished β1-integrin activation resulting in an adhesion defect of ADAP- and PFN1-deficient MKs on collagen I. However, WASP-deficient MKs exhibit normal integrin activation of adherent cells, but an overall reduced adhesion to collagen. In line with this, PFN1-deficient platelets also display a reduced αIIbβ3 and β1-integrin activation upon stimulation with commonly used agonists.[97] Considering that WASP-deficient MKs exhibit impaired adherence to Horm Collagen, but normal β1-integrin activation, this phenotype could be explained by

a selection process during spreading enabling only MKs with normal β1-integrin function to adhere. Thus, we speculated that β1-integrin activation or integrins in general contribute to transendothelial proplatelet formation.

Glanzmann thrombastenia (GT) is an inherited disorder of platelets and typically caused by the absence of platelet aggregation due to quantitative and/or functional deficiencies of the αIIbβ3-integrin. Classical GT patients exhibit normal platelet counts, however, reports of novel but rare point mutations in either *ITGA2B* and *ITGB3* genes have been associated rather with an altered platelet production than a true GT phenotype (reviewed in[141]). Interestingly, mutations in these patients are found in the intracytoplasmatic activation-restraining salt bridge of αIIbβ3, thus suggesting a role of the active conformation of these integrins in platelet production. However, deletion of α2- or β3-integrins in mouse models is not associated with changes in peripheral platelet counts or platelet morphology.[142,143] Interestingly, conditional deletion of the *Itga2* gene in MKs and platelets leads to a reduction in platelet size with unaltered platelet counts.[134,144] Regarding platelet counts, similar findings were made upon loss of β1-integrins in platelets and MKs taking advantage of the inducible Mx-cre system.[133] Since peripheral platelet counts were not affected in both systems, the findings strongly argue against a role of the mentioned integrins in platelet production *in vivo*. However, it is possible that in these genetic mouse models the loss of a single integrin can be compensated by another. Therefore, the generation and investigation of β1/β3-double-deficient mice with no functional integrins on platelets and MKs is required to answer the question, whether integrins *per se* are important for transendothelial platelet production.

Only little is known about integrin activation on MKs and their role in platelet biogenesis. Talin and kindlin are cytoplasmatic proteins interacting with the β-subunit of integrins and are known to be indispensable for integrin activation.[145] Knockout mouse models of these proteins with the Mx-cre system (talin 1) or bone marrow chimeras (kindlin 3) display overall normal platelet counts,[146,147] thus arguing against a role of integrin activation in platelet production. Of note, conditional MK- and platelet-specific talin knockout mice display a slightly reduced platelet count.[148] Although it is described that talin and kindlin are required for fast integrin activation in platelets, nothing is known

about their function in BM-situated MKs. Likely, due to the constant contact to ECM proteins, MK integrin regulation is following different rules compared to the fast activation described in platelets. It is tempting to speculate that for talin1-deficient MKs the time frame is sufficient to obtain enough integrins in an ‘extended open’ state due to fluctuations in the thermodynamic equilibrium of integrin conformations.[149] In addition, systems-wide proteomic studies in HeLa cells revealed that talin1 and kindlin3 display a protein half-life of 40.7 h and 47.1 h respectively. It is imaginable that talin protein is still expressed and functional on protein level in talin1-deficient MKs, although on gene level talin has already been deleted. A remnant of talin protein in MKs could be in line with the mild thrombocytopenia in conditional talin1-deficient mice with the PF4-cre system.[148]

Overall it is unclear, whether inside-out activation of integrins or outside-in signaling of integrins or both have a role for proplatelet formation of MKs *in vivo.* It will be of utmost importance to answer these questions in order to develop a model describing how integrins are involved in transendothelial proplatelet formation. Based on our *in vitro* studies of MKs deficient for ADAP, PFN1 and WASP on different ECMs and the ectopic release of (pro)platelet-like particles into the BM in these mice we suggest that integrin activation is important to establish a firm adhesion of MKs to the ECM in the BM. ADAP, PFN1 and WASP connect integrins to the cytoskeleton and disruption of this axis results in a cell intrinsic polarization defect of the F-actin cytoskeleton and the associated demarcation membrane system.

6. CONCLUDING REMARKS

The work presented here shows studies on mouse platelets and MKs deficient for ADAP, a cytosolic protein expressed in the hematopoietic system, which has been described to be affected by mutations in humans leading to a microthrombocytopenia (CARST patients). In addition, PFN1- and WASP-deficient MKs were analyzed regarding the ectopically released (pro)platelet-like particles into the BM compartment in these mice and the possible involvement of β1-integrin activation in this process.

The major findings are:

- ADAP-deficient mice (constitutive and conditional) display a microthrombocytopenia recapitulating the clinical feature of CARST patients.

- *Adap*$^{-/-}$ platelets show mildly impaired integrin activation.

- ADAP is associated with the F-actin cytoskeleton in platelets and loss of ADAP mildly affects F-actin dynamics upon platelet activation and under steady state conditions.

- Thrombocytopenia in ADAP-deficient mice is caused on the one hand by reduced platelet life span in the circulation due to enhanced clearing by macrophages and on the other hand by ectopic release of (pro)platelet-like particles into the BM compartment.

- ADAP-deficient MKs display an F-actin dependent polarization defect of the DMS.

- ADAP-deficient MKs show adhesion as well as F-actin cytoskeleton defects on collagen I and fibronectin with impaired β1-integrin activation.

- Ectopic release of (pro)platelet-like particles into the BM compartment of ADAP-, PFN1- and WASP-deficient MKs is comparable.

- ADAP-, PFN1- and WASP-deficient MKs display similar adhesion and spreading defects, with impaired β1-integrin activation, reduced F-actin content and podosome formation.

7. OUTLOOK

Studies regarding the ectopic release of (pro)platelet-like particles in ADAP-, PFN1-, WASP and ARPC2-deficient mice will provide a better understanding on how MKs polarize their cytoplasm including the DMS and how they produce directionally proplatelets into the vessel lumen. The knowledge about this fundamental process in platelet biogenesis could provide new therapeutic opportunities and targets to manipulate the platelet count in patients with thrombocytopenias. Therefore, it is of high interest to better understand the mechanisms underlying the ectopic release of platelet-like particles into the BM compartment. All other proteins known so far, involved in directional platelet production (PFN1, WASP, ARPC2), are regulators of the F-actin cytoskeleton. ADAP, however, is the first protein described that is indirectly connected to the F-actin cytoskeleton, suggesting that ADAP may act in a possible signaling pathway upstream of PFN1, WASP and ARPC2. In T-cells, ADAP becomes phosphorylated upon TCR stimulation and is present in a complex with SLP-76, Nck and Vav1 to regulate the F-actin cytoskeleton.[112] We are currently planning to detect such a complex in proplatelet-forming MKs *in vitro* performing co-immunoprecipitation studies of the ADAP protein and are analyzing ectopically released (pro)platelet-like particles and MKs of ARPC2-deficient mice.

To gain more insights into the underlying molecular mechanism and which domains and binding partners of ADAP are important for the ectopic release of (pro)platelet-like particles into the BM compartment, the expression of ADAP variants (point mutations of known phospho-sites, deletions of domains etc.) in MKs could be beneficial. It would also be of interest to detect possible truncated gene products of ADAP in CARST patients.

The challenge of studying a phenotype like the ectopic release of platelets lies in the limitations of culturing MKs *in vitro*. The culture system used in this study cannot mimic the complex microenvironment of the BM with its 3D architecture, different cell types, a complex ECM and gradients of blood-derived molecules. One possibility to include more of these aspects in MK *in vitro* cultures could be the use of 3D micropattern techniques

for cultivation and cell analysis in 3D microenvironments. With such approaches it is possible to engineer a micrometer-scale, soft, 3-dimensional, complex and dynamic microenvironment for individual cells or for multi-cellular arrangements.[150]

Another solution could be an adaption and further development of the recently engineered ‘organ-on-a-chip’ technology. Torisawa and colleagues developed a method for fabricating ‘bone marrow-on-a-chip’ that allows culture of living BM with a functional hematopoietic niche *in vitro* by first engineering new bone *in vivo*. In brief, a poly(dimethylsiloxane) device containing bone-inducing materials (collagen I gel containing bone-inducing demineralized bone powder and bone morphogenetic proteins) in its central cylindrical chamber is implanted subcutaneously into a mouse and after eight weeks, *in vivo* engineered BM is removed and inserted into a chip microdevice. The engineered BM retains hematopoietic stem and progenitor cells in normal *in vivo*-like proportions for at least one week in culture.[151] The combination of this method with knockout mouse models could provide a powerful platform for advanced analysis of platelet production *ex vivo*, with the freedom to manipulate the system and analyze MK behavior for a longer time period than with conventional intravital microscopy.

8. REFERENCES

1. Long MW, Williams N, Ebbe S. Immature megakaryocytes in the mouse: physical characteristics, cell cycle status, and in vitro responsiveness to thrombopoietic stimulatory factor. *Blood*. 1982;59(3):569-575.

2. Ogawa M. Differentiation and proliferation of hematopoietic stem cells. *Blood*. 1993;81(11):2844-2853.

3. Lefrancais E, Ortiz-Munoz G, Caudrillier A, et al. The lung is a site of platelet biogenesis and a reservoir for haematopoietic progenitors. *Nature*. 2017;544(7648):105-109.

4. Italiano JE, Jr., Lecine P, Shivdasani RA, Hartwig JH. Blood platelets are assembled principally at the ends of proplatelet processes produced by differentiated megakaryocytes. *J Cell Biol*. 1999;147(6):1299-1312.

5. Eto K, Kunishima S. Linkage between the mechanisms of thrombocytopenia and thrombopoiesis. *Blood*. 2016;127(10):1234-1241.

6. Machlus KR, Thon JN, Italiano JE, Jr. Interpreting the developmental dance of the megakaryocyte: a review of the cellular and molecular processes mediating platelet formation. *Br J Haematol*. 2014;165(2):227-236.

7. Stegner D, vanEeuwijk JMM, Angay O, et al. Thrombopoiesis is spatially regulated by the bone marrow vasculature. *Nat Commun*. 2017;8(1):127.

8. Kaushansky K. The molecular mechanisms that control thrombopoiesis. *J Clin Invest*. 2005;115(12):3339-3347.

9. Bartley TD, Bogenberger J, Hunt P, et al. Identification and cloning of a megakaryocyte growth and development factor that is a ligand for the cytokine receptor Mpl. *Cell*. 1994;77(7):1117-1124.

10. Kaushansky K. The mpl ligand: molecular and cellular biology of the critical regulator of megakaryocyte development. *Stem Cells*. 1994;12 Suppl 1:91-96; discussion 96-97.

11. Kaushansky K, Lok S, Holly RD, et al. Promotion of megakaryocyte progenitor expansion and differentiation by the c-Mpl ligand thrombopoietin. *Nature*. 1994;369(6481):568-571.

12. Kuter DJ, Beeler DL, Rosenberg RD. The purification of megapoietin: a physiological regulator of megakaryocyte growth and platelet production. *Proc Natl Acad Sci U S A*. 1994;91(23):11104-11108.

13. Lok S, Kaushansky K, Holly RD, et al. Cloning and expression of murine thrombopoietin cDNA and stimulation of platelet production in vivo. *Nature*. 1994;369(6481):565-568.

14. de Sauvage FJ, Hass PE, Spencer SD, et al. Stimulation of megakaryocytopoiesis and thrombopoiesis by the c-Mpl ligand. *Nature*. 1994;369(6481):533-538.

15. Sohma Y, Akahori H, Seki N, et al. Molecular cloning and chromosomal localization of the human thrombopoietin gene. *FEBS Lett*. 1994;353(1):57-61.

16. Wendling F, Maraskovsky E, Debili N, et al. cMpl ligand is a humoral regulator of megakaryocytopoiesis. *Nature*. 1994;369(6481):571-574.

17. Gurney AL, Carver-Moore K, de Sauvage FJ, Moore MW. Thrombocytopenia in c-mpl-deficient mice. *Science*. 1994;265(5177):1445-1447.

18. Ihara K, Ishii E, Eguchi M, et al. Identification of mutations in the c-mpl gene in congenital amegakaryocytic thrombocytopenia. *Proc Natl Acad Sci U S A*. 1999;96(6):3132-3136.

19. Thon JN, Italiano JE. Platelet formation. *Semin Hematol*. 2010;47(3):220-226.

20. Geddis AE, Kaushansky K. Endomitotic megakaryocytes form a midzone in anaphase but have a deficiency in cleavage furrow formation. *Cell Cycle*. 2006;5(5):538-545.

21. Eckly A, Heijnen H, Pertuy F, et al. Biogenesis of the demarcation membrane system (DMS) in megakaryocytes. *Blood*. 2014;123(6):921-930.

22. Antkowiak A, Viaud J, Severin S, et al. Cdc42-dependent F-actin dynamics drive structuration of the demarcation membrane system in megakaryocytes. *J Thromb Haemost*. 2016;14(6):1268-1284.

23. Schulze H, Korpal M, Hurov J, et al. Characterization of the megakaryocyte demarcation membrane system and its role in thrombopoiesis. *Blood*. 2006;107(10):3868-3875.

24. Brown E, Carlin LM, Nerlov C, Lo Celso C, Poole AW. Multiple membrane extrusion sites drive megakaryocyte migration into bone marrow blood vessels. *Life Sci Alliance*. 2018;1(2).

25. Thon JN, Italiano JE, Jr. Does size matter in platelet production? *Blood*. 2012;120(8):1552-1561.

26. Machlus KR, Italiano JE, Jr. The incredible journey: From megakaryocyte development to platelet formation. *J Cell Biol*. 2013;201(6):785-796.

27. Strassel C, Eckly A, Leon C, et al. Hirudin and heparin enable efficient megakaryocyte differentiation of mouse bone marrow progenitors. *Exp Cell Res*. 2012;318(1):25-32.

28. Aguilar A, Pertuy F, Eckly A, et al. Importance of environmental stiffness for megakaryocyte differentiation and proplatelet formation. *Blood*. 2016;128(16):2022-2032.

29. Junt T, Schulze H, Chen Z, et al. Dynamic visualization of thrombopoiesis within bone marrow. *Science*. 2007;317(5845):1767-1770.

30. Zhang L, Orban M, Lorenz M, et al. A novel role of sphingosine 1-phosphate receptor S1pr1 in mouse thrombopoiesis. *J Exp Med*. 2012;209(12):2165-2181.

31. Pecci A, Balduini CL. Lessons in platelet production from inherited thrombocytopenias. *Br J Haematol*. 2014;165(2):179-192.

32. Semeniak D, Kulawig R, Stegner D, et al. Proplatelet formation is selectively inhibited by collagen type I through Syk-independent GPVI signaling. *J Cell Sci*. 2016;129(18):3473-3484.

33. Balduini A, Pallotta I, Malara A, et al. Adhesive receptors, extracellular proteins and myosin IIA orchestrate proplatelet formation by human megakaryocytes. *J Thromb Haemost*. 2008;6(11):1900-1907.

34. Larson MK, Watson SP. Regulation of proplatelet formation and platelet release by integrin alpha IIb beta3. *Blood*. 2006;108(5):1509-1514.

35. Nieswandt B, Pleines I, Bender M. Platelet adhesion and activation mechanisms in arterial thrombosis and ischaemic stroke. *J Thromb Haemost*. 2011;9 Suppl 1:92-104.

36. Schmitt A, Guichard J, Masse JM, Debili N, Cramer EM. Of mice and men: comparison of the ultrastructure of megakaryocytes and platelets. *Exp Hematol*. 2001;29(11):1295-1302.

37. Aurbach K, Spindler M, Haining EJ, Bender M, Pleines I. Blood collection, platelet isolation and measurement of platelet count and size in mice-a practical guide. *Platelets*. 2018:1-10.

38. Jirouskova M, Shet AS, Johnson GJ. A guide to murine platelet structure, function, assays, and genetic alterations. *J Thromb Haemost*. 2007;5(4):661-669.

39. Ware J. Dysfunctional platelet membrane receptors: from humans to mice. *Thromb Haemost*. 2004;92(3):478-485.

40. Leon C, Dupuis A, Gachet C, Lanza F. The contribution of mouse models to the understanding of constitutional thrombocytopenia. *Haematologica*. 2016;101(8):896-908.

41. Sharda A, Flaumenhaft R. The life cycle of platelet granules. *F1000Res*. 2018;7:236.

42. Bentfeld-Barker ME, Bainton DF. Identification of primary lysosomes in human megakaryocytes and platelets. *Blood*. 1982;59(3):472-481.

43. Rayes J, Watson SP, Nieswandt B. Functional significance of the platelet immune receptors GPVI and CLEC-2. *J Clin Invest*. 2019;129(1):12-23.

44. Johnson B, Fletcher SJ, Morgan NV. Inherited thrombocytopenia: novel insights into megakaryocyte maturation, proplatelet formation and platelet lifespan. *Platelets*. 2016;27(6):519-525.

45. Savoia A. Molecular basis of inherited thrombocytopenias: an update. *Curr Opin Hematol*. 2016;23(5):486-492.

46. Thrasher AJ, Burns SO. WASP: a key immunological multitasker. *Nat Rev Immunol*. 2010;10(3):182-192.

47. Kahr WH, Pluthero FG, Elkadri A, et al. Loss of the Arp2/3 complex component ARPC1B causes platelet abnormalities and predisposes to inflammatory disease. 2017;8:14816.

48. Levin C, Koren A, Pretorius E, et al. Deleterious mutation in the FYB gene is associated with congenital autosomal recessive small-platelet thrombocytopenia. *J Thromb Haemost*. 2015;13(7):1285-1292.

49. Hamamy H, Makrythanasis P, Al-Allawi N, Muhsin AA, Antonarakis SE. Recessive thrombocytopenia likely due to a homozygous pathogenic variant in the FYB gene: case report. *BMC Med Genet*. 2014;15:135.

50. Levin C, Zalman L, Tamary H, et al. Small-platelet thrombocytopenia in a family with autosomal recessive inheritance pattern. *Pediatr Blood Cancer*. 2013;60(10):E128-130.

51. Patel-Hett S, Richardson JL, Schulze H, et al. Visualization of microtubule growth in living platelets reveals a dynamic marginal band with multiple microtubules. *Blood*. 2008;111(9):4605-4616.

52. Italiano JE, Jr., Bergmeier W, Tiwari S, et al. Mechanisms and implications of platelet discoid shape. *Blood*. 2003;101(12):4789-4796.

53. Bender M, Eckly A, Hartwig JH, et al. ADF/n-cofilin-dependent actin turnover determines platelet formation and sizing. *Blood*. 2010;116(10):1767-1775.

54. Janke C, Montagnac G. Causes and Consequences of Microtubule Acetylation. *Curr Biol*. 2017;27(23):R1287-R1292.

55. Janke C. The tubulin code: molecular components, readout mechanisms, and functions. *J Cell Biol*. 2014;206(4):461-472.

56. Gadadhar S, Bodakuntla S, Natarajan K, Janke C. The tubulin code at a glance. *J Cell Sci*. 2017;130(8):1347-1353.

57. Lecine P, Italiano JE, Jr., Kim SW, Villeval JL, Shivdasani RA. Hematopoietic-specific beta 1 tubulin participates in a pathway of platelet biogenesis dependent on the transcription factor NF-E2. *Blood*. 2000;96(4):1366-1373.

58. Schwer HD, Lecine P, Tiwari S, Italiano JE, Jr., Hartwig JH, Shivdasani RA. A lineage-restricted and divergent beta-tubulin isoform is essential for the biogenesis, structure and function of blood platelets. *Curr Biol*. 2001;11(8):579-586.

59. Strassel C, Magiera MM, Dupuis A, et al. An essential role for alpha4A-tubulin in platelet biogenesis. *Life Sci Alliance*. 2019;2(1).

60. van Dijk J, Bompard G, Cau J, et al. Microtubule polyglutamylation and acetylation drive microtubule dynamics critical for platelet formation. *BMC Biol*. 2018;16(1):116.

61. Iancu-Rubin C, Gajzer D, Mosoyan G, Feller F, Mascarenhas J, Hoffman R. Panobinostat (LBH589)-induced acetylation of tubulin impairs megakaryocyte maturation and platelet formation. *Exp Hematol*. 2012;40(7):564-574.

62. Patel SR, Richardson JL, Schulze H, et al. Differential roles of microtubule assembly and sliding in proplatelet formation by megakaryocytes. *Blood*. 2005;106(13):4076-4085.

63. Bender M, Thon JN, Ehrlicher AJ, et al. Microtubule sliding drives proplatelet elongation and is dependent on cytoplasmic dynein. *Blood*. 2015;125(5):860-868.

64. Melak M, Plessner M, Grosse R. Actin visualization at a glance. *J Cell Sci*. 2017;130(3):525-530.

65. Rohn JL, Baum B. Actin and cellular architecture at a glance. *J Cell Sci*. 2010;123(Pt 2):155-158.

66. Bearer EL, Prakash JM, Li Z. Actin dynamics in platelets. *Int Rev Cytol*. 2002;217:137-182.

67. Fox JE, Phillips DR. Inhibition of actin polymerization in blood platelets by cytochalasins. *Nature*. 1981;292(5824):650-652.

68. Fox JE, Phillips DR. Role of phosphorylation in mediating the association of myosin with the cytoskeletal structures of human platelets. *J Biol Chem*. 1982;257(8):4120-4126.

69. Seri M, Cusano R, Gangarossa S, et al. Mutations in MYH9 result in the May-Hegglin anomaly, and Fechtner and Sebastian syndromes. The May-Heggllin/Fechtner Syndrome Consortium. *Nat Genet*. 2000;26(1):103-105.

70. Kunishima S, Okuno Y, Yoshida K, et al. ACTN1 mutations cause congenital macrothrombocytopenia. *Am J Hum Genet*. 2013;92(3):431-438.

71. Derry JM, Ochs HD, Francke U. Isolation of a novel gene mutated in Wiskott-Aldrich syndrome. *Cell*. 1994;78(4):635-644.

72. Nurden P, Debili N, Coupry I, et al. Thrombocytopenia resulting from mutations in filamin A can be expressed as an isolated syndrome. *Blood*. 2011;118(22):5928-5937.

73. Pleines I, Dutting S, Cherpokova D, et al. Defective tubulin organization and proplatelet formation in murine megakaryocytes lacking Rac1 and Cdc42. *Blood*. 2013;122(18):3178-3187.

74. Bender M, Stritt S, Nurden P, et al. Megakaryocyte-specific Profilin1-deficiency alters microtubule stability and causes a Wiskott-Aldrich syndrome-like platelet defect. *Nat Commun*. 2014;5:4746.

75. Linder S, Kopp P. Podosomes at a glance. *J Cell Sci*. 2005;118(Pt 10):2079-2082.

76. Schachtner H, Calaminus SD, Thomas SG, Machesky LM. Podosomes in adhesion, migration, mechanosensing and matrix remodeling. *Cytoskeleton (Hoboken)*. 2013;70(10):572-589.

77. Schachtner H, Calaminus SD, Sinclair A, et al. Megakaryocytes assemble podosomes that degrade matrix and protrude through basement membrane. *Blood*. 2013;121(13):2542-2552.

78. Sabri S, Foudi A, Boukour S, et al. Deficiency in the Wiskott-Aldrich protein induces premature proplatelet formation and platelet production in the bone marrow compartment. *Blood*. 2006;108(1):134-140.

79. Carlsson L, Nystrom LE, Sundkvist I, Markey F, Lindberg U. Actin polymerizability is influenced by profilin, a low molecular weight protein in non-muscle cells. *J Mol Biol*. 1977;115(3):465-483.

80. Birbach A. Profilin, a multi-modal regulator of neuronal plasticity. *Bioessays*. 2008;30(10):994-1002.

81. Kang F, Purich DL, Southwick FS. Profilin promotes barbed-end actin filament assembly without lowering the critical concentration. *J Biol Chem*. 1999;274(52):36963-36972.

82. Alkam D, Feldman EZ, Singh A, Kiaei M. Profilin1 biology and its mutation, actin(g) in disease. *Cell Mol Life Sci*. 2017;74(6):967-981.

83. Pei W, Du F, Zhang Y, He T, Ren H. Control of the actin cytoskeleton in root hair development. *Plant Sci*. 2012;187:10-18.

84. Krishnamoorthy P, Sanchez-Rodriguez C, Heilmann I, Persson S. Regulatory roles of phosphoinositides in membrane trafficking and their potential impact on cell-wall synthesis and re-modelling. *Ann Bot*. 2014;114(6):1049-1057.

85. Yarmola EG, Bubb MR. How depolymerization can promote polymerization: the case of actin and profilin. *Bioessays*. 2009;31(11):1150-1160.

86. Shekhar S, Pernier J, Carlier MF. Regulators of actin filament barbed ends at a glance. *J Cell Sci*. 2016;129(6):1085-1091.

87. Wu CH, Fallini C, Ticozzi N, et al. Mutations in the profilin 1 gene cause familial amyotrophic lateral sclerosis. *Nature*. 2012;488(7412):499-503.

88. Tanaka Y, Nonaka T, Suzuki G, Kametani F, Hasegawa M. Gain-of-function profilin 1 mutations linked to familial amyotrophic lateral sclerosis cause seed-dependent intracellular TDP-43 aggregation. *Hum Mol Genet*. 2016;25(7):1420-1433.

89. Michaelsen-Preusse K, Zessin S, Grigoryan G, et al. Neuronal profilins in health and disease: Relevance for spine plasticity and Fragile X syndrome. *Proc Natl Acad Sci U S A*. 2016;113(12):3365-3370.

90. Zou L, Jaramillo M, Whaley D, et al. Profilin-1 is a negative regulator of mammary carcinoma aggressiveness. *Br J Cancer*. 2007;97(10):1361-1371.

91. Bae YH, Ding Z, Zou L, Wells A, Gertler F, Roy P. Loss of profilin-1 expression enhances breast cancer cell motility by Ena/VASP proteins. *J Cell Physiol*. 2009;219(2):354-364.

92. Karamchandani JR, Gabril MY, Ibrahim R, et al. Profilin-1 expression is associated with high grade and stage and decreased disease-free survival in renal cell carcinoma. *Hum Pathol*. 2015;46(5):673-680.

93. Zoidakis J, Makridakis M, Zerefos PG, et al. Profilin 1 is a potential biomarker for bladder cancer aggressiveness. *Mol Cell Proteomics*. 2012;11(4):M111 009449.

94. Yao W, Ji S, Qin Y, et al. Profilin-1 suppresses tumorigenicity in pancreatic cancer through regulation of the SIRT3-HIF1alpha axis. *Mol Cancer*. 2014;13:187.

95. Li Z, Zhong Q, Yang T, Xie X, Chen M. The role of profilin-1 in endothelial cell injury induced by advanced glycation end products (AGEs). *Cardiovasc Diabetol*. 2013;12:141.

96. Romeo GR, Moulton KS, Kazlauskas A. Attenuated expression of profilin-1 confers protection from atherosclerosis in the LDL receptor null mouse. *Circ Res*. 2007;101(4):357-367.

97. Stritt S, Birkholz I, Beck S, et al. Profilin 1-mediated cytoskeletal rearrangements regulate integrin function in mouse platelets. *Blood Adv*. 2018;2(9):1040-1045.

98. Alekhina O, Burstein E, Billadeau DD. Cellular functions of WASP family proteins at a glance. *J Cell Sci*. 2017;130(14):2235-2241.

99. Rivers E, Thrasher AJ. Wiskott-Aldrich syndrome protein: Emerging mechanisms in immunity. *Eur J Immunol*. 2017;47(11):1857-1866.

100. Thrasher AJ. New insights into the biology of Wiskott-Aldrich syndrome (WAS). *Hematology Am Soc Hematol Educ Program*. 2009:132-138.

101. Wang H, Rudd CE. SKAP-55, SKAP-55-related and ADAP adaptors modulate integrin-mediated immune-cell adhesion. *Trends in Cell Biology*. 2008;18(10):486-493.

102. Veale M, Raab M, Li Z, et al. Novel isoform of lymphoid adaptor FYN-T-binding protein (FYB-130) interacts with SLP-76 and up-regulates interleukin 2 production. *J Biol Chem*. 1999;274(40):28427-28435.

103. Rudolph JM, Guttek K, Weitz G, et al. Characterization of mice with a platelet-specific deletion of the adapter molecule ADAP. *Mol Cell Biol*. 2019.

104. Griffiths EK, Penninger JM. Communication between the TCR and integrins: role of the molecular adapter ADAP/Fyb/Slap. *Curr Opin Immunol*. 2002;14(3):317-322.

105. Kang H, Freund C, Duke-Cohan JS, Musacchio A, Wagner G, Rudd CE. SH3 domain recognition of a proline-independent tyrosine-based RKxxYxxY motif in immune cell adaptor SKAP55. *EMBO J*. 2000;19(12):2889-2899.

106. Liu J, Kang H, Raab M, da Silva AJ, Kraeft SK, Rudd CE. FYB (FYN binding protein) serves as a binding partner for lymphoid protein and FYN kinase substrate SKAP55 and a SKAP55-related protein in T cells. *Proc Natl Acad Sci U S A*. 1998;95(15):8779-8784.

107. Marie-Cardine A, Hendricks-Taylor LR, Boerth NJ, Zhao H, Schraven B, Koretzky GA. Molecular interaction between the Fyn-associated protein SKAP55 and the SLP-76-associated phosphoprotein SLAP-130. *J Biol Chem*. 1998;273(40):25789-25795.

108. Marie-Cardine A, Verhagen AM, Eckerskorn C, Schraven B. SKAP-HOM, a novel adaptor protein homologous to the FYN-associated protein SKAP55. *FEBS Lett*. 1998;435(1):55-60.

109. Raab M, Kang H, da Silva A, Zhu X, Rudd CE. FYN-T-FYB-SLP-76 interactions define a T-cell receptor zeta/CD3-mediated tyrosine phosphorylation pathway that up-regulates interleukin 2 transcription in T-cells. *J Biol Chem*. 1999;274(30):21170-21179.

110. Griffiths EK, Krawczyk C, Kong YY, et al. Positive regulation of T cell activation and integrin adhesion by the adapter Fyb/Slap. *Science*. 2001;293(5538):2260-2263.

111. Peterson EJ, Woods ML, Dmowski SA, et al. Coupling of the TCR to integrin activation by Slap-130/Fyb. *Science*. 2001;293(5538):2263-2265.

112. Comrie WA, Burkhardt JK. Action and Traction: Cytoskeletal Control of Receptor Triggering at the Immunological Synapse. *Front Immunol*. 2016;7:68.

113. Kasirer-Friede A, Cozzi MR, Mazzucato M, De Marco L, Ruggeri ZM, Shattil SJ. Signaling through GP Ib-IX-V activates alpha IIb beta 3 independently of other receptors. *Blood*. 2004;103(9):3403-3411.

114. Kasirer-Friede A, Kang J, Kahner B, Ye F, Ginsberg MH, Shattil SJ. ADAP interactions with talin and kindlin promote platelet integrin alphaIIbbeta3 activation and stable fibrinogen binding. *Blood*. 2014;123(20):3156-3165.

115. Kasirer-Friede A, Moran B, Nagrampa-Orje J, et al. ADAP is required for normal alphaIIbbeta3 activation by VWF/GP Ib-IX-V and other agonists. *Blood*. 2007;109(3):1018-1025.

116. Kasirer-Friede A, Ruggeri ZM, Shattil SJ. Role for ADAP in shear flow-induced platelet mechanotransduction. *Blood*. 2010;115(11):2274-2282.

117. Jarvis GE, Bihan D, Hamaia S, et al. A role for adhesion and degranulation-promoting adapter protein in collagen-induced platelet activation mediated via integrin alpha(2) beta(1). *J Thromb Haemost*. 2012;10(2):268-277.

118. Jarvis GE, Best D, Watson SP. Glycoprotein VI/Fc receptor gamma chain-independent tyrosine phosphorylation and activation of murine platelets by collagen. *Biochem J*. 2004;383(Pt. 3):581-588.

119. Tiedt R, Schomber T, Hao-Shen H, Skoda RC. Pf4-Cre transgenic mice allow the generation of lineage-restricted gene knockouts for studying megakaryocyte and platelet function in vivo. *Blood*. 2007;109(4):1503-1506.

120. Kawamoto T. Use of a new adhesive film for the preparation of multi-purpose fresh-frozen sections from hard tissues, whole-animals, insects and plants. *Arch Histol Cytol*. 2003;66(2):123-143.

121. Krause M, Sechi AS, Konradt M, Monner D, Gertler FB, Wehland J. Fyn-binding protein (Fyb)/SLP-76-associated protein (SLAP), Ena/vasodilator-stimulated phosphoprotein (VASP) proteins and the Arp2/3 complex link T cell receptor (TCR) signaling to the actin cytoskeleton. *J Cell Biol*. 2000;149(1):181-194.

122. Sorensen AL, Rumjantseva V, Nayeb-Hashemi S, et al. Role of sialic acid for platelet life span: exposure of beta-galactose results in the rapid clearance of platelets from the circulation by asialoglycoprotein receptor-expressing liver macrophages and hepatocytes. *Blood*. 2009;114(8):1645-1654.

123. Paul DS, Casari C, Wu C, et al. Deletion of the Arp2/3 complex in megakaryocytes leads to microthrombocytopenia in mice. *Blood Advances*. 2017;1(18):1398-1408.

124. Ong L, Morison IM, Ledgerwood EC. Megakaryocytes from CYCS mutation-associated thrombocytopenia release platelets by both proplatelet-dependent and -independent processes. *Br J Haematol*. 2017;176(2):268-279.

125. Lewis SA, Gu W, Cowan NJ. Free intermingling of mammalian beta-tubulin isotypes among functionally distinct microtubules. *Cell*. 1987;49(4):539-548.

126. Dutting S, Gaits-Iacovoni F, Stegner D. A Cdc42/RhoA regulatory circuit downstream of glycoprotein Ib guides transendothelial platelet biogenesis. 2017;8:15838.

127. Bender M, Giannini S, Grozovsky R, et al. Dynamin 2-dependent endocytosis is required for normal megakaryocyte development in mice. *Blood*. 2015;125(6):1014-1024.

128. Kuropka B, Schraven B, Kliche S, Krause E, Freund C. Tyrosine-phosphorylation of the scaffold protein ADAP and its role in T cell signaling. *Expert Rev Proteomics*. 2016;13(6):545-554.

129. Sabri S, Jandrot-Perrus M, Bertoglio J, et al. Differential regulation of actin stress fiber assembly and proplatelet formation by alpha2beta1 integrin and GPVI in human megakaryocytes. *Blood*. 2004;104(10):3117-3125.

130. Coppolino MG, Krause M, Hagendorff P, et al. Evidence for a molecular complex consisting of Fyb/SLAP, SLP-76, Nck, VASP and WASP that links the actin cytoskeleton to Fcgamma receptor signalling during phagocytosis. *J Cell Sci*. 2001;114(Pt 23):4307-4318.

131. Obergfell A, Judd BA, del Pozo MA, Schwartz MA, Koretzky GA, Shattil SJ. The molecular adapter SLP-76 relays signals from platelet integrin alphaIIbbeta3 to the actin cytoskeleton. *J Biol Chem*. 2001;276(8):5916-5923.

132. Kato K, Kanaji T, Russell S, et al. The contribution of glycoprotein VI to stable platelet adhesion and thrombus formation illustrated by targeted gene deletion. *Blood*. 2003;102(5):1701-1707.

133. Nieswandt B, Brakebusch C, Bergmeier W, et al. Glycoprotein VI but not alpha2beta1 integrin is essential for platelet interaction with collagen. *EMBO J*. 2001;20(9):2120-2130.

134. Holtkotter O, Nieswandt B, Smyth N, et al. Integrin alpha 2-deficient mice develop normally, are fertile, but display partially defective platelet interaction with collagen. *J Biol Chem*. 2002;277(13):10789-10794.

135. Abbonante V, Gruppi C, Rubel D, Gross O, Moratti R, Balduini A. Discoidin domain receptor 1 protein is a novel modulator of megakaryocyte-collagen interactions. *J Biol Chem*. 2013;288(23):16738-16746.

136. Smith CW, Thomas SG, Raslan Z, et al. Mice Lacking the Inhibitory Collagen Receptor LAIR-1 Exhibit a Mild Thrombocytosis and Hyperactive Platelets. *Arterioscler Thromb Vasc Biol*. 2017;37(5):823-835.

137. Abbonante V, Di Buduo CA, Gruppi C, et al. A new path to platelet production through matrix sensing. *Haematologica*. 2017;102(7):1150-1160.

138. Stritt S, Thielmann I, Dutting S, Stegner D, Nieswandt B. Phospholipase D is a central regulator of collagen I-induced cytoskeletal rearrangement and podosome formation in megakaryocytes. *J Thromb Haemost*. 2014;12(8):1364-1371.

139. Spuul P, Daubon T, Pitter B, et al. VEGF-A/Notch-Induced Podosomes Proteolyse Basement Membrane Collagen-IV during Retinal Sprouting Angiogenesis. *Cell Rep*. 2016;17(2):484-500.

140. Chen F, Tillberg PW, Boyden ES. Optical imaging. Expansion microscopy. *Science*. 2015;347(6221):543-548.

141. Nurden AT, Pillois X, Fiore M, Heilig R, Nurden P. Glanzmann thrombasthenia-like syndromes associated with Macrothrombocytopenias and mutations in the genes encoding the alphaIIbbeta3 integrin. *Semin Thromb Hemost*. 2011;37(6):698-706.

142. Poujol C, Tronik-Le Roux D, Tropel P, et al. Ultrastructural analysis of bone marrow hematopoiesis in mice transgenic for the thymidine kinase gene driven by the alpha IIb promoter. *Blood*. 1998;92(6):2012-2023.

143. Hodivala-Dilke KM, McHugh KP, Tsakiris DA, et al. Beta3-integrin-deficient mice are a model for Glanzmann thrombasthenia showing placental defects and reduced survival. *J Clin Invest*. 1999;103(2):229-238.

144. Habart D, Cheli Y, Nugent DJ, Ruggeri ZM, Kunicki TJ. Conditional knockout of integrin alpha2beta1 in murine megakaryocytes leads to reduced mean platelet volume. *PLoS One*. 2013;8(1):e55094.

145. Calderwood DA, Campbell ID, Critchley DR. Talins and kindlins: partners in integrin-mediated adhesion. *Nat Rev Mol Cell Biol*. 2013;14(8):503-517.

146. Moser M, Nieswandt B, Ussar S, Pozgajova M, Fassler R. Kindlin-3 is essential for integrin activation and platelet aggregation. *Nat Med*. 2008;14(3):325-330.

147. Nieswandt B, Moser M, Pleines I, et al. Loss of talin1 in platelets abrogates integrin activation, platelet aggregation, and thrombus formation in vitro and in vivo. *J Exp Med*. 2007;204(13):3113-3118.

148. Petrich BG, Marchese P, Ruggeri ZM, et al. Talin is required for integrin-mediated platelet function in hemostasis and thrombosis. *J Exp Med*. 2007;204(13):3103-3111.

149. Sun Z, Costell M, Fassler R. Integrin activation by talin, kindlin and mechanical forces. *Nat Cell Biol*. 2019;21(1):25-31.

150. Thery M. Micropatterning as a tool to decipher cell morphogenesis and functions. *J Cell Sci*. 2010;123(Pt 24):4201-4213.

151. Torisawa YS, Spina CS, Mammoto T, et al. Bone marrow-on-a-chip replicates hematopoietic niche physiology in vitro. *Nat Methods*. 2014;11(6):663-669.

9. APPENDIX

9.1. Abbreviations

3D	Three dimensional
ACTN1	Alpha actinin
ADAP	Adhesion and degranulation promoting adapter protein
ADF	Actin Depolymerizing Factor
ADP	Adenosine diphosphate
Akt	Protein kinase B
APS	Ammonium Persulfate
Arp2/3	Actin related protein 2/3
ARPC1B/2	Actin-related protein 2/3 complex subunit 1B/2
ATP	Adenosine triphosphate
BABB	Benzyl alcohol benzyl benzoate
BM	Bone marrow
BSA	Bovine serum albumin
CARST	Congenital autosomal recessive small platelet thrombocytopenia
CD	Cluster of differentiation
Cdc42	Cell division control protein 42 homolog
CLEC-2	C-type lectin-like receptor 2
Clod	Clodronate
Col	Collagen
CRP	Collagen related peptide
CVX	Convulxin
DAPI	4′,6-Diamidin-2-phenylindol
DDR	Discoidin domain receptor family, member 1
DMEM	Dulbecco's Modified Eagle Medium
DMS	Demarcation membrane system
DNA	Deoxyribonucleic acid
dNTP	Deoxynucleotide
ECL	Enhanced chemiluminescence

ECL	Erythrina cristagalli Lectin
ECM	Extracellular matrix
EDTA	Ethylenediaminetetraacetic acid
EGTA	Ethylene glycol-bis(β-aminoethyl ether)-N,N,N′,N′-tetraacetic acid
ER	Endoplasmatic reticulum
ERK1/2	Extracellular signal-regulated kinases
FACS	Fluorescence-activated cell sorting
F-actin	Filamentous actin
FAK	Focal adhesion kinase
FB	Fibrinogen
FC	Flow cytometry
FCS	Fetal calf serum
FITC	Fluorescein isothiocyanate
FLC	Fetal liver cell
FLNA	Filamin A
FN	Fibronectin
FYB	Fyn binding protein
G-actin	Globular actin
GAPDH	Glyceraldehyde-3-phosphate dehydrogenase
GATA-1/2	GATA-binding factor 1
GP	Glycoprotein
GT	Glanzmann thrombastenia
HEPES	4-(2-hydroxyethyl)-1-piperazineethanesulfonic acid
hESC H9	Human embryonic stem cell H9
HSCs	Hematopoietic stem cells
IF	Immuno-fluorescence
IgG	Immunoglobulin G
JNK	c-Jun N-terminal kinases
LAIR-1	Leukocyte-associated immunoglobulin-like receptor 1
LFA-1	Lymphocyte function-associated antigen 1
MAPK	Mitogen-activated protein kinase
MFI	Mean fluorescence intensity

MKs	Megakaryocytes
MMPs	Matrix metallopeptidases
MPV	Mean platelet volume
MYH9	Myosin, heavy chain 9
N	Nucleus
Nck	Non-catalytic region of tyrosine kinase adaptor protein 1
Neo	Neomycin
Neu	Neuraminidase
p42POP	Partner of profilin
Pak1/2/3	Serine/threonine-protein kinase PAK 1
PAR1/3	Protease-activated receptor-1/3
PBS	Phosphate-buffered saline
PCR	Polymerase chain reaction
PE	Phycoerythrin
PF4	Platelet factor 4
PFA	Paraformaldehyde
PFN	Profilin
PGI_2	Prostacyclin
P_i	Phosphate
PI3K	Phosphoinositide 3-kinases
PIP_2	Phosphatidylinositol 4,5-bisphosphate
PIPES	Piperazine-N,N′-bis(2-ethanesulfonic acid)
PLCγ1	Phospholipase C, gamma 1
Pld	Phospholipase
PLL	Poly-L-lysine
PPF	Proplatelet formation
PRP	Platelet rich plasma
PS	Phosphatidyl serine
PTMs	Posttranslational modifications
PVDF	Polyvinylidene fluoride
Pyk2	Proline-rich tyrosine kinase 2

Rac1	Ras-related C3 botulinum toxin substrate 1
RCC	Renal cell carcinoma
Rhod	Rhodocytin
RNA	Ribonucleic acid
ROCK	Rho-associated protein kinase
RT	Room temperature
RUNX1	Runt-related transcription factor 1
SCEM	Super cryo embedding medium
SCF	Stem cell factor
SDS	Sodium dodecyl sulfate
SDS-PAGE	Sodium dodecyl sulfate polyacrylamide gel electrophoresis
SH2/3	Src-homology 2/3
Skap55	Src-kinase-associated phosphoprotein of 55 kDa
SLAP-120/130	SLP-76–associated protein of 120/130 kD
SLP-76	SH2 domain–containing leukocyte protein of 76 kD
SMN	Survival of motor neuron protein
Syk	Spleen tyrosine kinase
TAE	Tris base, acetic acid, EDTA
Taq	Thermus aquaticus
TBS-T	Tris Buffered Saline with Tween
TCR	T-cell receptor
TEM	Transmission electron microscopy
TEMED	Tetramethylethylenediamine
Thpo	Thrombopoietin
Thr	Thrombin
TMR	Tetramethylrhodamine-dextran
TO	Thiazole orange
TRPV4	Transient receptor potential cation channel subfamily V member 4
TxA_2	Thromboxan A2
VASP	Vasodilator-stimulated phosphoprotein
Vav1	Vav Guanine Nucleotide Exchange Factor 1

VEGF	Vascular Endothelial Growth Factor
vWF	Von Willebrand factor
WAS	Wiskott-Aldrich syndrome
WAVE	WASP-family verprolin-homologous protein
WB	Western blot
WCA	WH2, connecting and acidic
WH2	Wiskott-Aldrich homology 2

9.2. **Acknowledgment**

The work presented here was performed at the Department of Experimental Biomedicine I, University Hospital/University Würzburg, in the group of Dr. Markus Bender.

During the period of my PhD work (2015 - 2019), many people helped and supported me. I would like to thank the following people for their help:

Dr. Markus Bender for allowing me to perform my PhD work in his laboratory and for his constant support, trust, useful advice and financing my projects, participations on workshops and scientific congresses.

all supervisors of my PhD work.

all present and past members of the lab for their experimental support, useful discussions and pleasant atmosphere in the lab.

the MK-meeting.

all external collaborators who contributed to this work.

all proof-readers of this thesis.

finally, I would like to thank my family and friends for their continuous support and patience.

9.3. **Publications**

First-author publication

Aurbach K., **Spindler M.**, Haining E.J., Bender M., Pleines I., Blood collection, platelet isolation and measurement of platelet count and size in mice-a practical guide. Platelets. 2018

Spindler M., van Eeuwijk J. M. M., Schurr Y., Nurden P., Nieswandt B., Stegner D., Reinhold A., Bender M., ADAP deficiency impairs megakaryocyte polarization with ectopic proplatelet release and causes microthrombocytopenia. Blood. 2018

Co-author publication

Gupta S., Cherpokova D., **Spindler M.**, Morowski M., Bender M., Nieswandt B., GPVI signaling is compromised in newly formed platelets after acute thrombocytopenia in mice. Blood. 2018

Schurr Y., **Spindler M.**, Kurz H., Bender M., The cytoskeletal crosslinking protein MACF1 is dispensable for thrombur formation and hemostasis. Sci Rep. 2019

International oral presentations

“Microthrombocytopenia and premature platelet release in ADAP-deficient mice.” 60th annual meeting of the Society of Thrombosis and Haemostasis Research (GTH); February 2016, Münster, Germany.

“Microthrombocytopenia and premature platelet release in ADAP-deficient mice.” 3rd EUPLAN conference; September 2016, Bad Homburg, Germany.

“Loss of the hematopoietic adaptor protein ADAP impairs megakaryocyte polarization and induces ectopic platelet release.” 26th Biennial Congress of the International Society on Thrombosis and Haemostasis (ISTH); July 2017, Berlin, Germany.

“Novel insights into mouse models with ectopic proplatelet release.” 27th Biennial Congress of the International Society on Thrombosis and Haemostasis (ISTH); July 2019, Melbourne, Australia.

International poster presentation

“Microthrombocytopenia and premature platelet release in ADAP-deficient mice.” 10th international Eureka! symposium; October 2015, Würzburg, Germany

“Microthrombocytopenia and premature platelet release in ADAP-deficient mice.” 11th international Eureka! symposium; October 2016, Würzburg, Germany

“Loss of ADAP impairs megakaryocyte polarization and induces ectopic platelet release.” 12th international Eureka! symposium; October 2017, Würzburg, Germany

International award

Young investigator award from the 26th Biennial Congress of the International Society on Thrombosis and Haemostasis (ISTH) for the highly rated abstract: “Loss of the hematopoietic adaptor protein ADAP impairs megakaryocyte polarization and induces ectopic platelet release.” July 2017, Berlin, Germany.

Young investigator award from the 27th Biennial Congress of the International Society on Thrombosis and Haemostasis (ISTH) for the highly rated abstract: “Novel insights into mouse models with ectopic proplatelet release.” July 2019, Melbourne, Australia.

9.4. **Curriculum vitae**

APPENDIX

9.5. **Affidavit**

I hereby confirm that my thesis entitled “The role of the *adhesion and degranulation promoting adapter protein* (ADAP) in platelet production” is the result of my own work. I did not receive any help or support from commercial consultants. All sources and/or materials applied are listed and specified in the thesis.

Furthermore, I confirm that this thesis has not yet been submitted as part of another examination process neither in identical nor in similar form.

Würzburg, August 2019 _____

Markus Spindler

Eidesstattliche Erklärung

Hiermit erkläre ich an Eides statt, die Dissertation “Die Rolle des *adhesion and degranulation promoting adapter* Proteins (ADAP) in der Thrombopoese” eigenständig, d.h. insbesondere selbständig und ohne Hilfe eines kommerziellen Promotionsberaters, angefertigt und keine anderen als die von mir angegebenen Quellen und Hilfsmittel verwendet zu haben.

Ich erkläre außerdem, dass die Dissertation weder in gleicher noch in ähnlicher Form bereits in einem anderen Prüfungsverfahren vorgelegen hat.

Würzburg, August 2019 _____

Markus Spindler